Second Harmonic (SH) spectroscopic studies on the effect of amphiphilic molecules-induced adsorption and transport characteristics of an organic cation across a POPG lipid bilayer

By

SRINIVASARAO KINTALI

Enrolment No. CHEM03201204001

Raja Ramanna Centre for Advanced Technology,

Indore-452013, India

A thesis submitted to the

Board of Studies in Chemical Sciences

In partial fulfillment of requirements

for the Degree of

DOCTOR OF PHILOSOPHY

of

HOMI BHABHA NATIONAL INSTITUTE

May 2019

Homi Bhabha National Institute[1]

Recommendations of the Viva Voce Committee

As members of the Viva Voce Committee, we certify that we have read the dissertation prepared by Srinivasarao Kintali entitled **"Second Harmonic (SH) spectroscopic studies on the effect of amphiphilic molecules-induced adsorption and transport characteristics of an organic cation across a POPG lipid bilayer"** and recommend that it may be accepted as fulfilling the thesis requirement for the award of Degree of Doctor of Philosophy.

Chairman – Prof. M. P. Joshi	**Date:** 08/01/2020
Guide / Convener – Prof. Arup Banerjee	**Date:** 08/01/2020
Examiner – Prof. Sobhan Sen, JNU Delhi	**Date:** 08/01/2020
Member 1- Prof. S. N. Jha	**Date:** 08/01/2020
Member 2- Prof. A. K. Das, IIT Indore	**Date:** 8/1/2020
External Member - Prof. K. I. Priyadarshini, BARC	**Date:**

Final approval and acceptance of this thesis is contingent upon the candidate's submission of the final copies of the thesis to HBNI.

I/We hereby certify that I/we have read this thesis prepared under my/our direction and recommend that it may be accepted as fulfilling the thesis requirement.

Date: 08/01/2020

Place: Indore

Arup Banerjee

(Guide)

[1] This page is to be included only for final submission after successful completion of viva voce.

STATEMENT BY AUTHOR

This dissertation has been submitted in partial fulfillment of requirements for an advanced degree at Homi Bhabha National Institute (HBNI) and is deposited in the Library to be made available to borrowers under rules of the HBNI.

Brief quotations from this dissertation are allowable without special permission, provided that accurate acknowledgement of source is made. Requests for permission for extended quotation from or reproduction of this manuscript in whole or in part may be granted by the Competent Authority of HBNI when in his or her judgment the proposed use of the material is in the interests of scholarship. In all other instances, however, permission must be obtained from the author.

Srinivasarao Kintali

DECLARATION

I, hereby declare that the investigation presented in the thesis has been carried out by me. The work is original and has not been submitted earlier as a whole or in part for a degree / diploma at this or any other Institution / University.

Srinivasarao Kintali

List of publications arising from the thesis

1. Effect of Three Pluronic Polymers on theTransport of an Organic cation Across a POPG Bilayer Studied by Second Harmonic Spectroscopy.

S. R. Kintali, G. K.Varshney, and K. Das.

Chem. Phys. Lett., **2017**, *684*, 267-272.

2. Interaction of Amphotericin B with Ergosterol/Cholesterol-containing POPG Liposomes Studied by Absorption, Fluorescence and Second Harmonic Spectroscopy.

S. R. Kintali, G. K.Varshney, and K. Das.

ChemistrySelect, **2018**, *3*, 10559-10565.

3. pH-Dependent Interaction of Four Different Bile salts with POPG Liposomes Studied by Dynamic Light Scattering and Second Harmonic Generation Spectroscopy.

S. R. Kintali, G. K.Varshney, and K. Das.

ChemistrySelect, **2019**, *4*, 1227-1231.

In conferences:

1. Effect of three pluronic polymers on the transport of an organic cation across an artificial membrane studied by Second Harmonic spectroscopy. **S. R. Kintali**, G. K. Varshney and K. Das, National Laser Symposium (NLS-25), held at KIIT University, Bhubaneswar, from December 20-23, 2016.

2. Effect of three bile salts on the transport of an organic cation across a negatively charged POPG membrane probed by Second Harmonic spectroscopy. **S. R. Kintali**, G. K. Varshney, and K. Das, National Symposium on Radiation and Photochemistry (NSRP-2017), held at Manipal University (MIT) Manipal, from March 2-4, 2017.

3. A comparative study on the effect of Curcumin & Chlorin-p6 on the transport of the LDS cation across a negatively charged POPG bilayer: Effect of pH.G. K. Varshney, **S. R. Kintali**, P. K. Gupta and K. Das, National Symposium on Radiation & Photochemistry (NSRP-2015), held at IIT Kanpur, from March 9-11, 2015.

4. Effect of Curcumin on the adsorption properties of a cationic dye across DPPG-POPG liposomes probed by Second Harmonic spectroscopy. G. K. Varshney, **S. R. Kintali**, and K. Das, National Symposium on Radiation and Photochemistry (NSRP-2017), held at Manipal University (MIT) Manipal, from March 2-4, 2017.

5. Determination of trace levels of mercury in aqueous solutions using gold nanostars as a probe-A spectrophotometric study. K. Das, A. Uppal, G Varshney, **S. Kintali**, B. Bose and S. K. Majumder. National Laser Symposium (NLS-27), held at RRCAT Indore, from December 3-6, 2018.

Other / Co-author Publications:

1. A comparative study on the effect of Curcumin and Chlorin-p6 on the transport of the LDS cation acrossa negatively charged POPG bilayers: Effect of pH.

G. K. Varshney, **S. R. Kintali**, P. K. Gupta and K. Das

Spectrochimica Acta Part A, **2017**, *173*, 132–138.

2. Effect of Bilayer Partitioning of Curcumin on the Adsorption and Transport of a Cationic Dye across POPG Liposomes Probed by Second-Harmonic Spectroscopy.

G. K.Varshney, **S. R. Kintali**, P. K. Gupta and K. Das

Langmuir, **2016**, *32*, 10415–10421.

3. Effect of Curcumin Addition on the Adsorption and Transport of a Cationic Dye across DPPG-POPG Liposomes Probed by Second Harmonic Spectroscopy.

G. K. Varshney, **S. R. Kintali**, and K. Das

Langmuir, **2017**, *33*, 8302-8310.

Srinivasarao Kintali

This work dedicated to…

My Ph. D. supervisor

Dr. Kaustuv Das (Late)

And

Parents, friends,

and family members.

ACKNOWLEDGEMENT

This thesis work is the culmination of whole Ph.D. journey. I realized though only my name appears on the cover page of this thesis, this journey would not have been possible without the efforts of many people, including the support of my family, supervisor, mentors, friends, and different departments have contributed to accomplish this big task. It is my pleasure to express acknowledge here to all those people who have helped me in this thesis. I really apologize for if I forgot it.

First and Foremost, I am extremely gratitude from bottom of my heart and will be truly indebted to throughout my lifetime to my supervisor Dr. Kaustuv Das (Late), Scientific Officer G, Laser Biomedical Applications Division (LBAD), RRCAT. He has encouraged me to pursue the research work in this research area. This research work would not have been possible without his guidance and active involvement in various stages like discussions about fundamentals in my research topic, the planning of experiments, analysis of the experimental data and scientific interpretation of the results, helping in the writing manuscripts, his constant support, patience, motivation, his immense knowledge in this research field, and enthusiasm about research which helped for my Ph. D. degree.

I am highly grateful to the members of doctoral committee, members are Dr. M. P. Joshi (Chairman), Dr. S. N. Jha, Dr. A. K. Das, (IIT Indore), Dr. K. I. Priyadarsini (External expert member, BARC Mumbai), I am also grateful to Dr. P. K. Gupta (former Chairman), Dr. S. K. Dixit (former Chairman), Dr. D. K. Palit (former external expert member, BARC Mumbai), Dr. Ramachari, Dr. R. Makde, Dr. D. Nayak, (IIT Indore), and all other members for their critical review and suggestions during the annual reviews and pre-synopsis viva voce. These valuable suggestions helped me a lot to improve the quality of the work presented.

I am so gratefully acknowledge to Dr. S. K. Majumder, Head, LBAD. I also thank to Dr. Alok Dube, Dr. Abha Uppal, Dr. Mrinalini Sharma, Dr. Biplap Bose, Dr. H. S. Patel, Dr. Raktimdas gupta, for corrections as well as suggestions of various drafts of this thesis and synopsis and which helped me to present the research work in an effective manner. Dr. R. Shrivastava, Dr. K Sahu, and Dr. Beena Jain, Shri Vijay kumar, Ms.

Anita, Ms. A. Shrivastava, Ms. Jyoti, Shri Anupam, Mr. Surjendu, and all the members of LBAS for providing their support, encouragement and creating friendly environment in research labs for carrying out the research work.

I am so gratefully to Dr. K. I. Priyadarsini (BARC Mumbai), Prof. Anindya Datta (IIT Bombay), Dr. Anjan chakraborty (IIT Indore), Dr. Tushar kanti Mukherjee (IIT Indore), Prof. Pramit K. Chowdhury (IIT Delhi) for corrections as well as suggestions of chapters of this thesis and synopsis.

I am forever thankful to my colleague, Dr. G. K. Varshney, I spent very nice moments with him in my Ph. D. journey. He always supports morally as well as helped in my research experiments. I got supportive seniors in our section Dr. R. K. Saini, Dr. Paromita Sarbadhikary, Dr. S. P. Singh, and Mr. Yashveer Singh for their support and creating a cordial working environment.

I am extremely grateful to Homi Bhabha National Institute, Department of Atomic Energy (DAE), RRCAT, Indore for provide DAE fellowship for making it possible for me to do research here. I am highly thankful for the opportunity given to work in Raja Ramanna Centre for Advanced Technology, Indore. I give deep thanks to the lectures at BARC training school, Mumbai, who taught me in different fields of sciences and enhances my knowledge in chemical sciences. Special thanks to Dr. Arup Banerjee (Dean Academics HBNI-RRCAT), who helped a lot in thesis submission. Thanks to Dr. C. P. Paul, Dean Student affairs-RRCAT, Administration staff of RRCAT and HBNI.

Millions of thanks go to my school teachers, lectures of N.M.R. Junior College, Srirama Degree College and NIT Warangal faculty members. Especially, special mention to who created interest in chemistry D. Palugunarao sir, Syambabu sir, Kiran Kumar sir, Srinivas sir, Aruna Kumari madam, and K. Rajarao sir.

I express my deepest gratitude to D. Sudhakar, K. Satheesh Kumar Reddy, R. Amar, and P. Bhaskar, for their encouragement, moral and financial support.

It is a pleasure to thanks my school friends K. Rajasehkar, K. Bhaskar, degree room mates K. Annaji, Ch. Ramu, and friends P. Srinu, P. Surapnaidu, K. Govind, Ch. Suresh, M. Mohan, K. Rajesh, S. Delhi, Raghu Yale. It's my fortune to gratefully acknowledge

my school, college classmates and 56th batch BARC training school friends Dr. Anita Kumari, Ms. Anita, Dr. Parvathi, Dr. Somunaidu, and TSO's.

My sincere thanks to my Ph. D. batchmates Dr. Tufan Roy, Dr. Paresh Chandra pradhan, Dr. Gangadhar Das, Dr. Arijit chakraborty, Dr. Debasis Mondal, Dr. Chitradip Banerjee, Dr. Sudheer, Dr. Adityanarayan H. Pandey, Dr.Vandna Kumari, Mrs. Sonal Saxena, and seniors and juniors for create enjoy full atmosphere in Ramanujan hostel, RRCAT Guest House. Thanks to guest house management and mess people.

I would like to express my profound gratitude to Dr. Srihari, who gives heart-warming support, combined with straightforward criticism for me in day to day life in RRCAT. I would also like to acknowledge Dr. Bhuvnesh, Dr.Nagaswer Rao, Dr. Venkat Narayana, K Gopi, and B Madhu for their well wishes and support.

I am extremely thankful to my cousin Ravi, for his encouragement, moral support and financial assistance whenever it's required. I owe my deepest gratitude to my family members grandparents and relatives. Namely, Ms. Annapurnamma, late Shri Suryam, Ms. Chinnammadu, late Shri Janardhanarao, Ms. Jayaamma, late Shri Suryanarayana, Ms. Kumari, Shri Govindarao, Ms. Akkamma, late Shri Sriramulu, Ms. Budemma, Shri Polinaidu, Mrs. Ravanamma, Shri Simachalam, my cousins Shri Ramana, Ms. Laxmi, Ms. Sarada, Ms. Girija, Ms. Nirmala, Ms. Suhasini, Mrs. Neelima, Mr. Appalanaidu, Ms. Punya, Mrs. Sarada, Mrs. Lavanya, Shri Simahachalam, Shri Venugopalarao, Ms. Padma, Mr. Sekhar. Sisters-in-law Ms. Jyothi, Ms. Srikalyani. Brothers-in-law Shri Mukundarao, Shri Atchutarao, Shri Lachhappa, Shri Sambamurthy, and their children.

I take my great pride and privilege to say to the people who mean a lot to me, my parents. I always knew that they trusted in me, given lot of opportunities and freedom to choose my career which I interest, Both of you supported my all decisions which I have chosen with full of liberty. I salute both of you for sacrifice, trust, guidance, wisdom, patience, unconditional love, moral support, selflessly encouraged, optimism, care, and pain.

Importantly, to my fiancée, Puspalatha, she recently entered into my life towards the end of my Ph.D. I wish to thank for your encouragement, support and care and all the excitement that you have brought into my life. I also thank for my mother-in-law

Ms.Prabavathi and father-in-law Shri BhaskarRao and brother-in-law Dr. Madhu babu have welcomed me into their family.

Finally, I would like to express my heartfelt gratitude to all those who have contributed to complete this research work directly or indirectly towards obtaining my doctorate degree, I hope, I could thank all of them, but time, space and conscience compel me to stop here and apologize if have missed out anyone.

Last but not least, I am thankful to Almighty for all time blessings.

- Srinivasarao Kintali

CONTENTS

ABSTRACT

The research work in the present thesis has been performed to investigate the effect of amphiphilic molecules (Pluronic polymers, antibiotic Amphotericin B and bile salts) on permeability of a negatively charged 1-palmitoyl-2-oleoyl-sn-glycero-3-phospho-(1'-rac-glycerol), sodium salt (POPG) lipid bilayer by monitoring the adsorption and transport characteristics of an organic ion, LDS-698 (LDS^+) as the second harmonic (SH) probe. The interfacial SH spectroscopy is performed using the quasi-CW output of a Ti-sapphire laser pumped by 532 nm wavelength of Nd-YAG green laser. The brief descriptions of research works presented in the thesis are given below.

Pluronic polymer induced transport of an organic cation across a negatively charged POPG membrane bilayer have been studied using interfacial selective second harmonic (SH) spectroscopic technique. The length of either hydrophilic (poly-ethylene oxide) or hydrophobic (poly-propylene oxide) unit in the polymer has been varied to investigate their effect on membrane transport. Membrane transport has been observed to depend critically on the length of the hydrophobic segment present in the polymer. Membrane transport studies using polymers which were either "incorporated" or "incubated" with the lipid bilayer suggested that bilayer packing plays a critical role in the insertion of polymers having a long hydrophilic chain.

The effect of Amphotericin B (AmB) in the transport properties of an organic cation (LDS-698) across either POPG liposomes or sterol (either Ergosterol (Ergo) or Cholesterol (Chol)) incorporated POPG liposomes have been studied by the interfacial selective SH spectroscopic technique. The transport of LDS^+ becomes faster at very low AmB/Liposome (A/L) ratio whereas Ergo present in the bilayer. As increasing A/L ratio, the average transport time constants (τ_{av}) of the LDS^+ ion fall into two kinetic re-

gimes which observed for the different liposomes. In POPG-Ergo liposomes, the effect of neutralizing either of the two charged functional groups of AmB reveals that interaction of AmB with Ergo is primarily dependent upon the charged amino group present in the mycosamine moiety of AmB. The spectral (absorption and fluorescence) properties of AmB were also studied to supplement the results obtained from SH studies. In summary, at low A/L ratio (< 1), the membrane permeability of the POPG membrane were observed to dependent upon the membrane composition or the pH of the medium, whereas at higher A/L ratio (> 1) the permeability becomes similar for all the cases. The spectroscopic properties of AmB with increasing A/L ratio suggest that the latter phenomena may be due to the aggregated states of AmB in the bilayer which enhance the bilayer permeability irrespective of the bilayer composition and solution pH.

In recent years the role of bile salts in colorectal cancer has been gaining importance. In addition, it has been observed that for diseases associated with gastrointestinal tract, the pH becomes slightly acidic. In this report we have investigated the pH dependent bile acid – bile salt transformation on the integrity and permeability of POPG liposomes by dynamic light scattering and the interfacial selective SH spectroscopic technique. Using four different bile salts whose chemical properties vary widely we have observed that in their neutral form (i.e bile acids) they are able to alter the POPG membrane properties significantly higher compared to their ionic (i.e. bile salts) form. Our results indicate that out of the four bile salts, Sodium Deoxycholate and Sodium Cholate have the potential to damage membranes in the colon as their pK_a is closer to the pH measured in the gastrointestinal tract. Therefore, one of the pathways of bile salt induced cytotoxicity in the gastrointestinal tract, may occur due to the potential membrane damaging action of these bile salts at acidic pH.

LIST OF FIGURES

LIST OF TABLES

LIST OF ABBREVIATIONS

SHG	Second harmonic generation
SFG	Sum frequency generation
HRS	Hyper-Rayleigh scattering
MG	Malachite green
TCSPC	Time correlated single photon counting
LDS-698	2-[4-[4-(dimethylamino)phenyl]-1,3-butadienyl]-1 ethylpyridinium monoperchlorate
BS	Bile salts
NaC	Sodium cholate
NaDC	Sodium deoxy-cholate
NaGDC	Sodium glycol deoxy-cholate
UDCA	Ursodeoxycholic acid
AmB	Amphotericin B
Chol	Cholesterol
Ergo	Ergoserol
τ_{av}	The average transport time constants
POPG	1-palmitoyl-2-oleoyl-sn-glycero-3-phospho(1'racglycerol) sodium salt

Chapter 1

Introduction

This chapter gives brief introduction to amphiphilic molecules and lipid membranes interactions. The interaction of amphiphilic molecules (pluronic polymers, Amphotericin B and bile salts) with membranes has been discussed in details. The fundamental theory and working principals on an interfacial selective second harmonic (SH) spectroscopic technique has been described briefly. The applications of SHG on the adsorption and the transport of molecules across the lipid bilayer available in the literature have been included.

1.1 Amphiphilic molecules-lipid membrane interactions

1.1.1 Bio-membranes

One of the most important constituent of a cell is its membrane which encompasses the cell in three dimensions. Fundamental researches on the membrane (Bio-membranes) have been carried out by different groups of basic sciences especially from biology, biophysics and biochemist background. The major constituents of bio-membranes are different type of lipid molecules which have either neutral or positively or negatively charged head groups. These lipids are arranged in highly organized manner and they also contain other molecules such as proteins, enzymes etc. embedded in the lipid matrix [1,2].

1.1.2 Molecular transport

One of the most important function of the bio-membrane is to regulate the transport of certain molecules [3]. In physiological state, the membrane permits crossing of substances that the cell requires and prevents the transport of those molecules that are harmful to cell. It is therefore crucial to understand how the membrane acts as gate for certain molecules. However, the biological membranes are structurally very complex, which makes difficult to understand their properties and functions. Therefore, membranes composed of pure lipids are used as model membranes which are popularly known as liposomes [4,5].

1.1.3 Membranes and amphiphilic molecules-Interactions

The bilayer properties of liposomes have been extensively studied to understand the effect of the interactions between amphiphilic molecules and lipid membranes [6]. Amphiphilic molecules can be either hydrophobic or hydrophilic depending upon the physical and chemical state of its surroundings. The interaction of amphiphilic molecules with membranes can have a significant effect on the physicochemical properties and function of the membrane [7]. Recent reviews on amphiphilic molecules interaction with lipid bilayers studied by computer simulation [8–11]. One of the most significant outcome of this interaction is alteration of membrane permeability i.e., transport of the molecules across a lipid bilayer. There are several molecular stimulation studies on the permeability of the membranes to understand how the changes in transport properties of bilayers take place upon interaction with different molecules [12]. In drug delivery systems, one of the most important processes is the interaction and then transport of drug molecules across the lipid bilayer. The latter process is more complex in nature due to

dependency on several physical and chemical parameters [13]. For example, in transport of the amphiphilic drug curcumin, from outer to inner lipid bilayer, the binding plays an important role. The binding of the drug has been described by a two state model, and depending upon the relative drug: lipid ratio, the membrane parameters were shown to change considerably [14]. The amphiphilic drug, Chlorpromazine Hydrochloride (CBZ) binds to phospholipid bilayers and then alters the molecular ordering of the phospholipids [15]. The modification of the bilayer structure due to binding of CBZ was observed to depend upon the nature of the phospholipid head groups [16]. The binding of several cationic amphiphilic drugs with phospholipid vesicles has been investigated by the surface plasmon resonance (SPR) spectroscopy. The SPR studies have demonstrated that drug-membrane binding interactions are dependent on membrane fluidity [17]. Theoretical studies like molecular dynamics (MD) simulations give better idea about local properties i.e. orientation and molecular positioning of these drugs in the membranes [18]. In this thesis, we have studied the membrane permeability of a negatively charged 1-palmitoyl-2-oleoyl-sn-glycero-3-phospho-(1'-rac-glycerol),sodiumsalt (POPG) liposomes in the presence of different types of amphiphilic molecules like pluronic polymer, amphotericin B (an antibiotic), and bile salts. The membrane permeability was measured by monitoring the transport characteristics of LDS-698 (2-[4-[4-(dimethylamino) phenyl]-1, 3-butadienyl]-1-ethylpyridinium monoperchlorate, (LDS^+)) across the bilayer using second harmonic (SH) spectroscopic technique. In the next section we have described how these amphiphilic molecules interact with liposomes.

1.2 Interactions of amphiphilic molecules with POPG liposomes.

1.2.1 Pluronic polymers

Pluronic polymers are amphiphilic triblock copolymers of type ABA (Figure1.1). The structural repeat unit of these polymers contains hydrophilic part Polyethylene Oxide (PEO) and hydrophobic part Polypropylene Oxide (PPO). The hydrophilic parts are located at the beginning and at end of the polymer while the hydrophobic part is located middle of the polymer. The amphiphilic characteristic of these molecules depends upon the relative chain length of the PEO and PPO groups [19,20]. These polymers are widely used in several industrial applications such as detergency, emulsification, forming, and formulation of cosmetics. Apart from their industrial applications, these are also used in medicines as biological response modifiers, drug delivery carriers, and ingredients in preparation of pharmaceuticals substances [21–24]. In addition, depending on their hydrophilic-lipophilic balance (HLB) values, studies have shown that these polymers can induce different effects in cell membrane [25,26]. The various physicochemical properties of amphiphilic pluronic polymers are presented in the table 1.1. In order to understand their interactions with cell membranes, several studies have been performed and summarized in recent reviews [27,28]. Pluronic polymers were observed to enhance the translocation behaviour (flip-flop) in membranes [29]. They bind to the membranes by incorporation of their hydrophobic units in the hydrophobic region of the lipid bilayer. The driving forces for these types of interactions are favoured by the hydrophobicity and the volume of the hydrophobic unit of the polymer [29]. These polymers were also observed to act as agents for drug penetration across biological membranes [20]. It has been observed that they interact differently with normal and malignant blood cells resulting in enhanced permeability of tumor cells [30]. The results of

the isothermal titration calorimetry (ITC) and electron cryomicroscopy indicate that the polymer insertion into lipid bilayer depend upon the phase structure of the lipid bilayer. [31].

$$HO-(CH_2CH_2O)_m-(CH_2(CH_3)CHO)_n-(CH_2CH_2O)_m-H$$

Figure 1.1: The chemical structure of pluronic triblock copolymers which contain two hydrophilic ethylene oxide (EO) segments and a hydrophobic propylene oxide (PO) segments. (Where m stands for the number of repeat units in the EO segment and n corresponds to the number of repeat units in the PO segment of the polymer).

Table 1.1: The various physico-chemical properties of amphiphilic pluronic polymers are tableted [29]**.**

Copolymer (trade name in parentheses)	**Molecular Weight**	**$\beta_{f\text{-}f}$ (uM^{-1})**	**Log K_p (Water/hexane)**	**$V_{hydrophobic}$ (nm^3)**
$EO_2\,PO_{30}\,EO_2$ (L61)	2090	0.16 ± 0.01	-0.24 ± 0.037	8.38
$EO_{13}\,PO_{30}\,EO_{13}$ (L64)	2900	0.07 ± 0.01	-1.83 ± 0.27	8.38
$EO_{76}\,PO_{30}\,EO_{76}$ (F68)	8400	0.01 ± 0.05	-3.5 ± 0.53	8.38
$EO_3\,PO_{40}\,EO_3$ (L81)	2750	0.56 ± 0.045	-0.11 ± 0.02	11.2
$EO_{26}\,PO_{40}\,EO_{26}$ (P85)	4500	0.22 ± 0.06	-2.65 ± 0.4	11.2
$EO_{61}\,PO_{40}\,EO_{61}$ (F87)	7700	0.06 ± 0.01	-3.19 ± 0.48	11.2
$EO_{76}\,PO_{30}\,EO_{76}$ (L101)	3800	1.35 ± 0.13	0.11 ± 0.017	16.4
$EO_{37}\,PO_{56}\,EO_{37}$ (P105)	6500	0.21 ± 0.03	-2.6 ± 0.4	15.6
$EO_{132}\,PO_{50}\,EO_{132}$ (F108)	14600	0.11 ± 0.02	-3.65 ± 0.54	13.9

In addition, the ITC studies have also indicated that the polymer insertion into fluid-phase liposomes increases with temperature [32]. There were also several theoretical studies to investigate the interactions of these polymers with membranes. Recent molecular simulation study demonstrated that if the hydrophobic part of the polymer is comparable in length to the bilayer thickness, polymer will insert itself across the bilayer.

However, if the hydrophobic part of the polymer is shorter than the bilayer thickness, it will insert into in the lipid bilayer partially [33]. In a recent Monte Carlo simulation study, it was revealed that the length of the hydrophobic part of the polymer plays a crucial role in governing the local permeability of the membrane [33]. The permeability increases significantly when the polymer present in the bilayer as transmembrane statewhile the polymer present as the hairpin state, the permeability of the lipid bilayer remains unaffected [34]. The results of atomistic molecular dynamics simulations have shown that the interactions of polymer and lipid bilayer critically depend on the hydrophilic/lipophilic balance of the polymer. The increase in polymer concentration initiates pore formation in the lipid bilayer [35]. All of above studies reveal that pluronic polymers interact with lipid membranes depending upon their structure, amphiphilic character, the hydrophilic/lipophilic balance of the polymer, and the length of the hydrophobic part of the polymer. Therefore, it would be interesting to explore the role of the length of the hydrophobic part of the polymer on the interaction between pluronic polymers and phospholipids membranes. The objective of first study is to investigate the role of chain lengths of the hydrophobic and hydrophilic units of pluronic polymers on the membrane permeability and bilayer mobility.

1.2.2 Amphotericin B

Amphotericin B (AmB) is an important antibiotic belonging to the class of polyene macrolides. This was first isolated from fermenter cultures of Streptomyces*nodosus* [36]. The preparation procedure of AmB was first described completely by Nicolaou et. al. 1988 [37]. Although it has some issues as drug, still it is using for the treatment of systemic fungal infections. There are several reviews which demonstrate that the mode of action of AmB on biological membranes depends on the type of sterol present in

membranes [38–41]. It is a rod-shaped amphiphilic molecule which has several the hydrophilic groups on the one side of the macrolide ring, namely the seven hydroxyl groups, carboxylic acid group, and the polar head mycosamine (Figure 1.2). The other side of the ring is hydrophobic and rigid due to the seven conjugated double bond (heptene) system [42].

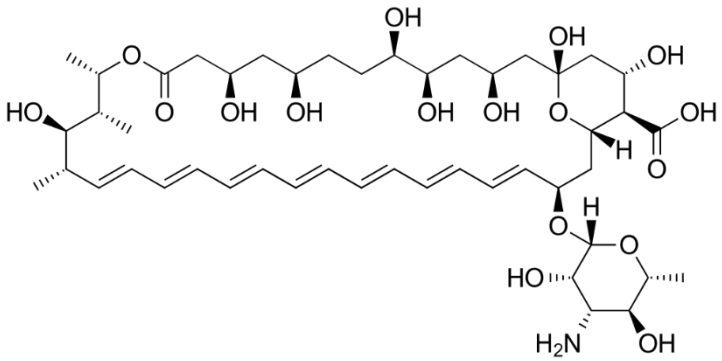

Figure 1.2: Chemical structure of Amphotericn B.

In the last 30 years, there has been significant progress in understanding the interaction of AmB with sterols in lipid membrane [43–46]. Sterols are necessary components of biological membranes and the functions of sterols regulate the membrane fluidity in membranes. In mammalian cells, the major membrane sterol is cholesterol (Chol) whereas in fungal cell membranes egrosterol (Ergo) is the major membrane sterol. The chemotherapeutic treatment of AmB, which is disruption of cell membrane activities, has been postulated due to its higher affinity for ergosterol containing cell membranes than for cholesterol containing cell membranes [47]. The surface pressure of the 1-palmitoyl-2-oleoylphosphatidylcholine (POPC) monolayers prepared with either ergosterol or cholesterol when allowed to interact with AmB in the membranes are studied. The results of study reveal that the surface pressure of POPC-ergosterol bilayer system is more significantly varied when AmB in the POPC-ergosterol bilayer as compared to the POPC and POPC-cholesterol bilayer [48]. The results of some studies indicate that

the antifungal activity of AmB is due to a change in the permeability of lipid membrane which occurs due to formation of an ion-channel assembly in lipid membrane with help of ergosterol [49]. These antibiotic/sterol channels are responsible for the transport of ions, which causes disruption in the cell integrity and ultimately cell lysis [50]. However, the results of recent findings reveal that the main cause for the antifungal activity of AmB is its binding with Ergo in the membrane as compared to the channel formation. This binding nature of AmB with Ergo inhibits essential physiological functions of Ergo in the yeast [51,52]. The studies by M Murata and co-workers reveal that the mode of molecular interactions of AmB-ergosterol in hydrated phospholipid bilayers is "head-to tail" orientation confirmed by rotational echo double resonance (REDOR) spectra [53]. The observed side effects of AmB have been attributed to the interaction with cholesterol containing biological cell membranes [54]. All of above studies reveal that AmB interact with lipid membranes depending upon membrane composition. Therefore, the objective of second study is to investigate the effect of AmB on the membrane permeability of POPG liposomes as a function of membrane composition (the presence of either ergosterol or cholesterol in the membrane) and the pH of the medium.

1.2.3 Bile salts

Bile salts (Figure 1.3) are amphiphiles secretion from cholesterol in the liver and stored in the gallbladder. Bile salts are covalently linked to glycine and taurine as conjugated bile acids and then excreted into the intestine. Bile acids participate in many physiological functions such as cholesterol homeostasis, digestion and adsorption of fats, solubilisation of lipids in the gut and in bile [55]. They are several bile salts available in the gut and in bile, in which some of listed here, sodium cholate (NaC), sodium deoxycholate (NaDC), sodium glycodeoxycholate (NaGDC), and ursodeoxycholic acid (UDCA).

During the last few years, there has been considerable interest in the effect of bile salts in the membrane systems [56]. The amphiphilic characteristics nature helps bile salts to interact with biological membranes and this phenomenon disturb membrane integrity. The membrane permeability might be changed by bile salts at below their critical micellar concentration (CMC) values due to the formation of mixed micelles and cell swelling. On the contrary, at concentration above their CMC, they interact with phospholipids of cell membranes is main cause for a membranolytic effect [57].

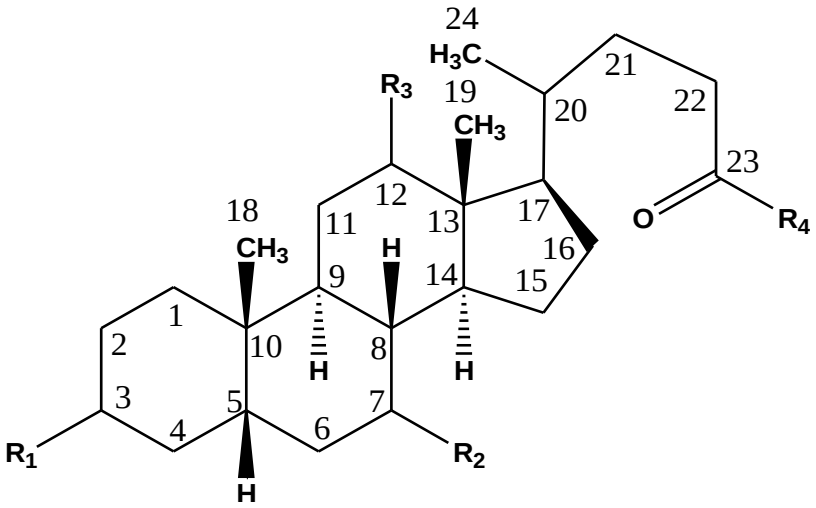

Bile salt	R_1	R_2	R_3	R_4
NaC	OH	OH	OH	O^-Na^+
NaDC	OH(α)	H	OH	O^-Na^+
NaGDC	OH	H	OH	$NHCH_2COO^-$
UDCA	OH(α)	OH(β)	H	OH

Figure 1.3: Chemical structure of bile salts shows the carbon atom numbering and the functional groups.

The bile salts may alter the behaviour of cholesterol in model systems at below their CMC values [58,59]. The passive movement of cholesterol in and out of the hepatocyte membranes depends on the bile salts as a function of their relative hydrophobicity [60].

Low concentration of bile salts can be disrupted phospholipid bilayers containg cholesterol. These results indicate that bile salts bind to membranes below their CMC and initiate by as yet unknown mechanism, and bile salts are transfer across the membrane [61–63]. Differential scanning calorimetry (DSC) study has shown that induction of membrane fluidity depends on the number and positioning of free hydroxyl groups on bile acids [64].

The steady state and time resolved fluorescence spectroscopy studies of cationic ellipticine drug with bile salts reveal that the binding capacity of cationic species to different bile salts depend on the pK_a of the corresponding bile acids. Concentration of bile salts increases the hydrophobic interaction between bile salts and cationic species increases due to formation of aggregates [65]. The interaction of bile acids, namely cytotoxic deoxycholic acid (DCA), and the cytoprotective ursodeoxycholicacid (UDCA) with model membranes has been reported earlier. It was found that DCA causes the fluidization of bilayers and UDCA helps a stabilization of membranes [66]. The recent study has shown that upon interaction with bile salts, the bioavailability of Phenothiazine tranquilizer drugs increases in aqueous medium and thus bile salts can be useful for drug delivery agents for phenothiazine drugs [67]. The interaction of anti-cancer drug, berberine chloride (BR) with bile salts aggregates of different hydrophobicity have been investigated by the time-resolved fluorescence spectroscopy. These interactions are sensitive to the structure and size of the bile salt aggregates [68]. The interaction of antipsychotic drugs with bile salts has been studied by UV–Visible and steady state fluorescence spectroscopy. The observed results shown that the extent of interaction between drug molecules and bile salts is dependent on hydrophobic nature of bile salts [69]. The studies of steady-state and time-resolved fluorescence of 1-naphthol indicate that monomeric bile

salt molecule (at very low concentration, 1 mM) induces appreciable wetting in the lipid bilayer [70]. All of above studies reveal that bile salts interact with lipid membranes depending upon their structure, hydrophobic nature and the pK_a of the corresponding of bile salts. Therefore, it would be interesting to explore the role of pH on the interaction between bile salts and phospholipids membranes as well as the role of the bile acid – bile salt transformation in the cytotoxic effects of bile salts.

1.3 Interfaces

In the physical science, an interface is defined as "the boundary between two different regions occupied by different matter, or by matter which has different physical states". Many biological, chemical, and physical phenomena occur at surfaces and interfaces. The study of surfaces and interfaces are important due to several phenomena which occur at the surfaces/interfaces such as molecular adsorption and transport, energy transfer, charge transfer, and several chemical reactions. These dynamic processes play a significant role in basic sciences, environmental sciences, medical field, and technology [71,72]. Generally, the bulk media experience by symmetrical environment but interfaces experience by asymmetrical environment. The latter is main cause for the chemical, physical, and biological properties that take place in the interface. So many bulk properties e.g. physical, chemical changes, charge and energy relaxation etc. are significantly altered at the interface. To study the properties of interface, require high intense electric filed. After invention of the optical high intensity laser in 1961, it has become easier to generate high intense electric field of radiation which is useful for development of the nonlinear spectroscopic techniques. Second harmonic generation (SHG) and sum frequency generation (SFG) are the powerful techniques often used to study of surfaces and interfaces [72,73,74-81,82-91]. The first optical second harmonic generation is ob-

served from the non-centrosymmetric quartz crystal [92]. The SHG signal is generated from the centrosymmetric calcite crystal also [93]. Both SHG and SFG are forbidden process in centrosymmetric media and isotropic environments due to electric dipole approximations [71,72,75,78,79,81]. The coherent optical SHG or SFG signals are not generated by the bulk liquids, gases and amorphous and centrosymmetric crystalline solids due to symmetry reasons. However, the interfaces are asymmetric in nature where inversion symmetry is no longer conserved. Thus the coherent SHG signal can be generated at interfaces. The Figure 1.4 describes schematic energy level diagram of SHG. The solid and the dashed lines represent the ground and virtual energy states respectively [94].

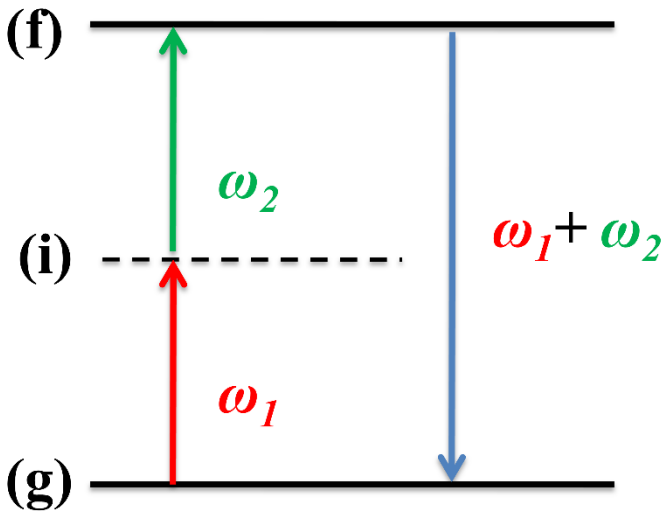

Figure 1.4: Energy-level diagram describing the SHG process. The electronic energy states (g) and (f) represents the atomic ground state and excited state respectively and (i) represents the virtual state. For SHG, $\omega_1 = \omega_2$.

1.3.1 Theory of second harmonic generation

1.3.1.1 Symmetry criteria for SHG

Generally, polarization of the medium interacts with the electromagnetic radiation and can be expressed as a power series [94]

$$\vec{P}(t) = \chi^{(1)}\vec{E}_{\omega}(t) + \chi^{(2)}\vec{E}_{\omega}(t)\vec{E}_{\omega}(t) + \chi^{(3)}\vec{E}_{\omega}(t)\vec{E}_{\omega}(t)\vec{E}_{\omega}(t)+\ldots \quad (1.1)$$

$$P(t) = P^{(1)}(t) + P^{(2)}(t) + P^{(3)}(t) \quad (1.2)$$

where, $\chi^{(1)}$ is the linear susceptibility, $\chi^{(2)}$, $\chi^{(3)}$ are the second and third order nonlinear susceptibility respectively etc. $E_{\omega}(t)$ is the incident electric field of the frequency of ω. The weak electric field of light interacts with matter followed by linear process, in this phenomenon, the induced polarization P (t) is proportional to linearly with strength of applied electric field.

$$P(t) = \chi^{(1)}E_{\omega}(t) \quad (1.3)$$

where, $\chi^{(1)}$ is the linear susceptibility and $E_{\omega}(t)$ is the incident electric field of the light. When high intense electric field of radiation is available for interact with the medium, higher order polarization terms are introduced to the linear polarization. Here, higher order polarization terms are nonlinear in nature, like, second harmonic generation, third order harmonic generation, become more observable.

The induced second order polarization $P^{(2)}(t)$ term is expressed as [95–98].

$$P^{(2)}(t) = \chi^{(2)}E_{\omega}(t)E_{\omega}(t) \quad (1.4)$$

where, $E_{\omega}(t)$ is incident electric field and $\chi^{(2)}$ is second order nonlinear susceptibility of the medium. We know that both the parameters i.e. the electric field of radiation and the induced polarization are vector quantities. Therefore, $p^{(2)}(t)$ and $E_{\omega}(t)$ can be expressed as vectors and the second order nonlinear susceptibility become a tensor.

$$P_i^{(2)}(t) = \sum_{j,k} \chi_{i,j,k}^{(2)} E_\omega^j(t) E_\omega^k(t) \quad (1.5)$$

where, i, j, k are the three normal Cartesian coordinates of laboratory system respectively.

In the polarization equation, even order terms are sensitive to the symmetry of the medium. It means that second harmonic generation is affected by centrosymmetric nature of the medium due to the induced polarization and the incident electric field of radiation. If inversion symmetry operation is performed on the nonlinear medium, the sign as well as magnitude of the second order polarization ($P^{(2)}(t)$) and the electric field of light (E_ω) are changed but the second order susceptibility ($\chi^{(2)}$) will remain same by sign and magnitude.

$$-P^{(2)}(t) = \chi^{(2)}\big(-E_\omega(t)\big)\big(-E_\omega(t)\big) \quad (1.6)$$

By combing equation 1.4 and 1.6, we get the final result as $-\chi^{(2)} = \chi^{(2)}$, which practically is not possible unless $\chi^{(2)} = 0$. It indicates that centrosymmetric media $\chi^{(2)}$ vanishes and in a centrosymmetric media, the second harmonic generation is not allowed. The inversion symmetry is no longer conserved at an interface, upon performing inversion symmetry operation at interfaces, $P^{(2)}(t)$ is not necessarily equal to $-P^{(2)}(t)$. Therefore, $\chi^{(2)}$ is not equal to zero at interfaces. The conclusion derived from above equations, is that SHG is allowed at interfaces. The unique characteristic of SHG is the nonlinear surface specific technique for the study of interfaces.

The bulk centrosymmetric systems do not contribute to coherent SHG due to symmetry reasons. We prove here a molecular point of view. Let us assume two similar neighbouring molecules present in bulk media which are oppositely oriented with respect to centre of symmetry. If the incident electric field of frequency (ω) interacts with oppositely ori-

ented molecules in bulk media, it produces induced polarizations which will be opposite phase with respect to each other. The distance between opposite phase is much less than compared to the coherence length of the process and thus will cancel each other. Therefore, the contributions of the net second order polarization become zero and the molecules present in bulk media do not produce coherent SHG or SFG signal. It is pertinent to note that the centrosymmetric bulk media generates incoherent second order light scattering called as hyper-Rayleigh scattering (HRS). This phenomenon arises by the fluctuations in orientation of molecules and molecular density in the isotropic bulk solutions, which disrupt the phase cancellation. The bulk HRS generated by centrosymmetric media has been reported [99,100].

1.3.1.2 The generation of SHG by microscopic centrosymmetric molecules

The SHG is allowed process in the non-centrosymmetric media, however, surfaces and interfaces which are the lack of inversion of symmetry systems, through the electric dipole approximation [72,101,102]. Bulk liquids are centrosymmetric systems, in which SHG thought to be forbidden process but Eisenthal and co-workers first demonstrated that SHG can be generated when molecules adsorbed at the surface of spherical centrosymmetric molecules [103]. The generation of SHG from centrosymmetric medium can be explained by a bare microsphere of diameter L (Figure 1.5). The adsorbed molecules on the opposite position of the microscopic particle surface oriented oppositely and the oppositely oriented surface structures generated second harmonic (SH) electric field will have opposite phases. The net SH field produced by a pair of oppositely oriented surface structures is

$$E_{2\omega} \propto \beta^{(2)} \mathrm{E}_{\omega} \mathrm{E}_{\omega} \left(1 - \mathrm{e}^{-\mathrm{i}\Delta\vec{\mathrm{k}}.\vec{\mathrm{L}}}\right) \tag{1.7}$$

where, $\beta^{(2)}$ is the second order polarizability of the microsphere, L is the diameter of the microsphere and Δk is scattering vector.

Δk derived by the equation is

$$\Delta\vec{k} = \vec{k}_{2\omega} - 2\vec{k}_{\omega} \tag{1.8}$$

where, $k_{2\omega}$ and k_{ω} are the light propagation vectors for the second harmonic light at 2ω and the fundamental light ω respectively.

The amplitude of the scattering vector is expressed as

$$\Delta k = \frac{4\pi(n_{\omega} - n_{2\omega})}{\lambda_{\omega}} = \frac{4\pi\Delta n}{\lambda_{\omega}} \tag{1.9}$$

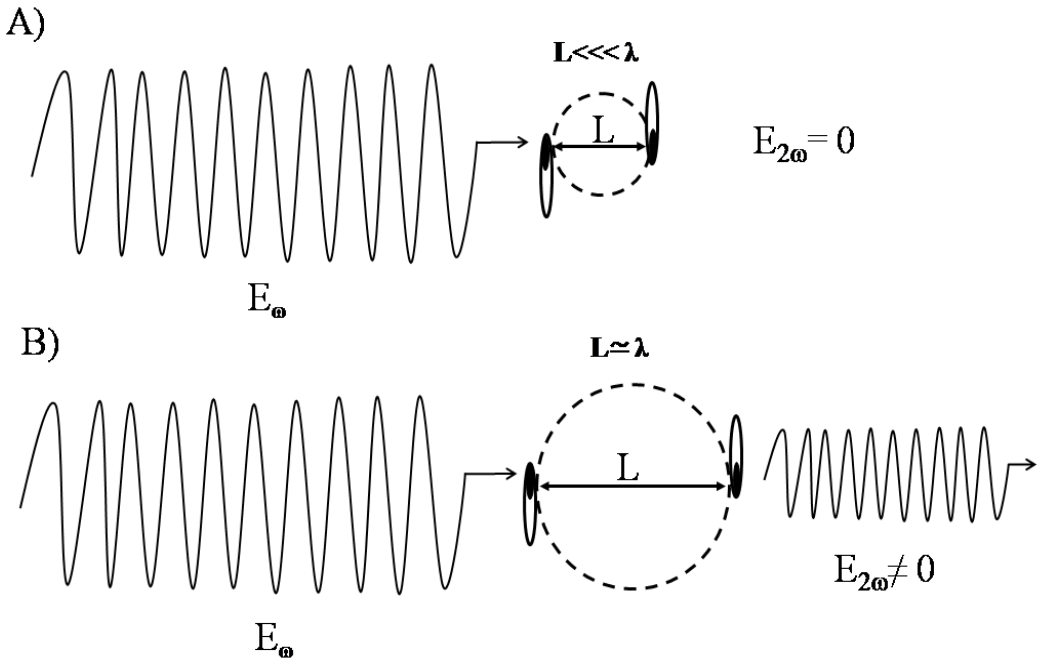

Figure 1.5: A schematic illustration of SHG how SH signal generates from molecules adsorbed at surface of centrosymmetric particles.

Case A: the distance between the two oppositely oriented surface structures (L) is much less than the wavelength of the incident light (Case A: Figure 1.5), then ($\Delta k \times L$) << λ the net $E_{2\omega}$ should be zero. Case B: the distance between the two oppositely oriented surface structures (L) is comparable to wavelength of the incident light (Case B: Figure 1.5), then ($\Delta k \times L$) ≈ λ, the net $E_{2\omega}$ should not be zero. The generated SH electric field signal depend upon the particle size as well as the wavelength of fundamental light. When ($\Delta k \times L$) = π the net $E_{2\omega}$ will be maximum.

Second harmonic generation from individual, isolated large non centrosymmetric molecules suspended in bulk solution [104]. In addition to semiconductor quantum dots and metallic crystals also generate SHG, due to their non-centrosymmetric structure [105].

1.4 SHG: A spectroscopic tool to monitor transport of molecules across a lipid bilayer

1.4.1 Molecules transport across a membrane

A primary role of biological membranes is the passage of chemical species into and out of cells as well as regulates the cell integrity [106]. The fundamental structure of bio-membrane is a bilayer. The main building blocks of bio--membranes are lipids. The bi-layers are made up of two monolayers which formed by a polar hydrophilic head group attached to two non-polar hydrophobic fatty acid tails. The lipid molecules exposed to polar environment, themselves are orientated as a spherical shape. Phospholipid molecules self-assembling into bilayer structure are called as liposomes [107,108]. The polar head groups of liposomes are exposed to aqueous environment and non-poplar carbon chains face to the hydrophobic environment. The structure of liposomes resemble to biological membrane bilayer which are often used as model membrane systems for

transport of molecules across lipid bilayer. Generally, the structure of liposome is spherical and centro symmetric in nature. The adsorption and transport of molecules across lipid bilayers have been investigated by various spectroscopic techniques like electron paramagnetic resonance (EPR) [109,110], nuclear magnetic resonance (NMR) [111–116], absorption [117,118] and fluorescence spectroscopy [119–126]. The advantage of the SHG technique over other conventional techniques is that SHG is sensitive to molecules that are located in the bilayer region.

1.4.2 The working principle of SHG for membrane transport

The SHG technique has been developed to monitor molecules transport across the bilayer in the real time. The SHG technique is extensively used by Eisenthal and coworkers using malachite cation (MG) to study the transport across a negatively charged bilayer of DOPG liposome [127]. The basic idea of the technique is based on molecules adsorbed on the outer surface of a liposome. The molecules are oriented in the preferred way in the interfacial region. With the progress in time, molecules cross the lipid span and are adsorbed on the inner surface of the liposome. These molecules will have opposite orientation with respect to molecules adsorbed on the outer surface of a liposome due to symmetry considerations. The working principle of SHG described below in the details manner.

The primary consideration of SHG is the molecule of interest should have a reasonable hyperpolarizability at the excitation wavelength. The excitation source for SHG studies is the quasi-CW output of a Ti-sapphire (Coherent Mira) laser pumped by Nd-YAG (532 nm, Coherent Verdi 5W) laser. The dipole moment increased significantly when molecules are excited from ground state to higher excited states. This type of phenome-

na is generally observed in the dye molecules due to extended electronic delocalizations. In addition, the necessary and sufficient condition for resonance enhancement of the SHG process is that the molecule of interest should have sufficient absorption at the SH wavelength of a Ti-sapphire laser. Finally, molecules should have a significant amphiphilic character, so that molecules are fairly distributed in the hydrophilic and hydrophobic environment and molecules can transport across lipid bilayer. The transport of molecules across the bilayer can be monitored by SHG process in real time is briefly described as follows. In our experiments, spherical shaped liposomes are used as model membranes to study the transport of the molecules because the size of liposomes is of the order of the wavelength of the incident radiation (~800 nm). Initially an aqueous liposomes solution is added in cuvette containing SH probe molecule followed by rapid mixing. Initially, the SH probe molecules are adsorbed on the outer surface of the liposome, which generate SH electric field due to in phase and will add up coherently (Figure 1.6). As time progress, the SH probe molecules pass through the bilayer and then get adsorbed to inner surface of liposomes oppositely oriented with respect to orientation at the outer surface. The oppositely oriented molecules are separated by the bilayer thickness (~5 nm) which is smaller than the coherence length of the SHG process, (typically about 1.0 nm). The SH electric field generated by oppositely oriented molecules will be out of phase and cancel each other. In contrast, molecules which are present in bulk aqueous solution cannot contribute to coherent SH signal because of randomly orientation but they can generate incoherent SH signal called as hyper-Rayleigh scattering (HRS) as discussed earlier. It is pertinent to note that the higher magnitude of the SH signal generated when molecules adsorbed on the outer surface of the liposome compared to the incoherent HRS generated from molecules present in the bulk aqueous medium. Therefore, the SHG technique can be used for monitoring transport process in

real time. From the measured SHG signal, $I_{2\omega}$, the second harmonicfield, $E_{2\omega}$, is calculated as follows:

$$E_{2\omega}(t) = \sqrt{I_{dye+liposome}(t) - I_{background}} \quad (1.10)$$

where, $I_{(2\omega)dye+liposome}(t)$ represents the total SH signal detected at 2ω after addition of the liposome solution into the SH probe solution at time t and $I_{(2\omega)\ Background}$ is the background SH signal coming from the SH probe molecules that remain in the bulk medium (HRS). Addition of the liposome solution to the dye solution (or vice-versa), generate the second harmonic electric field ($E_{2\omega}$) which is proportional to the second order susceptibility ($\chi^{(2)}$). This provides information of the finite population difference between the adsorbed SH probe molecules on the outer and inner surface of the liposome bilayer at time t. Here, $N_o(t)$ is the population of adsorbed molecules on outer surface at time t and $N_i(t)$ is the population of adsorbed molecules on inner surface at time t

$$E_{2\omega} \propto [N_o(t) - N_i(t)]E_\omega E_\omega \quad (1.11)$$

Generally, the measured experimental data can be converted to the SH electric field and is fitted to exponential decay functions per following equation.

$$E_{2\omega}(t) = A_0 + \sum_{i=1}^{n} a_i \exp\left(t/\tau_i\right) \quad (1.12)$$

It is pertinent to note that when equilibrium condition is attained, there was no changes in the SH electric field ($E_{2\omega}$) with time. It means the transport process might be finished. The observed SH electric field ($E_{2\omega}$) decay is parallel to the x-axes but the SH electric field signal does not approach zero. It indicates that the term A_0 in equation 1.12. The (N_{in} / N_{out}) ratio can be obtained by the term ($1-A_0$).

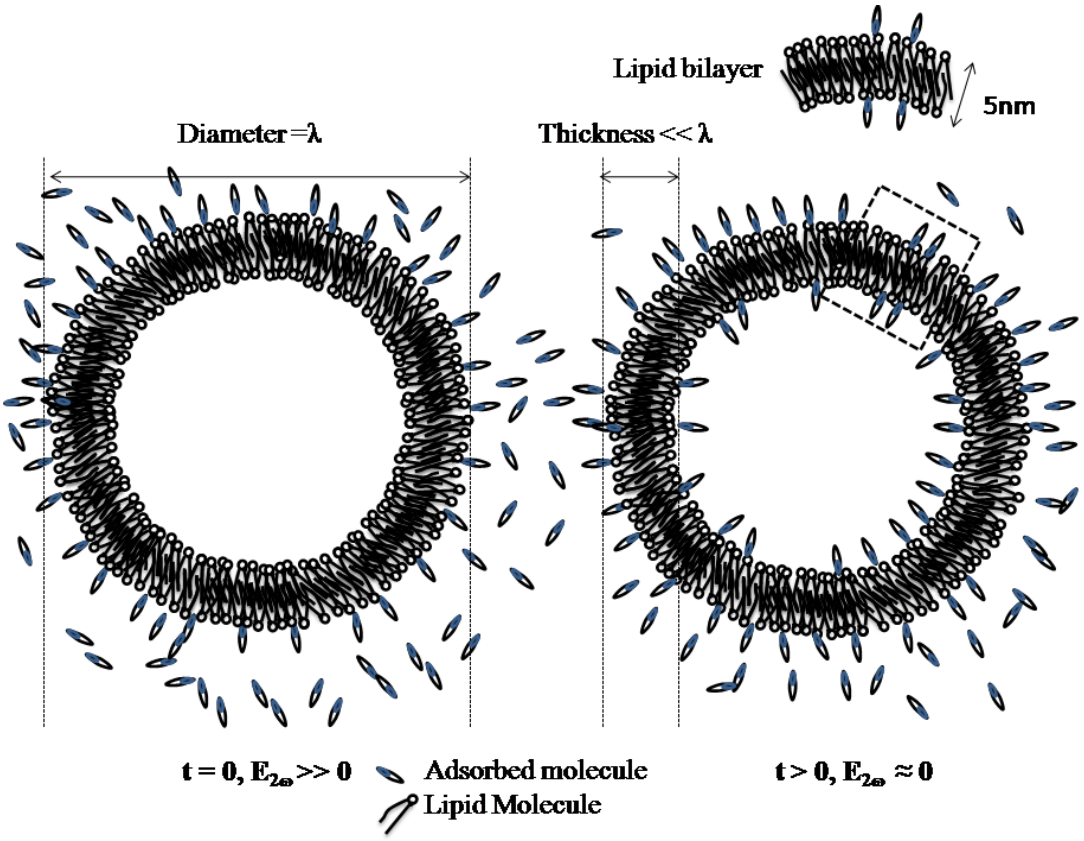

Figure 1.6: Schematic illustration of SHG to monitor molecules transport across the bilayer in the real time. At t = 0, the adsorption of SH probe molecules on the outer surface which generates a non-zero coherent SH signal. At time t > 0, as time progress, the SH probe molecules pass through the bilayer and then get adsorbed to inner surface of liposomes oppositely oriented with respect to orientation at the outer surface. The SH electric field generated by oppositely oriented molecules will be out of phase and cancel each other.

1.4.3 The membrane transport studies by SHG

Eisenthal and co-workers demonstrated a new method of second harmonic generation to monitor the transport of the positively charged malachite green (MG) cation across a negatively charged liposome in aqueous medium [127]. Several studies on surfaces and

interfaces have been reported by Eisenthal and co-workers using second harmonic generation spectroscopy. The effect of cholesterol on the molecular transport of MG cation across the unilamellar dioleolyphosphatidylglycerol (DOPG) liposomes membrane permeability is studied [128]. The results indicate that the transport rate of MG cation across bilayer decreases by six times when liposome contains 50 mol % cholesterol compared to cholesterol free liposomes. It means that cholesterol retards the rate of transport of MG cation across liposome bilayers due to enhancement in bilayer rigidity [128]. The SHG technique can successfully measure the surface potential and surface charge density of DOPG liposomes. The surface potential measured by SHG technique is dependent on the valence and concentration of the electrolyte. The charge density is found to be $1.3x10^{14}$ per cm^2, which is equal to 70 $Å^2$ per charge and this is in well agreement to the area of a phospholipid head group [129]. Eisenthal and co-workers have studied the effect of bilayer surface charge density on the adsorption and the transport kinetics of MG cation across liposomes of different lipid compositions by SHG technique in real time. The results show that the adsorption of MG cation onto the outer surface of bilayer and the transport rate of MG cation across the lipid bilayer increase linearly with the fraction of negatively charged lipids groups in the bilayer. The adsorption process is initiated by electrostatic interaction between the MG molecules on the outer surface of negatively charged bilayer. The potential gradient between the outer and inner bilayer is the driving force for the transport of MG molecules across the bilayer [130]. The transport rate of MG cation across DOPG liposomes have been studied by SHG technique in presence of different electrolytes used as counterions. The transport rate of MG cation across the DOPG liposome is independent up to 1 mM concentration of counterion, however, the transport rate becomes very much dependent at higher concentration of counterion [131]. Eisenthal's group also investigated the effect

of three different types of ionophores on the transport of MG across a lipid bilayer. These ionophores include are valinomycin (VAL) and gramicidin A (gA). The effect of these ionophores on the transport of MG and the extended transport of MG across a bilayer depends on their individual transport mechanisms [132,133].

So far, synthetic membrane systems are only used for the studies on the adsorption and the transport of the molecules across the bilayer by the SHG technique. Dai and coworkers used SHG technique to study the adsorption and transport of the MG ion across the living *Escherichia coli* membrane in real time. At low concentration of MG ion, the SH intensity of the MG ion is fitted with a multi process kinetic model which reveals that the transport of the MG ion across the outer membrane of the Gram-negative bacteria of *Escherichi coli* is much faster than through the cytoplasmic membrane [134]. In addition to all these works, uptake of small molecule into living *Escherichi coli* membranes and the transport of molecular ions (MG ion) across *Escherichi coli* bacteria membranes are also studied by two complementary techniques namely optical transmission microscopy (TM) and second-harmonic light scattering (SHS). Uptake and the transport measurements are carried out independently by individual technique [135]. The SHS results provide sequential differentiation of the molecular (MG ion) density at membrane surfaces. The transport rate constants of MG ion can be estimated by simultaneous global analysis of the TM and SHS data for all the traversed cellular barriers [136]. They have also investigated the adsorption and the kinetics of the hydrophobic molecules (MG cation and neutral bromocresol purple (BCP) molecule) across negatively charged murine erythroleukemia (MEL) cells by time and wavelength resolved SHS. The results have shown that the only MG ions adsorbs onto the surface of the MEL cell due to electrostatic interaction between the positively charged MG ion and the negative

charged MEL cell but it is not observed in case of BCP [135]. There are numerous studies available in literature on the interaction of MG cation and bio molecules with the living *Escherichia coli* membrane in real time using SHS technique [137–139].

Recently, Das and co-workers have reported several studies on the adsorption and transport of LDS^+ across lipid bilayer by second harmonic spectroscopy [140]. The transports of the photosensitizer Cp_6 across the egg PC lipid bilayer have been studied by SHG technique at different pH range. There are three ionizable carboxylic acid groups present in Cp_6 which can exist in different ionic forms at different pH of the medium. At low pH, Cp_6 exhibits strong interaction with liposomes and this is attributed to the hydrophobic character of the Cp_6. As the pH increases, the interaction with the like charged liposomes becomes weaker due to the abundance of the negatively charged hydrophilic species of the Cp6. The effect of the bilayer rigidity by the lowering temperature of the medium or by incorporating 50 mol % cholesterol in the lipid bilayer on transport of molecules also are studied. The obtained results show that lowering of temperature has more profound effect on the transport rates [140]. The effect of the lipophilic drug curcumin on the diffusion kinetics of LDS^+ ion across lipid bilayer has been studied in real time by the surface specific SHG technique. The transport time constants of LDS^+ have been found to be faster by ~56 times in presence liposomal curcumin (with the mole ratio of the curcumin/lipid of 0.2). The effect of curcumin is greater than the bilayer rigidity increased by any means on the trasport process. The results show that enhancement in transport of LDS^+ may depend on the interaction of the lipophilic molecule with the polar head group region of the lipid [141]. Das and co-workers also investigated how the curcumin partitioning affects the bilayer permeability during the adsorption and transport of the LDS^+ across a negatively charged POPG bilayer using

the nonlinear second harmonic (SH) spectroscopic technique [142]. The fractional increase in the SH electric field ($E^{f}_{2\omega}$) is observed upon addition of the curcumin to LDS^{+} containing liposomes solution. The observed results show that the neutral form of curcumin is more effective in increasing ($E^{f}_{2\omega}$) of LDS^{+} compared to the anionic form of curcumin [142]. Das and co-workers also studied the adsorption and the transport of LDS^{+} ion across liposome bilayer followed by the curcumin addition using the interfacial selective second harmonic (SH) spectroscopic technique. The results explained how the curcumin altered bilayer properties. Curcumin induced changes in the SH electric field signal of the LDS^{+} ions ($E_{2\omega}$ (LDS^{+})) is studied for two different cases in which liposomes are prepared by either only POPG or only DPPG lipids and the obtained results are distinctly different. In case, liposomes are prepared by different composition ratio of the POPG and DPPG lipids, the kinetics of LDS^{+} upon curcumin addition is found to exhibit a mixture of the individual kinetics characteristic. The results are explained on the basis of the relative strength of the Na^{+}-POPG and Na^{+}-DPPG interaction. Higher ordering of the lipid acyl chain in DPPG liposomes makes the Na^{+}-DPPG interaction much stronger than the Na^{+}-POPG interaction. The temperature dependent kinetic characteristics of the $E_{2\omega}$ (LDS^{+}) signal following curcumin addition is further studied using liposomes prepared by POPG-DPPG lipids at low temperature. The results explained that individual domains of POPG and DPPG lipids exist at low temperature. The formation these domains are dependent on the degree of the saturation/unsaturation (S/U) ratio of lipid chains and phase state of the bilayer. The effect of gel phase is more conducive for individual domain formation. [143].

1.5 Objectives and Scope of thesis

The organization of the remaining chapters of this thesis is as follows:

Chapter 2 describes details of the chemicals, methods and techniques used in the present thesis. Details of preparation method of liposomes and their characterizations have been described. This chapter also covers the details of various spectroscopic techniques (absorption, fluorescence and light scattering spectroscopy) used for the work described in this thesis. Finally, the experimental setup of SH spectroscopy used for measurements of the adsorption and the molecular transport across lipid bilayer in real time has been described in detail.

In chapter 3, the effect of lengths of the hydrophobic PO units and hydrophilic EO units of pluronic polymers on the bilayer permeability of the negatively charged 1-palmitoyl-2-oleoyl-sn-glycero-3-phospho-(1'-rac-glycerol), sodium salt (POPG) liposomes by the interfacial selective second harmonic (SH) spectroscopic technique has been described.

In chapter 4, the effect of Amphotericin B (AmB) on the transport properties of an organic cation (LDS-698) across either ergosterol incorporated POPG liposomes or cholesterol incorporated POPG liposomes have been investigated by monitoring the bilayer transport of the LDS^+ ion using the interfacial selective second harmonic spectroscopy. And also the spectroscopic properties (absorption and fluorescence) of the antibiotic in the POPG bilayer have been studied.

In chapter 5, the pH dependent affect of four bile salts (sodium cholate (NaC), sodium deoxycholate (NaDC), sodium glycodeoxycholate (NaGDC), and ursodeoxycholic acid (UDCA)) on the integrity and permeability of POPG liposomes have been investigated by dynamic light scattering (DLS) and interfacial second harmonic (SH) spectroscopic techniques.

Finally, in Chapter 6 a summary of the major observations is presented. A brief outline of future scopes that may evolve from the thesis is also provided.

Chapter 2

Materials & Methods

This chapter provides details of the chemicals, methods and techniques used in the various studies. Methods for preparation of liposomes and their characterization based on size and zeta potential are described. This is followed by description of absorption, fluorescence and light scattering spectroscopy techniques used to probe interaction of selected amphipihlic molecules (Pluronic polymers, Amphotericin B and bile salts) with liposomes. Finally, the experimental setup and procedure used to study of the adsorption and molecular transport of drug/substrate molecules across a lipid bilayer in real time by second harmonic (SH) spectroscopy is described in detail.

2.1 Materials

The lipid, polymers, and other reagents used in various studies are as follows. Sodium salt of L-α Phosphatidyl DL-Glycerol, POPG (Avanti Polar Lipid Inc. U.S.A), three pluronic polymers F-127, L-61, and F-68 (Sigma, U.S.A.), amphotericin B (Sigma, U.S.A.), the two sterols Ergosterol (Alfa Aesar, U.S.A.), Cholesterol (Titan Biotech limited, India) and four bile salts Sodium Cholate (NaC), Sodium Deoxycholate (NaDC), Sodium Glycodeoxycholate (NaGDC) and Ursodeoxycholic acid (UDCA) (Sigma, U.S.A.) were purchased and used as received. LDS-698 (Exciton, U.S.A.), the probe for SH spectroscopy was a gift from Prof. N. Sarkar (IIT Kharagpur, India) and used as received.

2.2 Preparation of liposomes

2.2.1 Thin film method

Biomimetic liposomes are self-assembled vesicles of natural or synthetic lipid molecules, which consist of an aqueous core entrapped by one or more lipid bilayers[144–146] . In the present study, various types of liposomes are prepared using POPG phospholipids. The chemical structure of POPG phospholipids is shown in Figure 2.1. The schematic diagram of liposome is shown in figure 2.2. The method used for preparation of these liposomes is described below in detail.

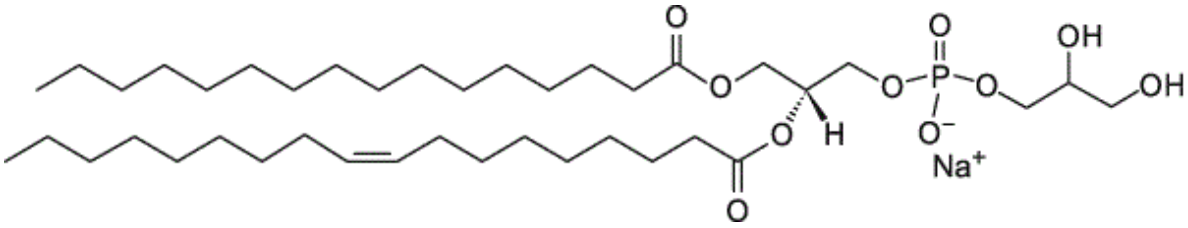

Figure 2.1*: *Chemical structure of POPG lipid.

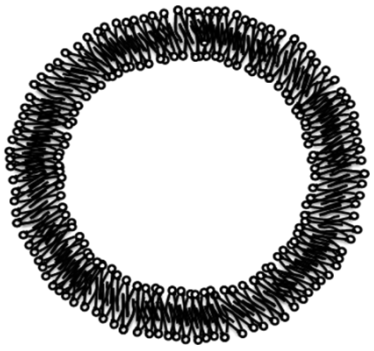

Figure 2.2*: *Schematic diagram of a liposome

The stock solution of POPG (0.1 M) is prepared in chloroform. To prepare liposomes by thin film method, 200 μL POPG solution in chloroform is taken in a 50 mL round bottom flask and the solvent is evaporated completely under reduced pressure in a rotary

evaporator at 40 rpm for overnight to make a thin film of lipid. The dry thin film of lipid is hydrated by adding appropriate buffer solution of desired pH. The liposomes suspension is then vortexed for 10 minutes to produce unilamellar liposomes [147]. The freshly prepared liposomes suspension is passed 10-15 times through cellulose-acetate membrane filters (pore size 0.45 μm and 0.20 μm) to minimize the polydispersity of liposomes suspension. The prepared liposomes are transferred in clean glass bottles and stored at 4 °C. The liposomes are used within a week of preparation. The final concentration of lipid in the liposomes prepared by thin film method is ~2 mM.

Calculation of liposome concentration:

The number of lipids in a spherical uni-lamellar liposome, N_{tot}, can be estimated as [148].

$$N_{tot} = \left(\pi/a_L\right)[d^2 - (d - 2t)^2] \quad (2.1)$$

where t is the bilayer thickness, d is the hydrodynamic diameter, and a_L is the average head group area per lipid. The bilayer thickness and average head group area of a POPG lipid is taken as 36 Å and 63 $Å^2$ respectively [149]. Liposome concentration in solution is calculated by dividing the lipid concentration by N_{tot}.

$N_{tot}= (\pi/63) \times [200^2 - (200 – 2\times3.6)^2]$ or 141 lipid molecules

Assuming a ~200 nm diameter POPG liposome, for 50 μM lipid, the liposome concentration is calculated to be ~ 350 nano Molar.

2.2.1.1 Preparation of pluronic polymer containing POPG liposomes

Liposomes containing various polymers (F-127, F-68 and L61) are prepared by two methods [150]. In the first method, required amount of the respective polymer is added to pre-formed liposomes, followed by incubation at room temperature for 1 hr. This in-

cubation time is chosen to ensure sufficient interaction between the polymer and the liposome. This interaction leads to insertion of the hydrophobic part (PO unit) of the polymer inside the bilayer while the hydrophilic parts (EO unit) remains outside the bilayer facing the solvent. Liposomes prepared in this manner are referred as polymer incubated liposomes [32,151]. In the second method, the required amount of the respective polymer is added directly to lipid thin film and then liposomes are prepared as described section 2.2.1. Liposomes prepared by this manner are referred as polymer incorporated liposomes. Addition of pluronic polymers during the preparation of liposomes ensures that the hydrophobic propylene oxide (PO) units of the polymer span the bilayer [152].

2.2.1.2 Preparation of sterol incorporated POPG liposomes

Ergosterol or Cholesterol incorporated POPG liposomes are prepared as follows. The stock solutions of ergosterol (0.1 M), cholesterol (0.1 M) and POPG (0.1 M) are prepared in chloroform. An aliquot of POPG solution (14 mL) is thoroughly mixed with 6 mL of either 0.1 M ergosterol or cholesterol. The solvent is evaporated completely under reduced pressure using the rotary evaporator. The dry lipid film is hydrated by adding appropriate buffer solution of desired pH. Subsequently liposome suspension is passed through cellulose-acetate membrane filters (0.45 μm and 0.20 μm) for 10-15 times to produce unilamellar POPG liposomes containing 30 mol % of either ergosterol or cholesterol.

2.2.1.3 Preparation of bile salts incubated POPG liposomes

Bile salts incubated POPG liposomes are prepared as follows. The stock solution of each bile salt (100 mM) is prepared in phosphate buffer pH 7.4. The stock solution of POPG (0.1 M) is prepared in chloroform. POPG liposomes are prepared fresh as de-

scribed in section 2.2.1. An aliquot of bile salt solution is added to pre-formed POPG liposomes followed by incubation at room temperature for 1 hr to ensure sufficient interaction time between the bile salts and the liposomes.

2.3 Characterization of liposomes

The prepared liposomes are characterized by size and zeta potential measurements using a Brookhaven 90 Plus size and zeta potential analyzer.

2.3.1 Measurement of the size of liposomes

Dynamic light scattering (DLS) also known as photon correlation spectroscopy (PCS) which is mostly used a noninvasive technique for measurement of the size and zeta potential of particles in suspension. The hydrodynamic radius and polydispersity index are calculated by DLS technique. The fundamental light source is 635 nm wavelength of solid state diode laser. The light passed through liposomes and scattered light from sample is collected at the right angle with respect to the incident light. The principle of technique is particles bombardment with surrounding molecules move randomly in suspension then particles in suspension undergoing Brownian motion. The speed of particles (translational diffusion coefficient, D) is calculated using the Stokes-Einstein equation.

$$D_T = \frac{k_B T}{6\pi\eta R_H} \tag{2.2}$$

where, D_T represents the translational diffusion coefficient, K_B is the Boltzmann constant, T is absolute temperature in Kelvin, η is the viscosity of the solvent and R_H is the hydrodynamics radius of the liposome.

From the Stokes-Einstein equation, the translational diffusion coefficient (D) of liposome correlated to the hydrodynamic radius of liposome which can be converted into size of liposome. The particle size depends upon the time dependent fluctuations in the intensity of the scattered light [153]. It means that large size of particles diffuse slower than small size particles. The measurements of the particle size measure in the range ~1 nm to ~6 μm with precision of 1%.

2.3.2 Measurement of zeta potential of liposomes

The zeta potential is the electric potential difference developed at the interface between a solid surface and its liquid medium. The magnitude of the zeta potential gives knowledge of the potential stability of the colloidal system. Higher value of zeta potential is considered as an indication of more stable colloidal system. The zeta potential is a quantity (expressed in mV) calculated from the electrophoretic mobility of the micro particle travel under an applied field [154]. Zeta potential directly cannot be measured. It is estimated experimentally by using some theoretical models, based on electrophoretic mobility. When an electric field is applied across a sample of liposome solution, the charge on liposome attracts towards opposite charge of the electrode. Simultaneously the viscous forces acting on the liposomes tend to oppose this movement. The constant speed of liposomes is attained due to once equilibrium between these two opposing forces. The velocity of the particle depends on the parameters such as the strength of electric field, the dielectric constant of the medium, and the viscosity of the medium. The velocity of the particle in a unit electric field is referred as its electrophoretic mobility. The zeta potential is correlated to the electrophoretic mobility which is derived by the Henry's equation (2. 2) using some approximations [155].

$$U_E = \frac{2 \in z\, f\, (ka)}{3\eta} \tag{2.3}$$

where, U_E is the electrophoretic mobility, z is the zeta potential, ε dielectric constant, η is the viscosity and f (ka) is the Henry's function. The zeta potential of suspension was measured from -150 mV to +150 mV (accuracy ± 2 mV).

Table 2.1*: *Size and zeta potential of POPG liposomes either incorporated or incubated with pluronic polymers and plain POPG liposomes at pH 7.4

Liposome system	Effective diameter (nm)	Zeta potential (mV)	Polydispersity
POPG only	185 ± 20	-78 ± 13	0.156 ± 0.009
POPG+ 0.5 µM F-127 (incorporated)	170 ± 23	-94 ± 11	0.150 ± 0.008
POPG+ 0.5 µM F-127 (incubated)	190 ± 18	-84 ± 17	0.174 ± 0.007
POPG+ 1 µM L-61 (incorporated)	195 ± 22	-95 ± 15	0.171 ± 0.008
POPG+ 1 µM L-61 (incubated)	194 ± 19	-84 ± 12	0.189 ± 0.006
POPG+ 5 µM F-68 (incorporated)	198 ± 25	-96 ± 20	0.165 ± 0.009
POPG+ 5 µM F-68 (incubated)	193 ± 17	-75 ± 10	0.185 ± 0.008

For studies carried out in Chapter 3, unilamellar POPG liposomes containing various pluronic polymers are used. The size, polydispersity and zeta potential of the plain liposomes and liposomes either incorporated or incubated with different pluronic polymers are given in Table 2.1

For studies carried out in Chapter 4, ergosterol and cholesterol incorporated unilamellar POPG liposomes are used. The size, polydispersity and zeta potential of the sterols containing POPG liposomes at different pH is given in Table 2.2.

Table 2.2: Size and zeta potential of POPG liposomes ergosterol and cholesterol incorporated POPG liposomes and plain POPG liposomes at different pH.

Liposome system	pH	Effective diameter (nm)	Zeta potential (mV)	Polydispersity
POPG only	7.4	178 ± 21	-90 ± 10	0.135 ± 0.008
POPG-Ergosterol	7.4	184 ± 18	-89 ± 12	0.147 ± 0.006
POPG-Cholesterol	7.4	177 ± 23	-84 ± 11	0.171 ± 0.008
POPG only	4.5	172 ± 26	-86 ± 15	0.133 ± 0.009
POPG-Ergosterol	4.5	181 ± 22	-76 ± 12	0.145 ± 0.007
POPG-Cholesterol	4.5	176 ± 26	-74 ± 16	0.134 ± 0.008
POPG only	11.0	175 ± 23	-93 ± 18	0.151 ± 0.007
POPG-Ergosterol	11.0	179 ± 16	-88 ± 14	0.142 ± 0.008
POPG-Cholesterol	11.0	172 ± 19	-90 ± 11	0.157 ± 0.007

For studies carried out in Chapter 5, unilamellar POPG liposomes incubated with four different bile salts are used.The size, polydispersity and zeta potential of POPG liposomes incubated with four different bile salts at two different pH is given in Table 2.3: The pH selected corresponds to pK_a of individual bile salt where first pH = pK_a + 1 and second pH = pK_a -1. The final concentration of both POPG and bile salt in liposomes is lipid 50 μM.

Table 2.3: Size and zeta potential of POPG liposomes incubated with four different bile salts at two different pH.

Liposome system	pH	Size (nm)	Zeta potential (mV)	Polydispersity
POPG Only	pH:4-8	180 ± 20	-84 ± 10 to-90 ± 10	0.146 ± 0.008
POPG + NaC	pKa-1	185 ± 17	-83 ± 15	0.150 ± 0.009
	pKa+1	208 ± 11	-78 ± 17	0.166 ± 0.008
POPG + NaDC	pKa-1	179 ± 18	-80 ± 19	0.159 ± 0.007
	pKa+1	207 ± 15	-69 ± 15	0.160 ± 0.008
POPG + NaGDC	pKa-1	162 ± 20	-93 ± 11	0.172 ± 0.009
	pKa+1	210 ± 16	-80 ± 13	0.169 ± 0.007
POPG + UDCA	pKa-1	188 ± 13	-75 ± 16	0.156 ± 0.008

2.4 Spectroscopic techniques

2.4.1 UV-Visible spectroscopy

UV-Visible spectroscopy is one of the most commonly used spectroscopic techniques by chemists and biologist. The basic principle of UV-Visible spectroscopy is to measure how much light is absorbed by a sample, to obtain qualitative and quantitative information regarding the ground state of an absorbing species and many physical and chemical processes [156–159] . The Beer-Lambert's law states that when a monochromatic light passes through a homogenous sample solution in a cell, the intensity of the transmitted light is directly proportional to product of concentration of the solution and the thickness of the solution at a particular wavelength λ. Absorbance also called as the optical density of the material. The Beer-Lambert's law writes mathematically given below.

$$log_{10}\left(\frac{I_0}{I}\right) = A = \varepsilon\, c\, l \qquad (2.4)$$

Where, I_0 *is* intensity of the incident light, I is intensity of transmitted light, A is Absorbance, ε is molar absorbance or absorption coefficient (in $dm^3\ mol^{-1}\ cm^{-1}$ units), *c* is concentration of the compound in the solution (in mol dm^{-3} units), and *l* is thickness of the sample (in cm units).

UV-Visible absorption spectrometer (duel beam, Model Cintra 20, GBC Scientific Equipment Ltd, Australia) is used for measurements of the steady state absorption spectra of the samples. This instrument contains dual light sources, for a visible region (35 W tungsten-halogen lamp) and UV region (30 W deuterium lamp). This instrument can be measured absorption spectrum of full wavelength scan range from 190 nm to 900 nm. Two light sources automatically work for selected wavelength range. The Czerny-Turner model monochromators with holographic grating determines the wavelength resolution which is ± 0.2 nm. Spectral band pass from 0.2 to 5 nm with increment of 0.1 nm changes by variable slit widths. The photomultiplier tube (PMT) which works as the detector in spectrophotometer. The quartz cuvette having path length of 1 cm is used for measurements of the absorbance of the sample.

2.4.2 Fluorescence spectroscopy

Fluorescence spectroscopy is widely used for the study of luminescence of biological, chemical and analytical samples. The basic principle of fluorescence is that the molecule in the ground electronic state upon absorption of photon of suitable energy within 10^{-15} seconds goes to a higher singlet excited state, then the excited state molecule returns to ground state by various processes, such as radiative or different non-radiative processes. The emission of light from any substances is called as luminescence. The process of luminescence is classified based on the nature of the excited state, which is

either fluorescence or phosphorescence. Fluorescence emission results from a thermally equilibrated excited state, that is, the lowest energy vibrational state of S_1 returns to a higher excited vibrational ground state level, S_0 of the molecule which then quickly reaches thermal equilibrium. Depending on relaxation dynamics, the important information of the molecule can be obtained such as the energy, polarity, lifetime, and radiative and non-radiative decay rates of the emitting state by the detection of these emitting photons. The radiative decay emits a photon while non-radiative decay through thermal energy transfer, collision quenching etc. [156,157,160]. A fluorescence emission spectrum of fluorophore is a plot of the fluorescence intensity of fluorophore versus wavelength (nm) or wave number (cm^{-1}). The phenomena of the absorption of energy and emission of light by various processes are usually illustrated by the Jablonski diagram. A schematic Jablonski diagram shows various processes before and after absorbing of light by a molecule is shown in the figure 2.3. The singlet ground, first, second and triplet electronic states are represented by S_0, S_1, S_2, and T_1 respectively.

The steady state emission measurements are performed by spectrofluorimeter (Model Spex Fluorolog 2, Horiba Jobin Yvon Inc. U.S.A.). It contains a 450 W xenon CW lamp works as steady state excitation light source in the spectrofluorimeter that generates a continuum output of wavelength range from 240 nm to 600 nm. The fluorophore in a sample upon excitation by the excitation light source emits a photon that passes through the emission monochromator which is placed at right angle with respect to the excitation source in order to avoid the detection of stray light by the photomultiplier tube. The experiments are carried out at constant temperature with help of temperature controller that is connected with the sample holder. The resolution in wavelength and intensity of

light are controlled by the entrance and exit slit (placed before each monochromator) widths. The PMT sensitivity for photon detection range starts from 250 to 850 nm.

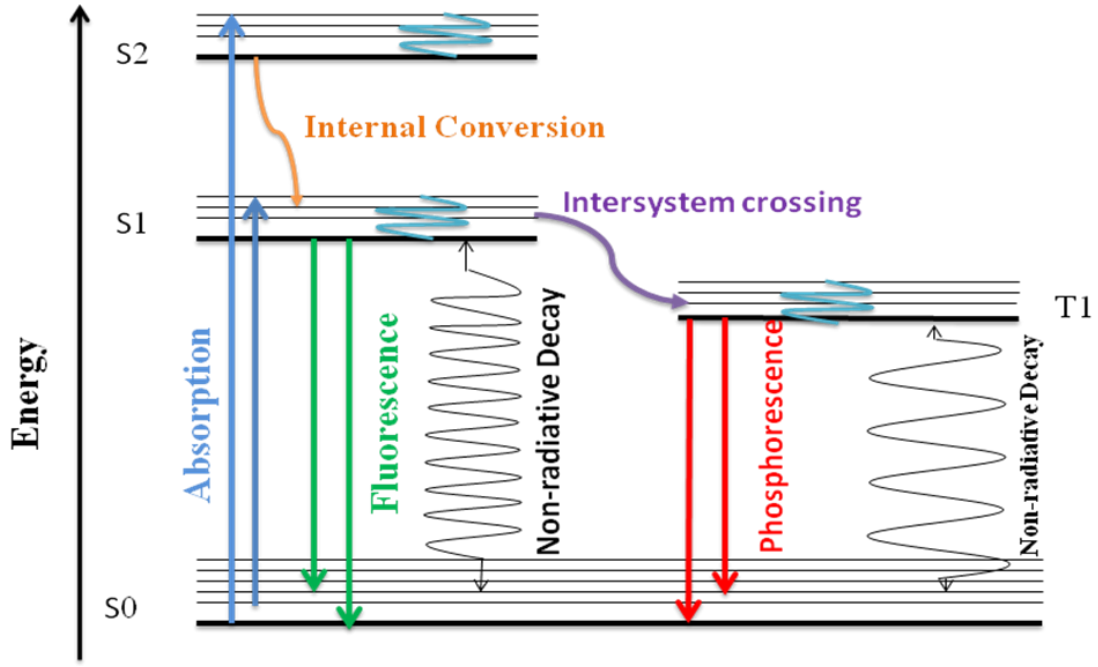

Figure 2.3: Schematic Jablonski diagram for a molecule.

The emission spectrum of a sample is recorded at fixed excitation wavelength (λ_{ex}) by scanning the require range of wavelength with help of the emission monochromator. Similarly, the excitation spectrum scan is performed by the excitation monochromator at constant emission wavelength (λ_{em}).

2.4.3 Fluorescence lifetime measurements

The fluorescence lifetime measurements are performed by the time correlated single photon counting (TCSPC) technique in the range of nanosecond to picosecond time scale [161–163]. The schematic block diagram of a TCSPC system is shown in Figure 2.4. Mode-locked femtosecond (fs) laser with high repetition rate is used as excitation light source for the TCSPC instrument. The laser pulse is split using a mirror and one of

the beams is used to excite the sample while another pulse is directed towards the photodiode detector as reference. The generated signal from photo diode is passed through a constant fraction discriminator (CFD), the working function of CFD is measured by the arrival time of the pulse accurately and generated electrical signal is passed to the time-to-amplitude converter (TAC) module, referred as START pulse. As the start pulse reach at TAC and generate a voltage ramp which linearly increases with time. In the meantime, the emitted photon from a fluorophore detected by MCP-PMT detector passe through CFD which is considered as STOP pulse to TAC. The function of TAC is to generate a voltage ramp which is proportional to time delay during the START and STOP pulse. The voltage is converted to a numerical value by Analog-to-Digital Converter (ADC). Finally a histogram is constructed which is the distribution of the counts against the channel number in MCA. Histogram provides information about the measured fluorescence intensity decay of the sample with time.

The measured fluorescence decay data are convoluted with the instrument response function (IRF) of the TCSPC system. IRF indicates the minimum time that can be measured by the instrument. It is considered to be the dead time of the TCSPC. The measurement is performed for IRF, first of all removing emission filters then the non-fluorescent scattering sample is placed in sample holder and collected signal is detected by the PMT. The intrinsic emission decay kinetics is deconvoluted from the IRF by applying iterative method. To minimize the pulse pile-up error, the sample concentration should be low and low pulse energy is recommended.The emission lifetime measurements are performed with the TCSPC system (Model: Lifespec-RED, Edinburgh Instruments Ltd, U.K.). The excitation light source is second harmonic output of a Ti-sapphire (Coherent Mira) laser pumped by Nd-YAG (532 nm, Coherent Verdi 5W) la-

ser. The pulse width of laser is (~150 fs). The repetation rate of the tunable Ti-sapphire laser is reduced to 3.8 MHz using a pulse picker (Coherent model 9200). The fluorescence signal is collected at right angle with respect to theexcitation source. An emission polarizer is placed before the collection optics and the fluorescence life time are measured at the magic angle 54.7° to the excitation light source. To minimize scatter light from the sample an appropriate emission filters is placed before the detector. The fluorescence emission photon from the sample is detected using a thermoelectric cooled micro channel plate (MCP)-PMT detector (Model: R3809U-50, Hamamatsu, Japan). The instrument response function (IRF) of the MCP-PMT detector is ~50 ps. The fluorescence decays are convoluted with the IRF, the data which decovoluted from IRF by iterativemethod software provided by the manufacture, it works based on global least squares analysis algorithm. The measured decays are fitted to whether single or multi exponential dacay functions are shown in the equation 2.5.

$$I\,(t) = \sum_{i}^{n} a_i \;\; exp^{-\left(\frac{t}{\tau_i}\right)} \qquad (2.5)$$

In this expression τ_i are the fluoresecnce decay life times, a_i represents the pre-exponential factor of the i^{th} components at t=0, and n is the number of the flurosencnce dacay life times. The lifetime values obtained from fitted data is confirmed by the goodness-of-fit parameters such as weighted residuals randomly distributed around zero line and reduced chi-square value near to 1.0 [164].

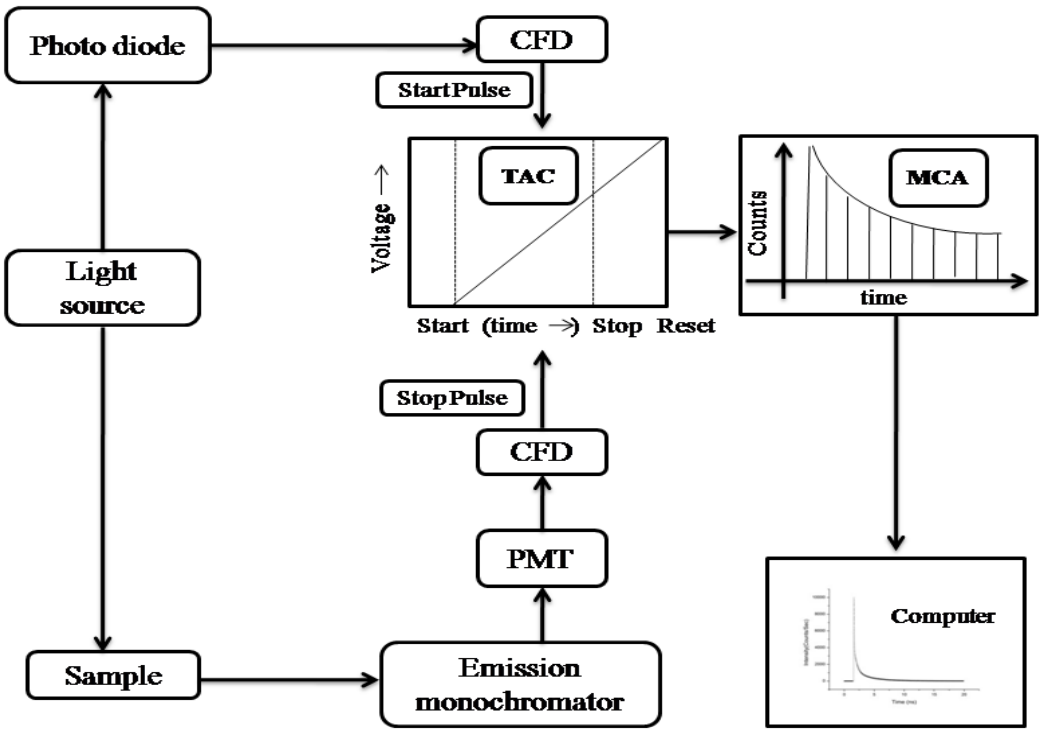

Figure 2.4: A schematic block diagram of various electronic parts of TCSPC instrument.

2.5 Measurements of SHG

2.5.1 Experimental setup

The second harmonic (SH) spectroscopy is used for monitoring the transport of molecules or ions across the lipid membranes in real-time using TCSPC system (Model Lifespec Red, Edinburgh Instruments Ltd, U.K.). The schematic diagram of the experimental setup of the SH technique is shown in Figure 2.5. The excitation source for SHG studies is the quasi-CW output of a Ti-sapphire (Coherent Mira) laser pumped by Nd-YAG (532 nm, Coherent Verdi 5W) laser. The quasi-CW output of a Ti-sapphire laser is tunable from 780 to 850 nm and generates femto second pulses at a repetition rate of 82 MHz. The Full Width at Half Maximum (FWHM) of the pulse of the laser is ~150 fs at

this range of wavelength as certified by the supplier. The high peak power laser is necessary for the nonlinear optical process to be efficient and generates femto second pulse. The SHG signal of SH probe-liposomes solution is quadratically dependent on the intensity of the incident of laser light. All SH measurements are carried out at the average laser power of 500 mW. The polarization of the laser pulse is fixed by using a half wave plate (HWP) in the vertical plane. The fundamental laser beam passes through a convex lens which has the focal length of 10 cm.

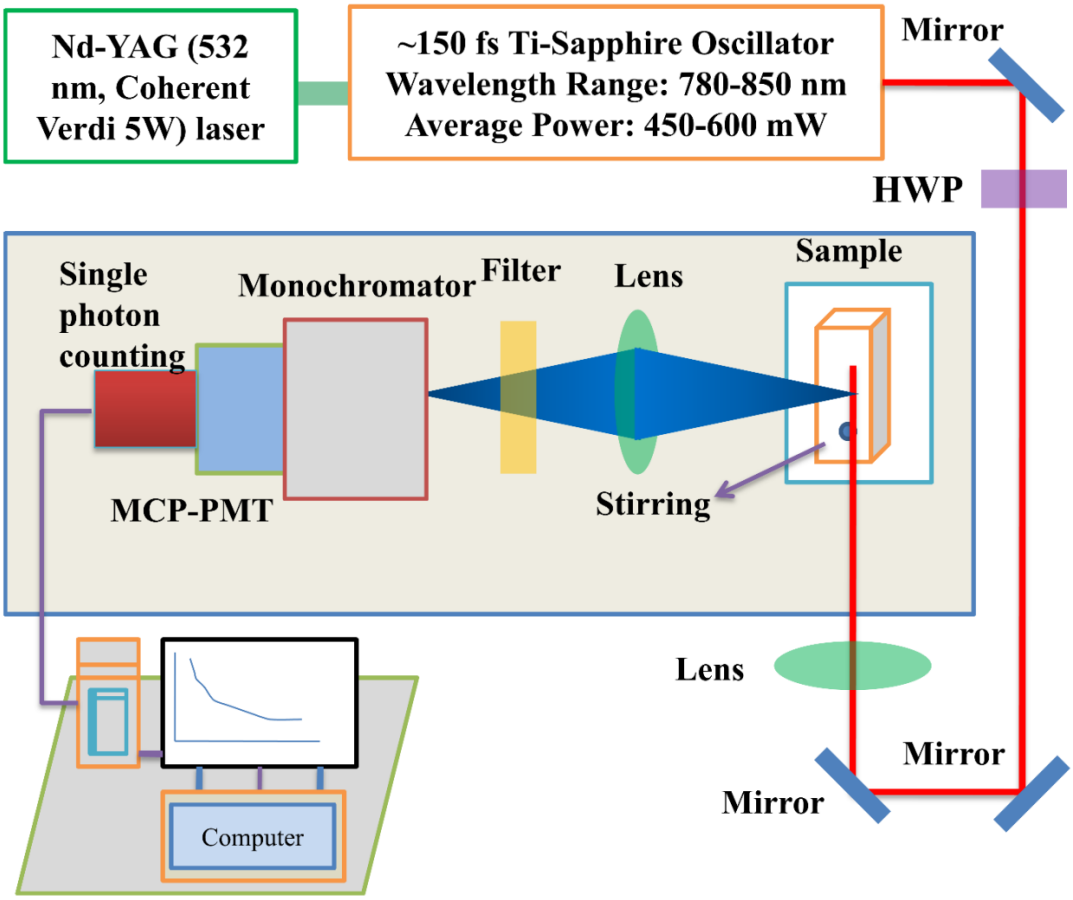

Figure 2.5: A schematic block diagram of the SH experimental set up. It is used to measure HRS and SH signals.

The focused laser light falls on the sample, excites the sample and the generated SH signal passes throgh a band pass filter placed before the monochromator of the TCSPC sys-

tem to avoid fundamental light and other source of light. The wavelength resolution of monochromator is 2 nm. The SH signal is collected at right angle with respect to the laser beam (800 nm) and The generated SH signal is detected in the transmitted direction using a cooled MCP-PMT (Hamamatsu, Japan). After detecting the SH signal proceeds through single photon counting technique. Here, the TAC does not require for collecting SHG signal. The integration time of SH signal is one second.

2.5.2 The SH probe: LDS-698

Most of earlier SHG studies have been carried out with the organic cation, Malachite green (MG) as a SH probe. It works at only acidic pH as the SH probe but loses its positive charge at neutral pH (becomes a neutral molecule), as a result loses its non-linear characteristics at neutral and basic pH. A suitable molecule that should work as SH probe at wide range of pH is necessary to findout. The family of hemicayanine dyes having strong hyperpolarizability values are being considered for SH probe [165–168]. A hemicayanine dye (LDS-698), has sufficient absorption at the SH wavelength of a Ti-sapphire laser. Das and co-workers have previously shown that LDS^+ ion act as suitable SH probe at wide range of pH [169]. The chemical structure of the LDS-698 is shown in the figure 2.6.

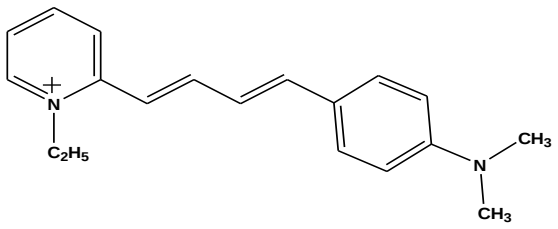

Figure 2.6: Chemical structure of the LDS-698.

2.5.3 The procedure for SH experiments

The procedure for conducting SH experiments is as follows. Initially 2 mL buffer solution is added in cuvette and the SH is recorded for a few seconds as a base level. Now aliquot of SH Probe (LDS^+) is added to the buffer solution and recording of SH signal is continued for another few seconds. The signal is slightly increased above the base level due to hyper-Rayleigh scattering (HRS) from the LDS^+ ions. Subsequently the liposome suspension (100 μL) is added into the solution in the cuvette. There is an instantaneous increase in SH intensity due to the electrostatic adsorption of positively charged LDS^+ ions onto a negatively charged outer surface of lipid bilayer of POPG liposomes. The SH signal from the sample starts decay with time which indicates that the transport of LDS^+ ions from the outer lipid bilayer to inner lipid bilayer of POPG liposomes. The experiment is stopped when there is no change in SH decay with time. A typical SH intensity decay profile of LDS^+ions across the POPG liposome in pH 7.4 buffer with time at room temperature is shown in the figure 2.7.

The sample temperature is controlled by a Neslab (JULABO Labortechnik GmbH, Germany) circulating water chiller having a temperature accuracy of ± 1 ^{0}C. The sample solution is constantly stirred with a magnetic stirrer to avoid photo bleaching of the sample due to high peak power laser as excitation source. The SH intensity decay data are first converted to the SH electric field then the data are fitted with the exponential decay functions. Finally, the transport time constants ((τ_{av}; where, $\tau_{av} = a_1\tau_1 + a_2\tau_2$) can be extracted by fitting of the SH electric field traces following the liposome solution addition to the buffer containing the LDS^+ solution with the exponential decay functions. The observed bi-exponential decays of $E_{2\omega}$ could arise due to initial rapid transport of the cation from the outer bilayer to the inner bilayer (~100 seconds). As the inner bi-

layer gets populated with the LDS^+ ions, the potential difference decreases which causes the transport rate of the LDS^+ ions to be slower (~1000 seconds). It is clearly observed that the SH intensity decay profile does not reach to zero. It means the adsorbed sites on the lipid bilayer is quite difference in both inner and outer surface of lipid bilayer. Because of the surface area of inner lipid bilayer is smaller than the outer lipid bilayer and potential difference also. And the second harmonic signal approaches a steady state value at long times that is determined by the balance between the electrostatic forces and the chemical concentration gradient.

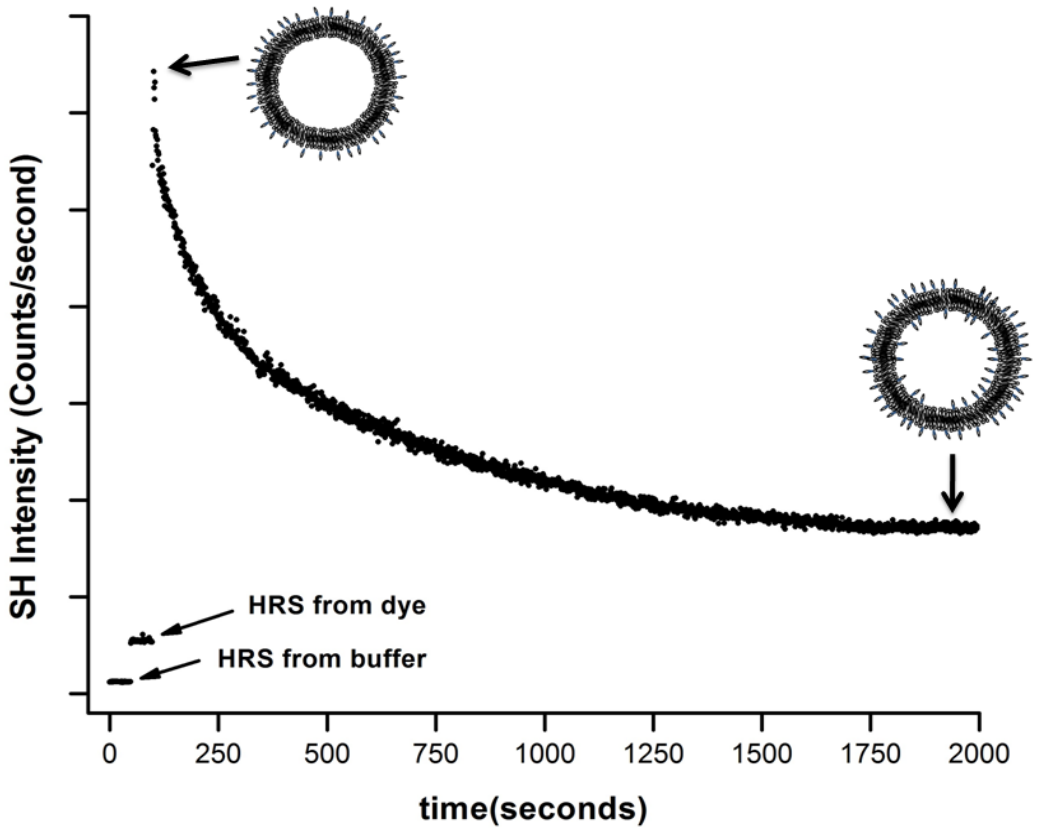

Figure 2.7: A typical SH decay profile of LDS^+ across a lipid bilayer monitored in real time.

Chapter 3

Effect of Three Pluronic Polymers on the Transport of an Organic Cation, LDS^+ ions Across a POPG Bilayer Studied by Second Harmonic Spectroscopy

3.1 Introduction

Pluronic polymers are neutral, nonionic amphiphilic triblock copolymers. The general chemical structure of pluronic polymers is EO_n-PO_m-EO_n. The hydrophilic poly-ethylene oxide (PEO) parts are located at the beginning and at end of the polymer, while the hydrophobic poly-propylene oxide (PPO) part is located in the middle of the polymer. Pluronic polymers are one among the important class of compounds for pharmaceutical and bio-medical applications [19]. These polymers play a significant role in drug formulation, drug delivery systems, tumor therapy, DNA transfection, chemo-sensitizing agents and healing of injured cell membranes etc. [20]. This can be attributed to specific interactions between polymers and biological membranes. These interactions are important for regulating transport of molecules across the membranes. Hence, it is necessary to understand the interaction between polymers and membrane systems [29,170,171]. During the past few decades, several studies have been performed to characterize the polymer-membrane interactions by both experimental and theoretical methods [29,30-35,170–195]. The fluorescence spectroscopic and microscopic studies have suggested that pluronic polymers affect membrane organization. This implies that the membrane permeability depends on the chemical architecture of polymer [29,30,172–178,180,187,188,192]. As we know, the pluronic polymer consists of both hydrophobic

as well as hydrophilic part in which the hydrophobic (PO) part of the polymer insertion into the membrane is another topic. The effect of hydrophobic and hydrophilic units of pluronic polymers on membrane systems are studied using experimental [31,32,176,177,181,184–186] and theoretical [34,35,190–195] techniques. Based on all these studies, it is concluded that the number of hydrophobic (EO) and hydrophilic (PO) segments present in the polymers play a significant role in the interaction of pluronic polymers with artificial and natural membranes. This indicates that the changes in membrane permeability depend on the composition of hydrophobic and hydrophilic units of pluronic polymer.

In this work, we investigate the effect of lengths of the hydrophobic PO units and hydrophilic EO units of pluronic polymers on the bilayer permeability of the negatively charged L-α Phosphatidyl DL-Glycerol (POPG) liposomes. The transport properties of an organic cation (LDS-698) across a POPG bilayer with and without pluronic polymers have been studied by the interfacial selective second harmonic (SH) spectroscopic technique. Three different pluronic polymers are used for all the SH studies. The chemical formula of each pluronic polymer is: F-127 (EO_{100} PO_{65} EO_{100}), L-61 (EO_2 PO_{30} EO_2), and F-68 (EO_{76} PO_{30} EO_{76}). The SH technique is advantageous as it can monitor the transport of amphiphilic molecules across a lipid bilayer (liposome) in real time. The transport of molecules across the bilayer can be monitored by SHG process in real time is briefly described as follows: The principle of this technique lies on the fact that the SH probe (LDS^+) molecules are adsorbed on the outer surface of the liposome and the orientations of adsorbed molecules on liposome are in preferred way in the interfacial region. The distance between adsorbed molecules on outer surface of liposome is separated by the diameter of the liposome. Two oppositely oriented

molecules on outer surface of liposome generate the SH electric field which will be added coherently when the generated SH electric fields are in phase. The necessary and sufficient condition for coherent addition of electric fields is comparable in size of liposomes and of the order of the wavelength of the incident radiation (~800 nm). In contrast, molecules which are present in bulk aqueous solution cannot contribute to coherent SH signal because of random orientation but they can generate incoherent SH signal called as hyper-Rayleigh scattering (HRS).

3.2 Results

Spherical shaped liposomes from POPG lipid in 10 mM of phosphate buffer solution having a pH of 7.4 are prepared according to procedure mentioned in Chapter 2. Liposomes containing various polymers (F-127, F-68 and L61) are prepared by two methods: In the first method, required amount of the respective polymer is added to pre-formed liposomes, followed by incubation at room temperature for 1 hr. This incubation time is chosen to ensure sufficient interaction between the polymer and the liposome. This interaction leads to the insertion of the hydrophobic part (PO unit) of polymer inside the bilayer, while the hydrophilic parts (EO unit) are exposed to the aqueous buffer medium. Liposomes prepared in this manner are referred to as “polymer incubation liposomes”. In the second method, the required amount of the respective polymer is added directly to the lipid thin film and then liposomes are prepared as described section 2.2.1. Liposomes prepared in this manner are referred to as “polymer incorporation liposomes”. Addition of polymers during the preparation of liposomes ensures that the hydrophobic poly-propylene oxide units of the polymer span the bilayer. The first and second methods are referred as “incubated” and “incorporated” throughout this work. The polymers containing liposomes are prepared by the above

two methods which are used for all the SH experiments. The chemical formula, HLB, CMC values of the three pluronic polymers used in this study are presented in Table 3.1. The composition of hydrophobic and hydrophilic units of three polymers are described here. The number of propylene oxide (PO) units are similar in case of L-61 and F-68 polymers but they differ in ethylene oxide (EO) units. Whereas, the number of propylene oxide (PO) units significantly differ in F-68 and F-127 polymers but more-or-less equal number of EO units.

Table 3.1: The chemical formula, HLB, CMC, and other properties of pluronic block copolymers.

Pluronic polymer	**Chemical formula**	**[182]HLB**	**[182]CMC**	**[190]Log K_p (water/hexane)**
L-61	$EO_2 PO_{30} EO_2$	3	1.1×10^{-4}	-0.24 ± 0.037
F-68	$EO_{76} PO_{30} EO_{76}$	29	4.8×10^{-4}	-3.5 ± 0.53
F-127	$EO_{100} PO_{65} EO_{100}$	22	2.8×10^{-6}	N.A.

(HLB: hydrophilic−lipophilic balance; CMC: critical micelle concentration.)

The effective diameter (the average size of liposome), zeta potential and poly-dispersity of polymer containing liposomes have been studied for polymer incubated and incorporated POPG liposomes at various lipid : polymer molar ratio. The Figure 3.1 (top panel) describes the size of liposome and polydispersity changes with the variation in polymer concentration, and bottom panel shows that zeta potential changes with the variation in polymer concentration. From Figure 3.1, it is observed that the size and zeta potential of liposomes prepared by polymer incubation/incorporation liposomes do not show any significant change with variations in concentration of polymers. This indicates stability

of liposomes (integrity of liposome) is not compromised below their CMC values of polymers. This is consistent with previous reports [31,172,179–185,187].

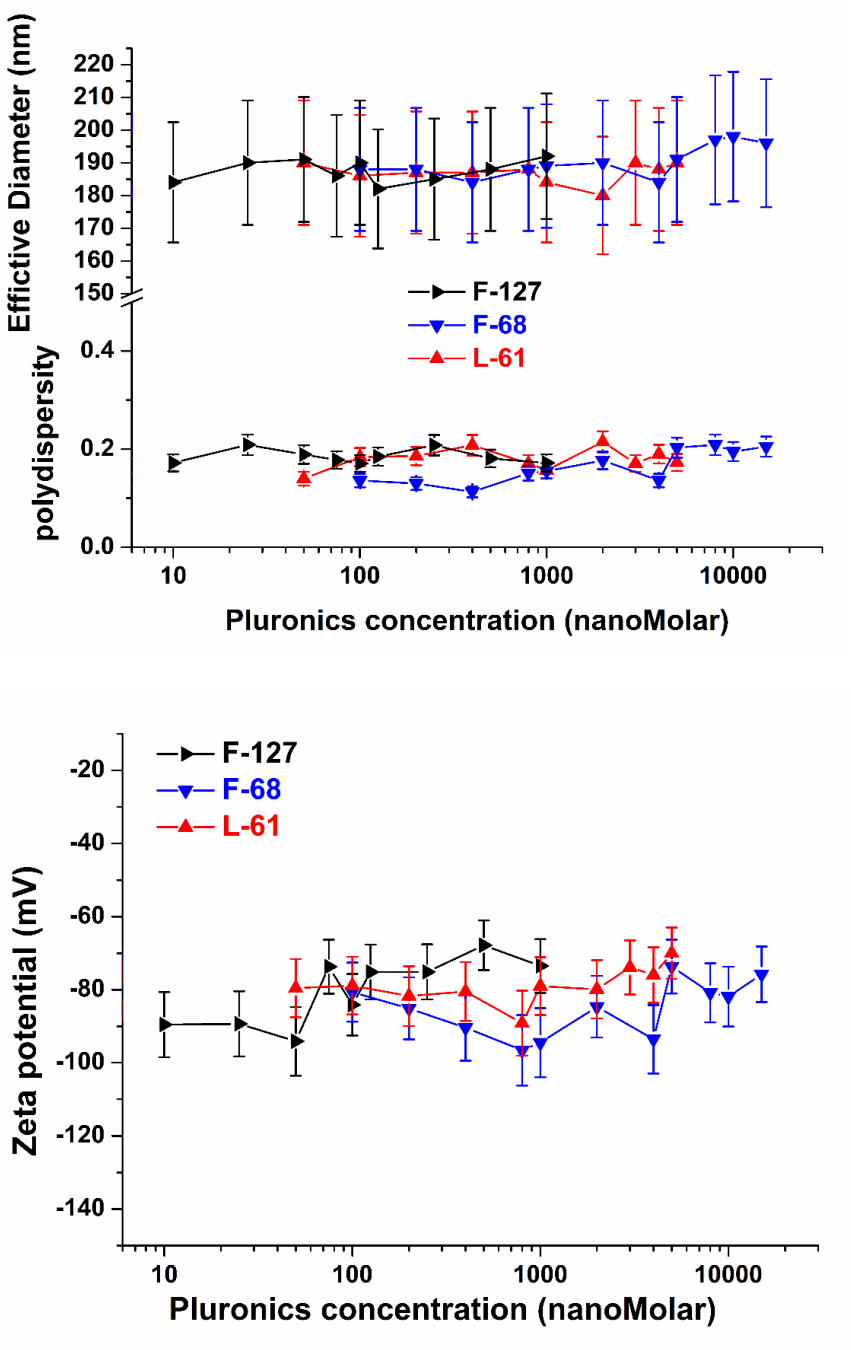

Figure 3.1: Changes in the size and polydispersity (top) and zeta potential (bottom) of pluronic polymers incubated POPG liposomes with variation in concentration of polymers. Error bar represents standard deviation of three independent measurements.

Details of the SH and hyper-Rayleigh scattering (HRS) measurements are carried out as described in Chapter 2. The SH experiments are done as per the given procedure: Here, the SH experimental procedure is briefly explained. Initially, 2 mL buffer solution is added in cuvette and the SH signal is recorded for a few seconds as a base level. Then, aliquot of SH Probe (LDS^+) is added to the buffer solution having desired pH and, recording of SH signal is continued for a few seconds. The signal is slightly increased above the base level due to HRS from the LDS^+ ions. Further, a concentration of 1 μM of the individual polymer incubated in POPG liposome suspension is added into the buffer solution having 5 μM LDS^+ ions in the cuvette. There is an instantaneous increase (< 1 second) in SH intensity due to the electrostatic adsorption of positively charged LDS^+ ions onto a negatively charged outer surface of POPG liposomes as demonstrated earlier [141]. After addition of POPG liposomes to LDS^+ solution, the generated SH electric field of ($E_{2\omega}$) of LDS^+ decreases gradually with time. This is attributed to the LDS^+ ions are passed through the lipid bilayer. It ensures that the transport process occurs in the POPG liposomes. The measured experimental data can be converted to the SH electric field and is fitted to exponential decay functions per following equation 1.12. The SH decay curves are fitted from their maximum value of the SH electric filed ($E_{2\omega}$) i.e., just after the addition of the liposomes to the buffer solution containing LDS^+ ions. The transport time constants (τ_1 and τ_2 values) are extracted by exponential fitting of the decay curves of the SH electric field of LDS^+ ions and calculated τ_{av} values.

Figure 3.2 illustrates time dependent changes in the SH electric field of LDS^+ ($E_{2\omega}$) under different liposomes systems: POPG liposomes incubated with same concentration of each pluronic polymer (F-127, F-68, and L-61). The polymer-liposomes suspension is

added to buffer solution containing the LDS^+ ions (5 µM) at 50 seconds. The experiments are performed at 25 ^{0}C. These liposomes systems are:

1. The black curve represents the SH electric field of LDS^+ ions across the POPG liposomes (control, i.e., without polymer). Similarly,

2. The red curve represents the SH electric field of LDS^+ ions across the 1 µM of F-127 polymer incubated in POPG liposomes.

3. The blue curve represents the SH electric field of LDS^+ ions across the 1 µM of F-68 polymer incubated in POPG liposomes.

4. The green curve represents the SH electric field of LDS^+ ions across the 1 µM of L-61 polymer incubated in POPG liposomes.

From Figure 3.2, it is clearly shown that the presence of pluronic polymers in POPG liposomes enhance the transport of the LDS^+ across the liposome bilayer. The fitted parameters are obtained for the decay of SH electric field of LDS^+ after addition of polymer-POPG liposomes. The τ_{av} values of LDS^+ in POPG liposomes with or without polymers are summarized in Table 3.2. The τ_{av} values of LDS^+ in POPG liposomes are found to be significantly affected in the presence of polymers.

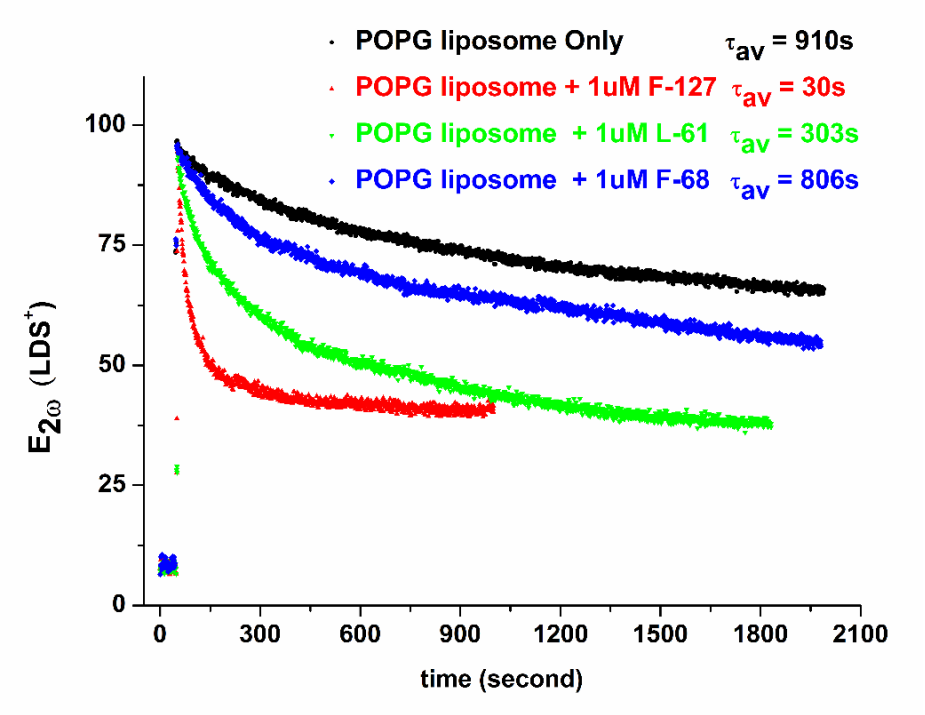

Figure 3.2: Time dependent changes in the SH electric field of LDS^+ ($E_{2\omega}$) under different liposomes systems. The liposome systems are POPG liposomes and polymer (F-127, F-68, and L-61) incubated POPG liposomes. The liposomes suspension is added to buffer solution containing the LDS^+ ions (5 µM) at 50 seconds.

***Table 3.2*: Fitted parameters are obtained for the decays of SH electric field of LDS^+ after addition of polymer-POPG liposomes.**

Liposome + Polymer (Concentration)	a_0	a_1	τ_1	a_2	τ_2	τ_{av} (sec.)
POPG liposome only	0.11	0.54	1640	0.35	83	914.6
POPG liposome + F-127 (1 µM)	0.05	0.05	183	0.90	24	30.29
POPG liposome + L-61 (1 µM)	0.15	0.36	724	0.49	82	302.82
POPG liposome + F-68 (1 µM)	0.13	0.52	1468	0.35	110	806.11

In order to understand the membrane permeability of liposome, the effect of the copolymer composition of polymer (variation in number of EO and PO units of polymer) on the transport of LDS^+ across POPG liposomes with polymers are also studied. For this,

the experiments are carried out with different concentration of individual pluronic polymer present in POPG liposomes. The selection of concentration of individual polymer is to get more or less equal to τ_{av} values of LDS^+. This gives an idea about how different copolymer composition of individual polymers affects the transport of LDS^+ in POPG liposomes.

Similar to Figure 3.2, Figure 3.3 describes time dependent changes in the SH electric field of LDS^+ ($E_{2\omega}$) under different liposomes systems. These curves represent the SH electric field of LDS^+ ions across POPG liposomes incubated with different concentration of each polymer (0.1 µM of F-127, 10 µM of F-68, and 3 µM of L-61).

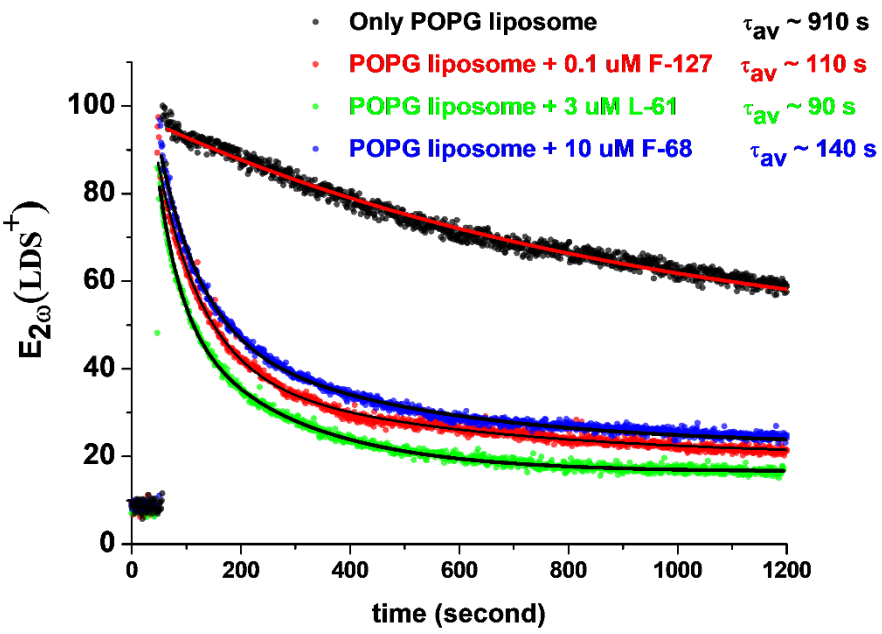

Figure 3.3*: *Time dependent changes in the SH electric field of LDS^+ ($E_{2\omega}$) under different liposomes systems: The liposome systems are POPG liposomes and the respective polymer (0.1 µM of F-127, 10 µM of F-68, and 3 µM of L-61) incubated POPG liposomes. The liposomes suspension is added to buffer solution containing LDS^+ ions (5 µM) at 50 seconds.

The fitted parameters for decay of SH electric field of LDS^+ ions are obtained in the presence of different concentration of pluronic polymers incubated in POPG liposomes. The τ_{av} values of LDS^+ ions across the POPG liposomes in the presence of each polymer are summarized in Table 3.3. The τ_{av} values of LDS^+ ions becomes ~ 9 times faster in presence of pluronic polymers present in POPG liposomes as compared to only POPG liposomes (without polymer). However, Figure 3.3 indicates that the transport of LDS^+ ions depends upon the concentration of individual polymers. The results demonstrated that the membrane permeability of POPG liposomes is severely dependent on the copolymer composition of the pluronic polymers. In order to get an idea about how the number of polymer molecules per liposome affects the transport of LDS^+ ions across the lipid bilayer, further, the experiments are carried out with variation in the number of polymer molecules per liposomes ratio (variation in polymer concentration).

Table 3.3: ***Fitted parameters for the decays of SH electric field of LDS^+ after addition of pluronic polymer in POPG liposomes.***

Liposome + Polymer (Concentration)	a_0	a_1	τ_1	a_2	τ_2	τ_{av} **(sec.)**
POPG liposome only	0.11	0.54	1640	0.35	83	914.6
POPG liposome + F-127 (0.1 µM)	0.16	0.17	578	0.67	94	105.00
POPG liposome + L-61 (3 µM)	0.11	0.28	230	0.61	43	90.75
POPG liposome + F-68 (10 µM)	0.17	0.23	400	0.60	77	140.02

Figure 3.4 describes the effect of the number of polymer molecules per liposome on the transport rate constant (k_{av} i.e. $1/\tau_{av}$) of LDS^+ in the POPG liposomes incubated with respective polymer. In Figure 3.4, both axes are kept deliberately in logarithmic scale in order to capture the entire variation in polymer concentration and k_{av} values. Out of

three pluronic polymers, the transport of LDS^+ across the POPG liposomes incubated with F-127 polymer is observed to be faster when compared to the other two polymers, L-61 and F-68. As discussed earlier, the length of the hydrophobic PO unit is the highest in F-127 (EO_{100} PO_{65} EO_{100}) whereas, in the other two polymers the length of the hydrophobic PO unit is comparatively less. Based on the results obtained, it can be speculated that the membrane permeability depends on the length of hydrophobic unit of the polymer.

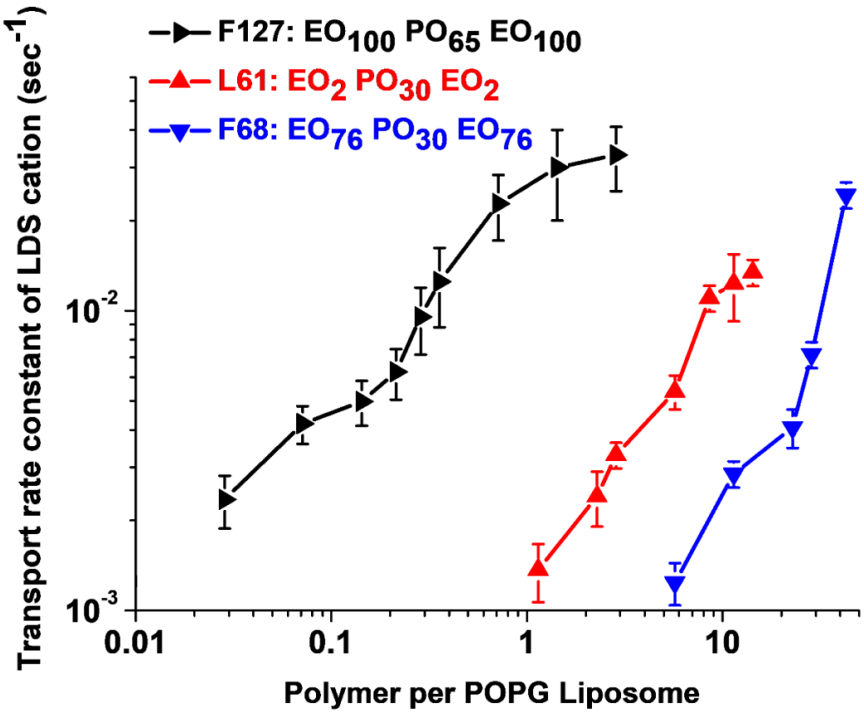

Figure 3.4: Changes in the transport rate constants (τ_{av}) of LDS^+ with number of polymer molecules per liposome (P/L) ratio for polymer incubated POPG liposomes. The line connecting the data points are only meant for guidance.

So far, the pluronic polymers incubated POPG liposomes are used for the SH studies. When the experiments are performed with polymer incubated liposomes, there might be an issue of polymer localization with respect to the lipid bilayer. To address this, we

carried out a comparative study of the transport rates of LDS^+ using two different type of liposomes which are prepared by two different methods. These are referred as polymer incubated and polymer incorporated POPG liposomes (methods of preparation are described in the Chapter 2). As discussed earlier, it is reasonable to assume that the PO unit of the polymer spans the entire bilayer in the case of polymer incorporated liposomes. In polymer incubated liposomes, the insertion of the hydrophobic (PO unit) of the polymer into the bilayer, while the hydrophilic parts (EO unit) can be accompanied by the translocation state across the bilayer. Further, variation in temperature of the system (5-45 ^{0}C) can give an idea about how the bilayer rigidity changes with temperature. Figure 3.5 describes time dependent changes in the SH electric field of LDS^+ ($E_{2\omega}$) before and after addition of either POPG liposomes or POPG liposomes incubated/incorporated with individual pluronic polymer (added at t = 50 sec.) for three different pluronic polymers (F-127, F-68, and L-61) at 10 ^{0}C and 25 ^{0}C. At 10 ^{0}C, the transport of LDS^+ in POPG liposomes or POPG liposomes incubated/incorporated with individual polymer (F-127, F-68, and L-61) is observed to be similar for all polymer-POPG systems except F-68 and F-127 incorporated POPG liposomes. The transport of LDS^+ ions is observed to be significantly faster in case of F-68 and F-127 incorporated POPG liposomes. As the temperature is increased to 25 ^{0}C, the transport of LDS^+ ions across the polymer incubated (L-61 and F-68) POPG liposomes is faster as compared to their polymer incorporated liposomes. The transport of LDS^+ ions is more or less similar for both F-127 polymer incubated and incorporated POPG liposomes.

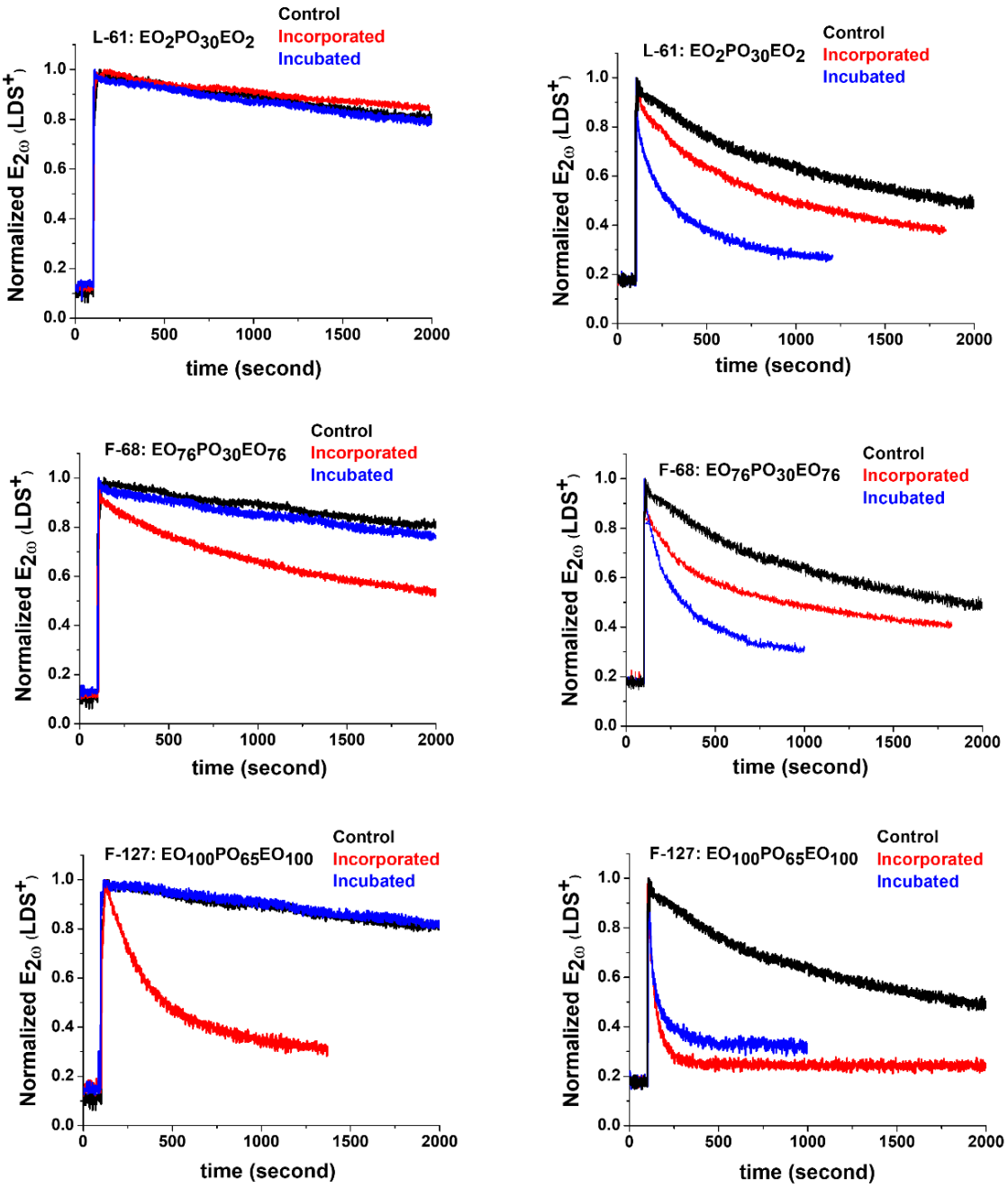

Figure 3.5: Time dependent changes in the SH electric field of LDS^+ before and after addition of either POPG liposomes or POPG liposomes incubated/incorporated with pluronic polymer (added at t = 50 sec.) for three pluronic polymers (F-127, F-68 and L-61). The experiments are performed at 10 ^{0}C (left panel) and 25 ^{0}C (right panel).

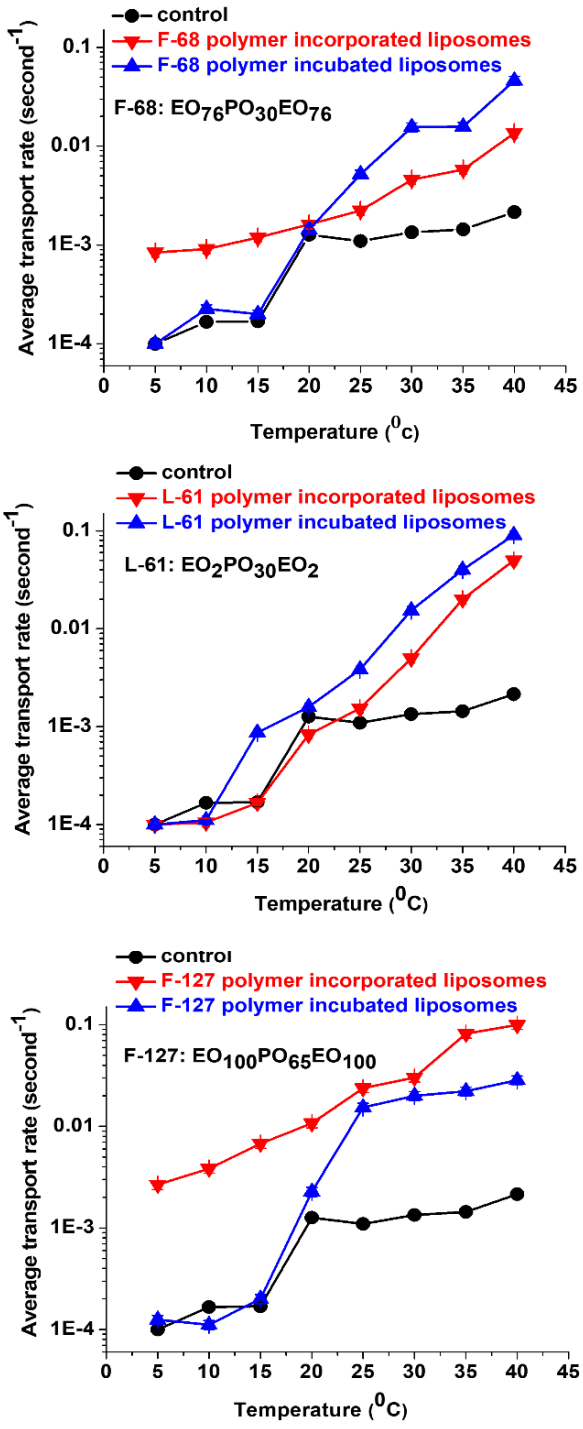

Figure 3.6: Temperature dependent changes in the transport rate constants (k_T) of the LDS^+ under different conditions: Top, middle and bottom panel represents POPG liposomes which are either incubated or incorporated with L-61, F-68 and F-127 polymers respectively. In all the panels, POPG liposomes (without polymer) are also shown for comparison.

Finally, Figure 3.6 describes temperature dependent changes in the transport rate constants (k_T) values of LDS^+ ions across POPG liposomes (control, incorporated, and incubated liposomes) for three different polymers (F-127, F-68, and L-61). In Figure 3.6, the Y-axis is kept deliberately in logarithmic scale in order to capture the entire variation in the transport rate constants. The sample temperature in the SH experiments are varied from 5 to 40 ^{0}C with increment of 5 ^{0}C. For temperature variation experiments, the sample temperature is controlled by a Neslab (JULABO Labortechnik GmbH, Germany) circulating water chiller having a temperature accuracy of ± 1 ^{0}C. The integrity of liposome may be compromised at higher temperature (> 40 ^{0}C) which limits the experimental conditions to 40 ^{0}C. Control experiment means POPG liposomes without polymer as reference.

The following observations from SH experiments can be summarized.

1. There is no significant variation in the k_T values of LDS^+ across POPG bilayer (control) till 15 ^{0}C after which is increased sharply (~10 x) and thereafter remained more or less constant.

2. As temperature is increased from 5 to 40 ^{0}C, the k_T values of LDS^+ increases monotonically with temperature in case of L-61 polymer incubated and incorporated POPG liposomes.

3. At temperature range of 5-15 ^{0}C, F-127 and F-68 polymer incorporated liposomes is observed to be substantially higher compared to their polymer incubated liposomes.

4. There is no significant variation in the k_T values of LDS^+ in case of F-127 or F-68 incubated POPG liposomes after which it increases sharply then starts to level off after 30 ^{0}C.

3.3 Discussions

The membrane permeability properties of POPG liposome bilayer altered by pluronic polymers have been studied by using the interfacial selective SH spectroscopic technique. In literature, the membrane permeability properties is studied by the lipid flip-flop rates using fluorescently labelled lipids and the trans-membrane transport of some fluorescent probes [29,172,174,175,179,180]. In one study, the adsorption of F-127 polymer (a polymer: lipid (P/L) mole ratio of 0.10) onto small unilamellar vesicles (SUVs) of egg phosphatidylcholine has released a fluorescent dye (Carboxy fluorescein) by 100 times. A similar rate of the transport of the LDS^+ ions is observed at a P/L ratio of 0.010 in this study (Figure 3.6). In another study, the permeation rate of Doxorubicin (an anti-cancer drug) across unilamellar egg phosphatidylcholine vesicle in presence of ~20 molecules of L-61 pluronic polymer per vesicle has been reported to increase threefold and the flip-flop rate of fluorescently labelled lipids increased six fold [175]. In this study, it is observed that the transport rate of LDS^+ increases ten fold in presence of ~5 molecules of L-61 polymer per liposome at room temperature. The calculation of liposomes concentration is described in Chapter 2. The results from the SH spectroscopic technique, which provides better sensitivity to probe the bilayer permeability induced by the pluronic polymers. Results presented in Figure 3.4 indicate that the permeability of POPG membrane against LDS^+ ions is critically dependent on the length of hydrophobic (PO) segment in the polymer. The chemical formula of pluronic polymers shows that the length of the hydrophobic PO unit is the highest in F-127 (EO_{100} PO_{65} EO_{100}). Whereas, it is lowest in both L-61 (EO_2 PO_{30} EO_2) and F-68 (EO_{76} PO_{30} EO_{76}). In F-127 polymer, the length of the hydrophobic PO unit is roughly twice the order of membrane thickness whereas, in L-61 and F-68 polymers this is of

the order of membrane thickness (~ 5 nm). Therefore, the results of SH spectroscopic technique have shown that the permeability of the LDS^+ ions is enhanced by the length of the hydrophobic PO unit present in these polymers. Now, comparing the results of almost similar lengths of the hydrophobic PO units (L-61 and F-68 polymers) and differences in the length of the hydrophilic (EO) unit have shown that membrane permeability increases as the length of the hydrophilic (EO) unit gets smaller. Thus, it is inferred that the hydrophilic−lipophilic balance (HLB) values get smaller. In general, HLB values determine the hydrophilic/lipophilic character of the respective polymer. These values are shown in the HLB index (Table 3.1) and are calculated by using the empirical formula: HLB = −36n / (2m + n) + 33 [196]. Where, *m* and *n* represent to the number of repeated units in the PO segment and EO segment of the polymer, respectively.

The liposome concentration is calculated to be ~350 nM as described in Chapter 2. At this point it is worthwhile to consider the number of polymer molecules present per liposome in our experimental conditions. The average transport time constants of the LDS^+ (τ_{av}) across the POPG membrane in the presence of respective polymers (0.1 µM of F-127, 3 µM of L-61, 10 µM of F-68) become ~ 9 times faster as compared to the τ_{av} values of LDS^+ for only POPG liposome. This means that ~0.3 molecules of F-127, ~9.0 molecules of L-61, and ~ 29.0 molecules of F-68 polymers are available per liposome. Thus, F-127 polymer significantly affects the τ_{av} values of LDS^+ (Figure 3.3). At this point, it is also worthwhile to consider the partition co-efficient ($Log\ K_{p\ water\text{-}hexane}$) of the individual polymers. This decides how many polymer molecules are *adsorbed* per liposome. As expected, the actual number of polymer molecules adsorbed on the surface of an individual liposome will be less than the number of polymer molecules added to the liposome solution. Further, from Table 3.1, the $Log\ K_p$ values of polymers indicate that

more number of L-61 polymer molecules can be adsorbed on the surface of liposome compared to F-68 and F-127. It is reasonable to expect that the membrane permeability depends on the mobility of lipids constituting the membrane. Therefore, in presence of pluronic polymers, the enhanced mobility of the membrane components may originate from two mechanisms: 1) Either the global mobility of all the lipid constituents or 2) the formation of small patches on the surface of the membrane where polymers get adsorbed onto the surface of liposome. These mechanisms increase the mobility of membrane components drastically. It is difficult to assume that presence of $\backsim$10 molecules or less pluronic polymer molecules per liposome would affect the global mobility of the lipids constituting the liposome. This is inferred as the size of the liposome does not alter at all the pluronic concentrations used in this study (Figure 3.1). The mobility of the lipid constitutents of membrane gets compromised at the locations where the polymers are adsorbed onto the surface of liposome. In F-127 polymer, the length of the hydrophobic PO unit is twice the order of membrane thickness (~ 5 nm). The insertion of large hydrophobic PO units of F-127 polymer molecule in the hydrophobic region of lipid bilayer affects the region severely. We propose that the cause of the membrane permeability of the LDS^+ across the membrane containing pluronic polymers is due to the formation of localized "highly mobile" areas. A similar type of hypothesis has already been proposed earlier [175]. It might be noted that several molecular dynamics (MD) simulation studies are performed under equilibrium conditions. The final conclusion from these studies show that the hydrophobic PO segment of pluronic polymer adapted a folded conformation in the lipid bilayer [34,35,190,191,193–195]. In particular, the hydrophobic PO segment of F-127 polymer has adapted a folded conformation even in trans-membrane state [193]. The ordered arrangement of the lipid molecules get disturbed by the adsorbed polymer molecules onto liposome due to adapted in a fold

conformation in the bilayer. At this point it is important to note that transport of ions across a bilayer is driven by the creation of a trans-membrane potential difference. This occurs due to the adsorption of oppositely charged ions on the outer bilayer surface. However, the transport rate will also depend upon the rigidity of the bilayer. Therefore, if by any means the rigidity is compromised, the transport rate will increase. We propose that due to the folded conformation of the PO unit of F-127 inside the bilayer, the lipid molecules in the immediate vicinity will lose their ordering arrangement. The main consequence is reduced rigidity which will result in an enhanced permeability of the LDS^+ ions around this localized area.

So far, the effect of polymers on the transport of LDS^+ ions across the POPG liposome have been discussed. The interaction between polymer and membranes consists of two processes. In the first process, the polymer gets adsorbed on the surface of membrane. In the second process, the hydrophobic part (PO unit) of the polymer is inserted into the bilayer [32,177,181,184,188,190,192]. The insertion mechanism of the hydrophobic part (PO unit) of the polymer (whose the length of the hydrophobic PO unit is of the order of bilayer thickness or more) in the lipid bilayer can be of two types: the hydrophobic part (PO unit) of the polymer spans across bilayer or localization of the hydrophobic part (PO unit) of the polymer in the outer surface (leaflet) of the membrane. Since the polymer consists of the hydrophobic part (PO unit) as well as hydrophilic part (EO unit), the transport of the hydrophilic (EO unit) segment of the polymer passes through the hydrophobic region of the bilayer which is an energetically costly process. Thus, it can be slow process [32,187,188] at room temperature. However, the transport of the hydrophilic (EO unit) segment of the polymer may be faster at elevated temperatures as the mobility of lipid constituents is more at higher temperature.

POPG liposomes are prepared by polymer incubated or incorporated in POPG liposomes. The results of k_T values of the LDS^+ ions for all systems (POPG liposomes, polymer either incubated or incorporated liposomes) have shown that temperature plays a crucial role in the interaction between the F-68 and F-127 polymers and membranes (Figure 3.6). The changes in k_T values of LDS^+ across POPG bilayer with temperature do not follow similar trends over a range of temperature (5-40 ^{0}C). The k_T values of LDS^+ ions across POPG bilayer suddenly increase with temperature near the temperature range of 15-20 ^{0}C. This occurs because the mobility of the POPG lipids increases significantly at this temperature. Similar trend is also followed by F-68 and F-127 polymers incubated with POPG liposomes (polymer F-68 and F-127 are more-or-less equal number of EO units).

A comparison of the k_T values of the LDS cation across a POPG bilayer and POPG bilayer containing pluronic polymers which were present either in the incorporated or incubated state (Figure 3.6) indicates that temperature plays a crucial role in controlling the interaction of the F-68 and F-127 polymers with the bilayer. The k_T values of LDS cation across POPG bilayer shows an abrupt increase near the temperature range of 15-20 ^{0}C indicating that at this temperature the mobility of the POPG lipids increases significantly. This trend is also followed by F-68 and F-127 polymers (which have a long chain hydrophilic EO groups) when they are incubated with POPG liposomes which leads us to conclude that insertion of the PO chain in F-127 and F-68 polymers in the POPG bilayer starts when the mobility of the bilayer gets reduced abruptly around the 15-20 ^{0}C temperature range. Although the reason behind this sudden change in the POPG bilayer mobility is not clear at this point, it is relevant to note that liposomes made from egg PE (phosphatidyl ethanolamine) were observed to show a transition near

10°C, which has been attributed to the lipid hydrocarbon chain order-disorder conformational transition [197]. It is possible that a similar transition in the POPG liposomes occurs in the temperature range of 15-20 ^{0}C causing the above mentioned effect. Further experiments are needed to corroborate this possibility. Since above 20 ^{0}C the observed changes in the k_T values of the LDS cation with temperature are more or less similar for both incubated or incorporated complexes of F-127 or F-68 polymers with POPG liposomes further leads to the conclusion that above this temperature polymer incorporation in the bilayer is similar for both incorporated and incubated polymer-lipid complexes and this is likely to be in a bilayer spanning state. The reduction of the lipid mobility is likely to assist the translocation of the bulky EO chains in these polymers across the bilayer. In the schematic diagram shown in Figure 3.7 the POPG lipid bilayer gets disturbed by the presence of pluronic polymers and variation in temperature.

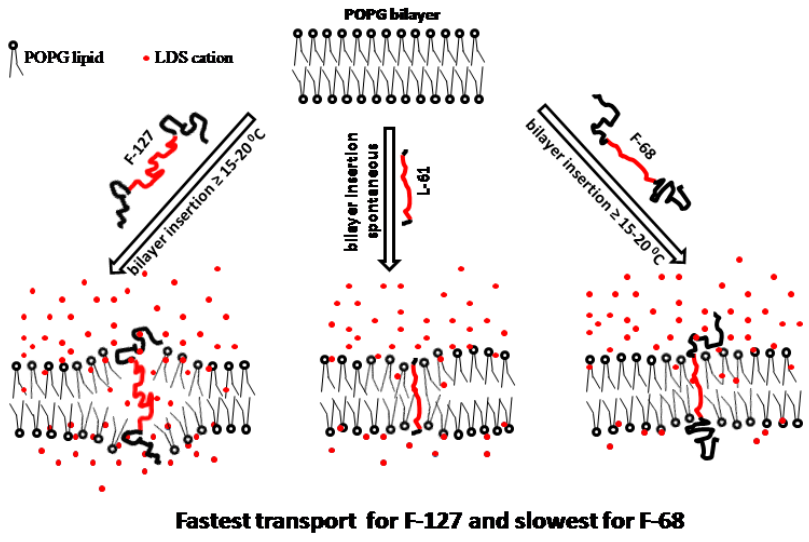

Figure 3.7: A schematic illustration of how the POPG lipid bilayer get disturbed by the presence of pluronic polymers and variation in temperature.

The insertion of the hydrophobic part (PO unit) of L-61 polymer into the POPG bilayer is followed by a similar trend for both L-61 polymer incubated and incorporated liposomes system. It is clearly observed that the preparation of liposome is independent of method of preparation because L-61 polymer has the highest HLB value among the three polymers. This indicates that L-61 inserts itself in the bilayer when added externally (incubated). Therefore, L-61 polymer is expected to bind more strongly to the POPG bilayer.

3.4 Summary and conclusions

It is concluded that, the transport of LDS^+ across POPG liposomes containing tri-block pluronic polymers depends on the copolymer composition of polymer (variation in the individual sub-units of the polymer). Using three different polymers (F-127, F-68 and L-61), the effect of variation in the length of the hydrophobic PO unit and the length of the hydrophilic EO unit on the transport properties of LDS^+ across POPG liposomes has been investigated. The results of transport of LDS^+ across the bilayer show that the length of the hydrophobic PO unit remarkably affects the permeability of POPG liposomes when compared to the length of the hydrophilic EO unit. The permeability of POPG liposomes are significantly altered. This is attributed to the accommodation of the hydrophobic PO unit of the polymer in the hydrophobic region of the bilayer. The effect is higher in the case of F-127 polymer as the hydrophobic PO unit length is almost double to that of the bilayer thickness. In the schematic diagram shown in Figure 3.8, the POPG liposome bilayer gets disturbed by methods of preparation. They are prepared either by polymer incubated liposomes or by polymer incorporating in the liposomes. The role of polymer structure and temperature (5-40 ^{0}C) on the insertion of the hydrophobic PO unit in the bilayer has also been investigated by monitoring the

transport of the LDS^{+}. L-61 polymer, which is the most hydrophobic of the series, is observed to insert itself spontaneously into the bilayer. We further studied the insertion of the hydrophobic PO unit in the bilayer is a function of temperature (5-40 ^{0}C) and the copolymer composition of polymer. L-61 polymer is the most hydrophobic in character out of three polymers used in this study. It is observed that L-61 polymer inserts itself spontaneously into the bilayer. The insertion of the hydrophobic part (PO unit) of F-127 and F-68 polymer into the POPG bilayer starts above 15-20 ^{0}C. These changes occur as increased temperature significantly enhance the mobility of the POPG lipids. Results obtained in this study are expected to provide further insight into the nature of pluronic polymer induced membrane permeability.

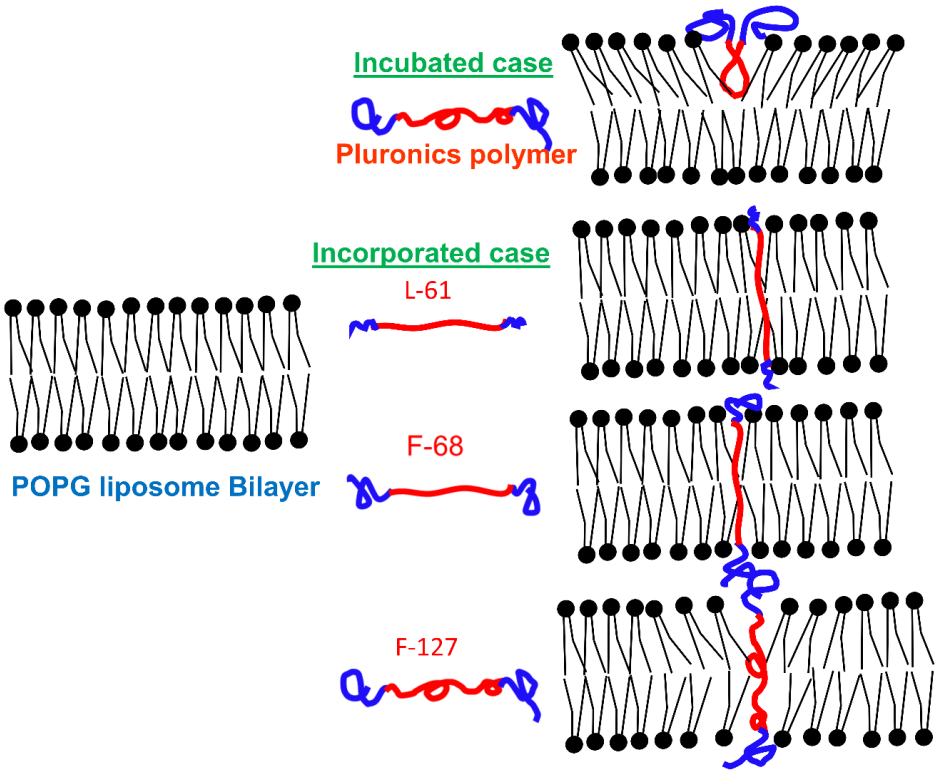

Figure 3.8: A schematic illustration of pluronic polymer insertion in the POPG liposome differs in methods of preparation.

Chapter 4

Interaction of Amphotericin B with Ergosterol/Cholesterol-Containing POPG liposomes Studied by Absorption, Fluorescence and Second Harmonic Spectroscopy

4.1 Introduction

Amphotericin B (Figure 4.1) is a polyene antibiotic belonging to a class of structurally related macrolides. The polyene antibiotics are used clinically for their anti-fungal activity. In the last few decades it has emerged as drug of choice for treatment of systemic fungal infections [36,38–41]. The usage of antibiotic amphotericin B (AmB) is, however, limited as it damages certain biological membranes. Inspite of its severe side effect, it is still the most popular drug mainly due to lack of better alternatives. The antifungal action of AmB arises from its binding to membrane sterols and formation of ion-channels in fungal cell membranes [42]. This leads to disruption of cell membranes activities followed by cell death [50]. The antifungal action of AmB described above are widely accepted. According to these two modes of action, the main cause of antifungal action of AmB is due to its interactions with sterols. Several studies reported in the literature suggest that the binding affinity of AmB with ergosterol (Ergo) containing membranes (fungal cells) is higher in comparison with cholesterol (Chol) containing membranes (mamelian cells) [198,199]. However, the results of recent findings reveal that the main cause for the antifungal activity of AmB is its binding with Ergo in the membrane as compared to the ion-channel formation in the membranes. When AmB binds

with Ergo in fungal cells it cannot perform its essential physiological functions which leads to cell death [51,52]. The chemical structures of amphotericin B, ergosterol and cholesterol are shown in Figure 4.1. The structural differences between ergosterol and cholesterol are discussed in Chapter 1. The binding affinity of sterols with amphotericin B is considerably influenced by these minor structural differences between sterols. Several experimental and theoretical studies [43,44,46,48,200–208] suggest that the binding affinity of Ergo with AmB (K_a = 6.9 ×10^5 M^{-1}) is higher compared to Chol and AmB (K_a = 5.2×10^4 M^{-1}). Figure 4.1 represents the interaction between ergosterol and amphotericin B which is highlighted as obtained from literature [51,52].

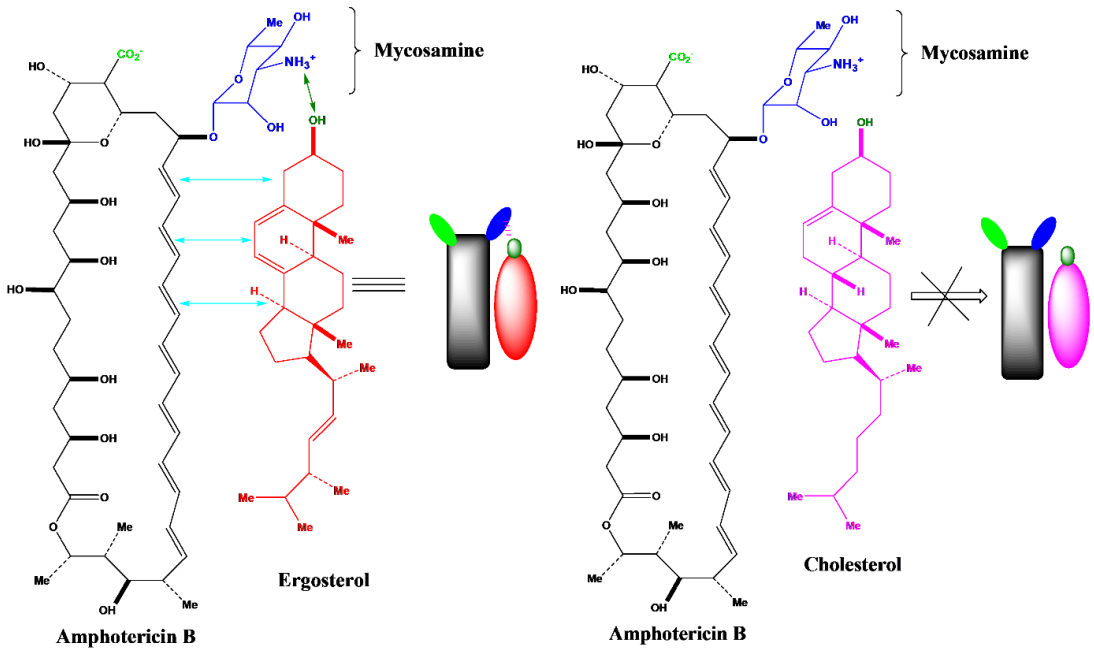

Figure 4.1: Chemical structures of Amphotericin B, Ergosterol, and Cholesterol. The interaction between ergosterol and amphotericin B which is highlighted as obtained from literature [51,52].

In this present work, we report the effect of Amphotericin B on the membrane permeability of sterol incorporated POPG liposomes. The effect of AmB in the transport prop-

erties of an organic cation (LDS-698) across either POPG liposomes or sterol incorporated POPG liposomes have been studied by the interfacial selective second harmonic (SH) spectroscopic technique. An antibiotic, AmB molecule has two ionisable functional groups i.e., carboxylic and amine groups (Figure 4.1). The effect of neutralization of the two oppositely charged functional groups of AmB on the transport of LDS^+ ions in POPG liposomes with sterols has been investigated. Two different sterols namely ergosterol (Ergo) and cholesterol (Chol) are used for SH studies to elucidate interactions of AmB with sterols. As regards membrane composition, the choice of lipid:sterol ratio is one of the important parameter. Control experiments have performed with different mole fraction of membrane sterol (either ergosterol or cholesterol) present in the POPG liposomes in presence of the antibiotic molecule (AmB). The results are shown that the transport rate is varied with different mole fraction of sterol present in liposomes. The fungal membranes which contain typically 29-31 mol % of ergosterol and the human cell membranes have cholesterol typically 30-50 mol % are reported. In light of these observations and given the additional practical constraint that membrane containing levels of sterol exceeding 30 mol % exhibit significant lateral inhomogeneity [239]. In this study, 30 mol % of sterol have been selected for all spectroscopic experiments. In addition to this, the absorption and fluorescence properties of AmB in either POPG liposomes or sterol incorporated POPG liposomes are also studied. The LDS^+ ion has been employed as an optical SH probe in the present studies due to strong second-order non linearity at the wavelength (800 nm) of a Ti-sapphire laser. The use of positively charged LDS^+ ion in the SH experiments facilitates monitoring of membrane transport process across a negatively charged lipid bilayer of liposome in real time.

Details of the principle of SH technique are described in Chapter 1. A brief description of generating SH signal from interfacial region in an aquous liposome system is ex-

plained here. The principle of this technique lies on the fact that initially the LDS^+ molecules are adsorbed on the outer surface of the liposome due to electrostatic interactions between liposomes head groups and LDS^+ ions. The SH electric field generated by oppositely oriented molecules on outer surface of liposome are in phase and will add up coherently when the diameter of the membrane is of the order of the excitation wavelength. With progress in time, the LDS^+ ions pass through the bilayer and then get adsorbed to inner surface of liposomes that are oppositely oriented with respect to orientation at the outer surface. The oppositely oriented molecules are separated by the bilayer thickness (~5 nm) which is smaller than the coherence length of the SHG process. The SH electric field generated by oppositely oriented molecules are out of phase and cancel each other. In contrast, molecules which are present in bulk aqueous solution cannot contribute to coherent SH signal because of random orientation but they can generate incoherent SH signal called as hyper-Rayleigh scattering (HRS). The SH technique is used as it can monitor the transport of amphiphilic molecules across a lipid bilayer (liposome) in real time. Several studies on adsorption and transport kinetics of organic ions across a lipid bilayer that can be monitored in real time by the SHG technique have been investigated [127,128,132,133,141].

4.2 Results

The liposomes used in present study are POPG, POPG-Ergo and POPG-Chol liposomes prepared in desired pH medium. Details of preparation of POPG, POPG-Ergo, POPG-Chol liposomes according is mentioned in Chapter 2. The effective diameter (the average size of liposome), zeta potential and poly-dispersity of respective sterol incorporated POPG liposomes and only POPG liposomes (control, i.e., sterol free) are measured at various pH using a Brookhaven 90 Plus size and zeta potential analyzer (Brookhaven

Instrument Corp., USA). The average size, polydispersity and zeta potential of only POPG and POPG liposomes incorporated with each sterol (Ergo or Chol) at three different pH is given in Table 2.3 (Chapter 2). From table. 2.2, it is observed that the size and zeta potential of liposomes prepared by sterol incorporated POPG liposomes do not significantly change with variation in pH. This indicates that the liposomes are stable in this pH range. Details of the SH and hyper-Rayleigh scattering (HRS) measurements are performed as described in Chapter 2. The SH experiments are carried out at constant temperature. The sample temperatures are controlled by a Neslab (JULABO Labortechnik GmbH, Germany) circulating water chiller having a temperature accuracy of ± 1 ^{0}C.

The time dependent change in the SH electric field ($E_{2\omega}$) for a solution of these liposomes is recorded as per the procedure briefly explained as given here. The time dependent changes in the SH electric field of LDS^+ ($E_{2\omega}$) from three different POPG liposomes solution are measured for two cases: Case I: Absence of AmB in respective liposomes and Case II: presence of 50 nM AmB in respective liposomes. The pH value of the solution in both the cases is maintained at 7.4.

Case I: Absence of AmB in respective liposomes.

The concentration of 30 mole % of the respective sterol (either ergosterol or cholesterol) incorporated POPG liposomes suspension is added into the solution having LDS^+ ions in the cuvette. For all cases, there is an instantaneous increase (< 1 second) in SH intensity due to the electrostatic adsorption of positively charged LDS^+ ions onto a negatively charged outer surface of lipid bilayer of POPG liposomes as demonstrated in numerous studies earlier [26-30]. After the addition of POPG liposomes with sterols or without sterol (control experiment) to the solution containing 5 μM LDS^+ ions, the SH electric field of ($E_{2\omega}$) of LDS^+ ions decreases gradually with time. This indicates the transport of

LDS^+ ions from the outer lipid bilayer to the inner lipid bilayer of POPG liposomes. The measured experimental data can be converted to the SH electric field and is fitted to exponential decay functions per following equation 1.12. The transport time constant (τ_1 and τ_2 values) have been extracted by exponential fitting of the decay curves of the SH electric field of LDS^+ ions and then calculated τ_{av} values. The SH decay curve is fitted from their maximum of the SH electric filed ($E_{2\omega}$), i.e., just after the addition of the liposomes to the buffer solution containing LDS^+ ions.

Case II: Presence of AmB in respective liposomes.

A similar procedure described for *case I* is followed. Here, the required concentration of AmB is added to respective liposomes suspension before start the SH measurement. Figure 4.2 describes time dependent changes in the SH electric field of LDS^+ ($E_{2\omega}$) are measured in respective liposomes systems for two cases: Absence of AmB in liposomes systems (a, left panel) and presence of 50 nM of AmB in liposomes systems (b, right panel). The liposomes suspension is added to buffer solution containing the LDS^+ ions (5 μM) at 100 seconds.

The black curve describes POPG liposomes (control, i.e., sterol free)

The red curve describes cholesterol incorporated POPG liposomes.

The blue curve describes ergosterol incorporated POPG liposomes.

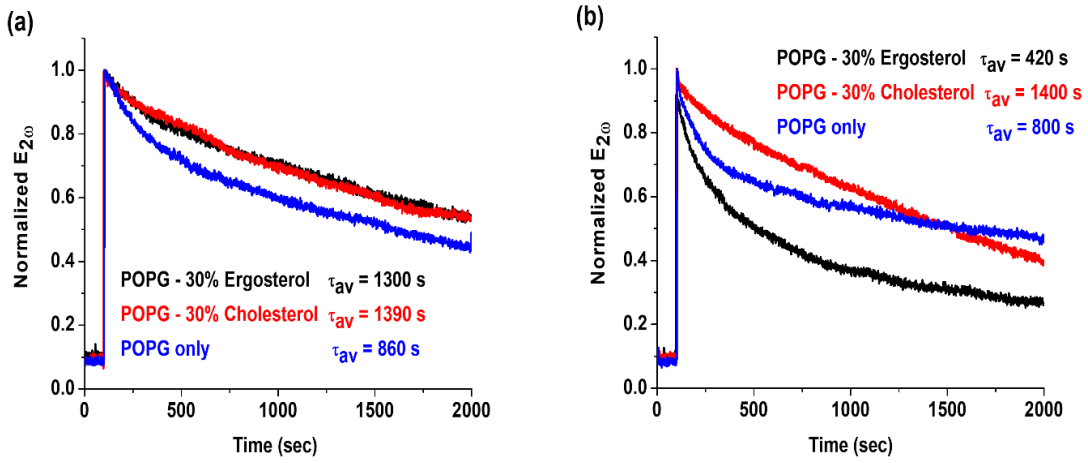

Figure 4.2: Time dependent variations in the SH electric field of LDS^+ ($E_{2\omega}$) in respective liposomes systems for two cases: Absence of AmB in liposomes systems (a, left panel) and presence of 50 nM of AmB in liposomes systems (b, right panel). The liposomes suspension is added to buffer solution containing the LDS^+ ions (5 µM) at 100 seconds. These sterol-POPG liposomes systems are POPG liposomes (black curve), POPG-Chol liposomes (red curve) and POPG-Ergo liposomes (blue curve).

Two cases are considered in Figure 4.2.

Case I: In the absence of AmB, it is clearly observed that the transport of LDS^+ in POPG liposomes with sterols is slower as compared to POPG liposomes without sterols. However, the transport of LDS^+ in presence of sterol incorporated liposomes is slower as sterols increase the bilayer rigidity.

Case II: In the presence of AmB, these results show that the transport of LDS^+ becomes significantly fast for POPG liposomes containing Ergo in presence of AmB. The effect of AmB on the transport of LDS^+ is minimum for similar concentration of AmB present in POPG liposomes and POPG-Chol liposomes. These results suggest that the permeability of the POPG membrane against LDS^+ is critically dependent on the sterol composition of the POPG liposomes. The liposome concentration is calculated to be ~350 nM

as described in Chapter 2. At an AmB/liposome (A/L) value as low as ∽ 0.14, i.e., when 0.14 molecules of AmB are present per liposome, the presence of less than one molecule of AmB per liposome significantly affects the transport of LDS^+ in the POPG-Ergo lipid bilayer. The transport time constants (τ_{av}) are extracted by exponential fitting of the decay curves of the SH electric field of LDS^+ ions across each POPG liposomes system and the sterols incorporated POPG liposomes for two cases (Absence of AmB in respective liposomes and presence of AmB in respective liposomes). The τ_{av} values of LDS^+ for all liposome sytems have been summarized in Table 4.1.

Figure 4.3 shows the change in τ_{av} of LDS^+ ions with varying concentration of AmB. The X-axis represents number of AmB molecules per liposome (A/L) which gives an idea on the change in τ_{av} with the number of AmB molecules present in the bilayer. In Figure 4.3 it is clearly shown that there are two kinetic regimes associated with increasing A/L values. In the first regime, it is clear that when the value of AmB/liposome (A/L) is less than one, the τ_{av} values for all the three liposomes decreases with different slopes almost in a linear fashion. For A/L values greater than unity, the τ_{av} values for all the three liposomes saturate and remains more or less similar. In the inset of Figure 4.3, a linear fit of the τ_{av} values is shown for all the three cases along with their respective slopes. The effect of AmB is more prominent in POPG-Ergo liposome system compared to POPG and POPG-Chol liposomes.

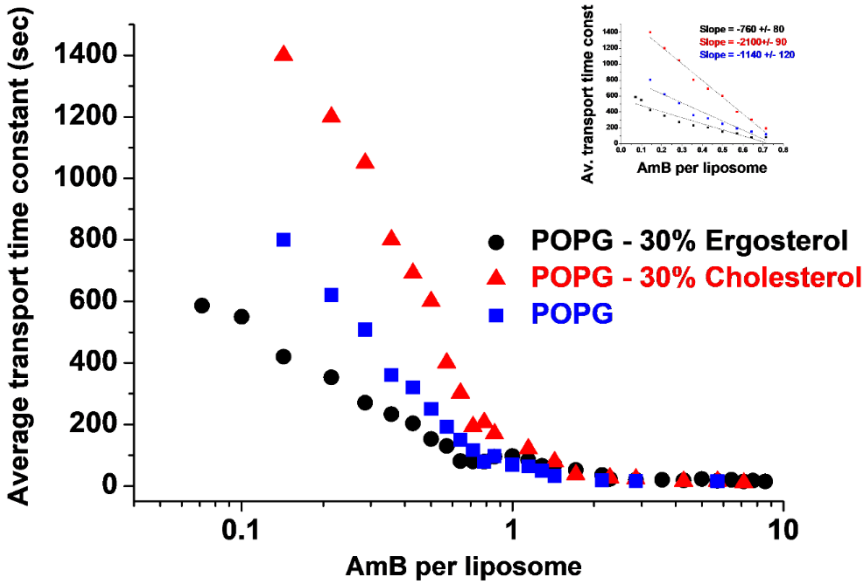

Figure 4.3: Changes in the transport time constants (τ_{av}) of LDS^+ with number of AmB molecules per liposome (A/L) ratio for three different POPG liposomes systems (POPG-Ergo, POPG-Chol, and POPG only).

So far, the effect of the sterol composition of the POPG liposomes on the transport rates of LDS^+ across a POPG bilayer with and without antibiotic AmB are studied. The amphotericin B molecule has two oppositely charged functional groups. The AmB molecule has zwitterionic characteristics in buffer solution. Recent studies reveal that the interaction of Ergo with AmB is due to the interaction of positively charged mycosamine group of AmB with hydroxyl group of Ergo (Figure 4.1). The carboxyl functional group of AmB is not involved in any type of interactions with sterols (Ergo or Chol). At this point, it is worthwhile to consider the binding of two charged functional groups of AmB with ergosterol in the liposomes systems. These experiments have been planned with the objective of neutralizing the charge on the functional groups (either amino group or carboxyl group) of AmB, one at a time, by varying the pH of the liposomes solution. The pK_a values of the functional groups of AmB are obtained from sigma website. The pK_a

value of the mycosamine group is ~10.0, and the pK_a value of the carboxyl group is ~5.5. The studies (The SH experiments, size and zeta potential) are performed at pH 4.5, 7.4 and 11. The AmB molecule has zwitterionic in nature at pH 7.4. A pH = 4.5 (pK_a-1, here the pK_a corresponds to the carboxyl group) indicates that 90% of the carboxyl functional group is present in their unionized state (neutral form). Similarly, at pH = 11 (pK_a+1, here the pK_a corresponds to the mycosamine group) 90% of the mycosamine functional group is present in their ionized state (charged form).

Figure 4.4 shows time dependent changes in the SH electric field of LDS^+ ($E_{2\omega}$) are measured in POPG-Ergo liposomes at three different pH for two cases: *case I*: Absence of AmB in POPG-Ergo liposomes (a, left panel) and *case II*: presence of 50 nM of AmB in POPG-Ergo liposomes (b, right panel). The liposomes suspension is added to buffer solution containing the LDS^+ ions (5 µM) at 100 seconds. These studies are performed at 25 ^{0}C

The blue curve describes POPG-Ergo liposomes at pH 4.5

The black curve describes POPG-Ergo liposomes at pH 7.4

The red curve describes POPG-Ergo liposomes at pH 11

Case I: In the absence of AmB in POPG –Ergo liposomes, it is clearly observed that the transport of LDS^+ moderately changes with variation in pH.

Case II: The presence of AmB in the POPG-Ergo liposomes, shows that the transport of LDS^+ gets significantly faster as pH is lowered from 11 to 4.5. The concentration of AmB in POPG-Ergo liposomes corresponds to ~0.14 AmB molecules per liposome.

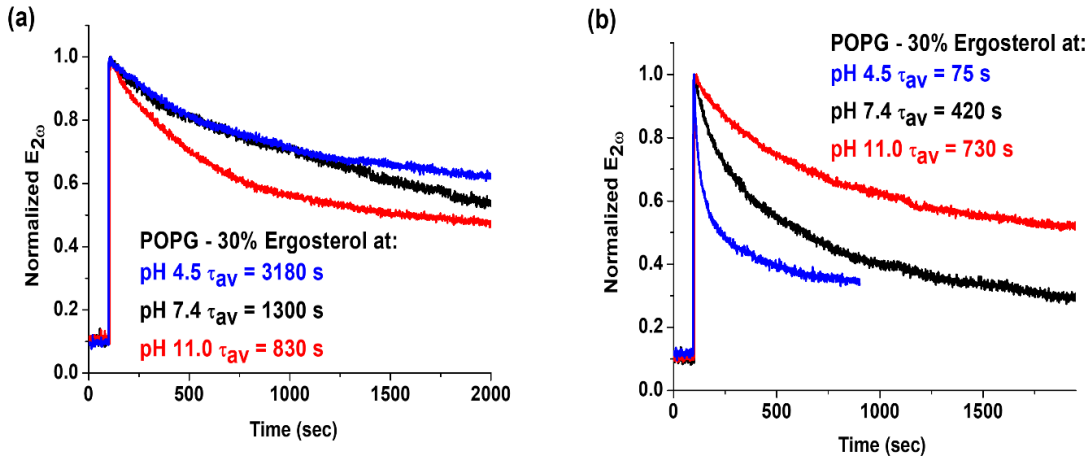

Figure 4.4: Time dependent variations in the SH electric field of LDS^+ ($E_{2\omega}$) in POPG-Ergo liposomes at three different pH for two cases: Absence of AmB in POPG-Ergo liposomes (a, left panel) and presence of 50 nM of AmB in POPG-Ergo liposomes (b, right panel). The liposomes suspension is added to the LDS^+ ions (5 µM) solution at 100 seconds. The POPG-Ergo liposomes at three pH are pH 7.4 (black curve), pH 4.0 (blue curve), and pH 11.0 (red curve).

These results clearly demonstrate that the effect of neutralizing the amino/carboxylic group of AmB is more significant on the transport of LDS^+ across the POPG-Ergo liposomes (the permeability of POPG-Ergo liposomes). The carboxylic group is neutralized at pH 4.5 (pK_a-1, here the pK_a corresponds to the carboxyl group). The AmB enhances the permeability of POPG-Ergo liposomes at low concentration of AmB per POPG-Ergo liposome. i.e., this concentration of AmB is equal to 0.14 AmB molecules per POPG-Ergo liposome. On the other hand, the amino group is neutralized at pH 11 (pK_a+1, here the pK_a corresponds to the amino group). At this pH, there is no significant effect on the permeability of POPG-Ergo liposomes.

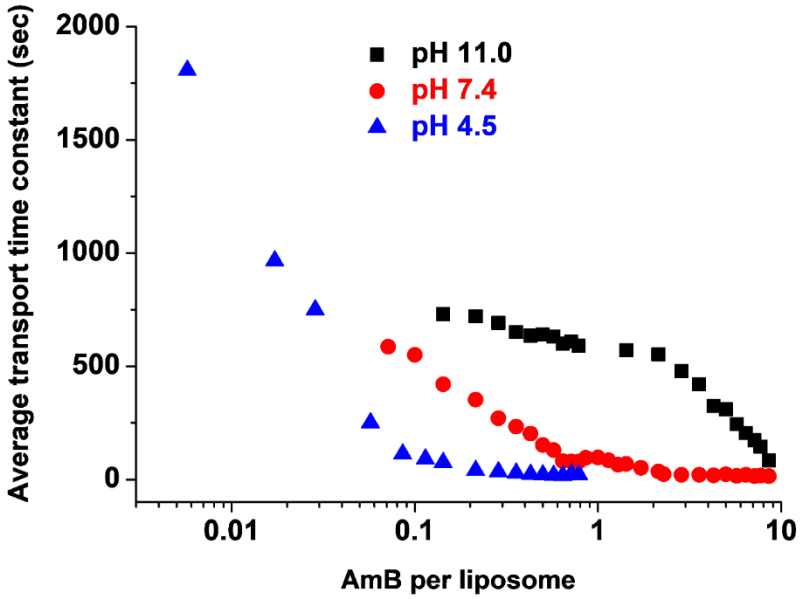

Figure 4.5: Changes in the transport time constants (τ_{av}) of LDS^+ with number of AmB molecules per liposome (A/L) ratio for POPG-Ergo liposomes at three different pH. The X-axis is shown in logarithmic scale so as to capture the entire range of variation of τ_{av} value.

Figure 4.5 describes the variation in the τ_{av} values of LDS^+ in POPG –Ergo liposomes with AmB concentration at three different pH similar to Figure 4.3. The net charge on either amino group or carboxyl group changes with variation in pH accordingly. It gives an idea on the neutralization of either of the two charged functional groups (amino/carboxylic) of the AmB molecule. This affects the bilayer permeability in POPG-Ergo liposomes by varying the pH of the buffer. In Figure 4.5, it is clearly shown that the rate of decrease in the τ_{av} values of LDS^+ with changing AmB/Liposome (A/L) value is faster at pH 4.5 followed by pH 7.4 and pH 11. For A/L values greater than unity, the rate of change in the τ_{av} values of LDS^+ with A/L ratio is similar for pH 4.5 and 7.4. The τ_{av} values of LDS^+ for all the systems studied are summarized in Table 4.1 and these τ_{av} values are used for plotting in Figure 4.3 and 4.5. The lifetime values have an error of

10%. The observed changes in the transport time constants (τ_{av}) values of LDS^+ with increasing AmB/Liposome (A/L) ratio distinctly fall into two kinetic regimes for POPG, POPG-Ergo, and POPG-Chol liposomes. In the first regime, the τ_{av} values of LDS^+ decrease linearly with different slopes and converge at an A/L value of ~1.0. In the second regime, the τ_{av} values of LDS^+ remain almost constant at higher A/L value. i.e., the permeability becomes similar for all the three systems. This indicates that the A/L values are independent of the liposome without/with sterol.

So far, we have studied the effects of variation in AmB/ liposome value on the τ_{av} values of LDS^+ of POPG liposomes by SH technique for two cases.

Case I: three different liposomes (POPG, POPG-Ergo, and POPG-Chol)

Case II: at three different pH (pH 4.5, 7.4, and 11).

At this point it is worthwhile to consider the absorption and fluorescence properties of AmB with varying A/L value in these three liposomes in pH 7.4. The spectral properties of AmB in presence of POPG-Ergo liposomes at different pH are studied. The results of SH studies show that the τ_{av} of LDS^+ ions in the three different liposomes follow two kinetic regimes with increasing A/L values. This indicates the mode of action of AmB on liposomes systems at minimum and maximum A/L values that are followed by two different types of mechanisms. Therefore, absorption, fluorescence emission, and fluorescence lifetime of AmB in these liposomes are studied at two extreme A/L values. In the control experiment, interactions of LDS^+ with AmB in different pH buffer solutions are studied. For this, the absorption spectra of AmB in buffer solution having LDS^+ at different pH are studied. The results indicate that there are no interactions between AmB and LDS^+ at different pH. The concentration of AmB is fixed at 2.0 μM for absorption,

fluorescence emission, and fluorescence lifetime measurements, while the liposomes concentration is varied.

Figure 4.6, consists of two set of experiments. Figure 4.6 (a & b) describes the absorption spectra of AmB for three different liposomes (POPG, POPG-Ergo, and POPG-Chol) at minimum and maximum A/L values. These three liposomes are prepared in pH 7.4 medium. Similarly, Figure 4.6 (c & d) shows the absorption spectra of AmB in POPG-Ergo liposomes for three different pH (pH 4.5, 7.4, 11) at minimum and maximum A/L values. From Figure 4.6 (a), it is clearly observed that the spectra of these three liposomes are slightly different at the region of 410-416 nm when A/L value is 0.14. This corresponds to the $S_0 \rightarrow S_2$ transition [209–211]. Whereas at higher A/L value, the spectra of AmB in POPG-Ergo liposomes are distinctly red-shifted. At the same time, no differences are observed in the spectra of AmB in presence of POPG-Chol and POPG liposomes. The spectra of AmB in the presence of POPG-Ergo liposomes are similar for three pH at minimum A/L value, while it changes significantly for pH 11 at maximum A/L value (Figure 4.6 (c & d)).

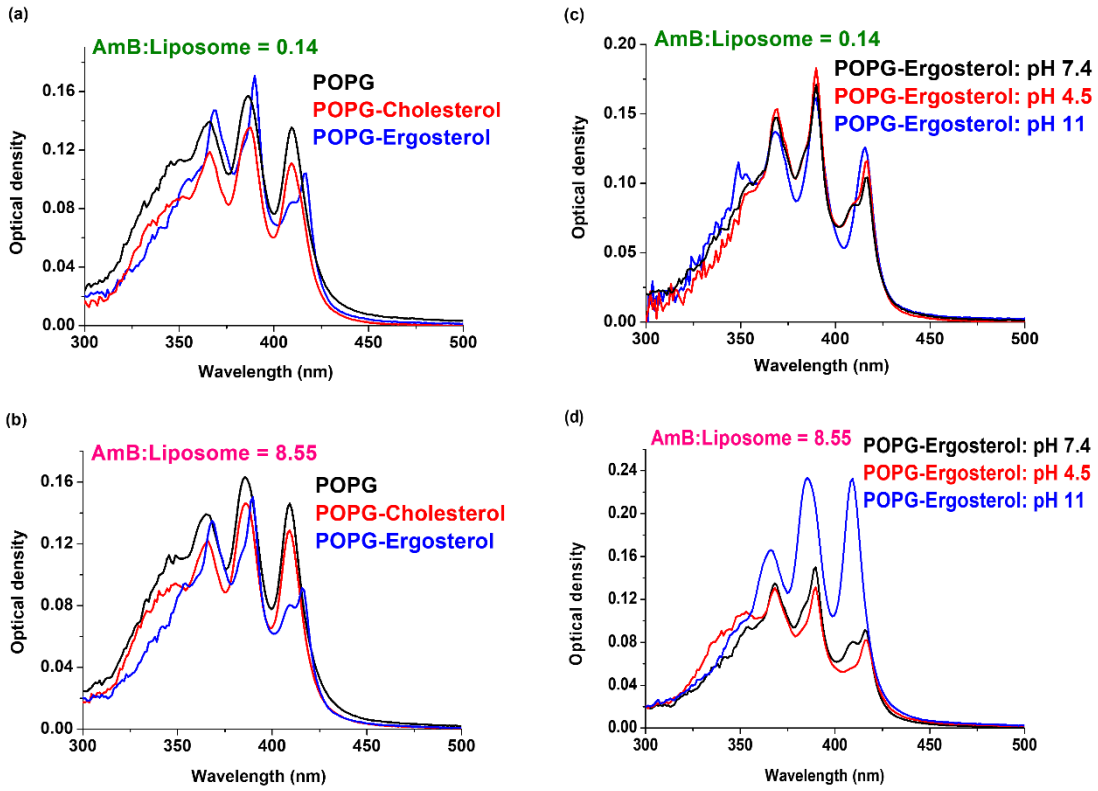

Figure 4.6: Left panel (a, b): Absorption spectra of AmB (2 μM) in the presence of three different POPG liposomes (as described in Figure 4.2) with minimum and maximum A/L values. Right panel (c, d): Absorption spectra of AmB (2 μM) in the presence of POPG-Ergo liposomes at three different pH (as described in Figure 4.4) with minimum and maximum A/L values.

Figure 4.7, consists of two set of experiments. Figure 4.6 (a, b and c) describes the peak normalized fluorescence spectra of AmB at minimum and maximum A/L values for each liposomes system (POPG, POPG-Ergo, and POPG-Chol liposomes in pH 7.4). Figure 4.7 (c, d, and f) shows the peak normalized fluorescence spectra of AmB in POPG-Ergo liposomes at minimum and maximum A/L values for three different pH (pH 4.5, 7.4, and 11). Figure 4.7, it is clearly observed that the fluorescence spectra of AmB in POPG-Ergo and POPG-Chol liposomes are significantly shifted to higher

wavelength region (red shift). The same shift is observed in POPG-Ergo liposomes at pH 4.5 and 11. A similar shift is modest in the case of POPG liposomes at pH 7.4.

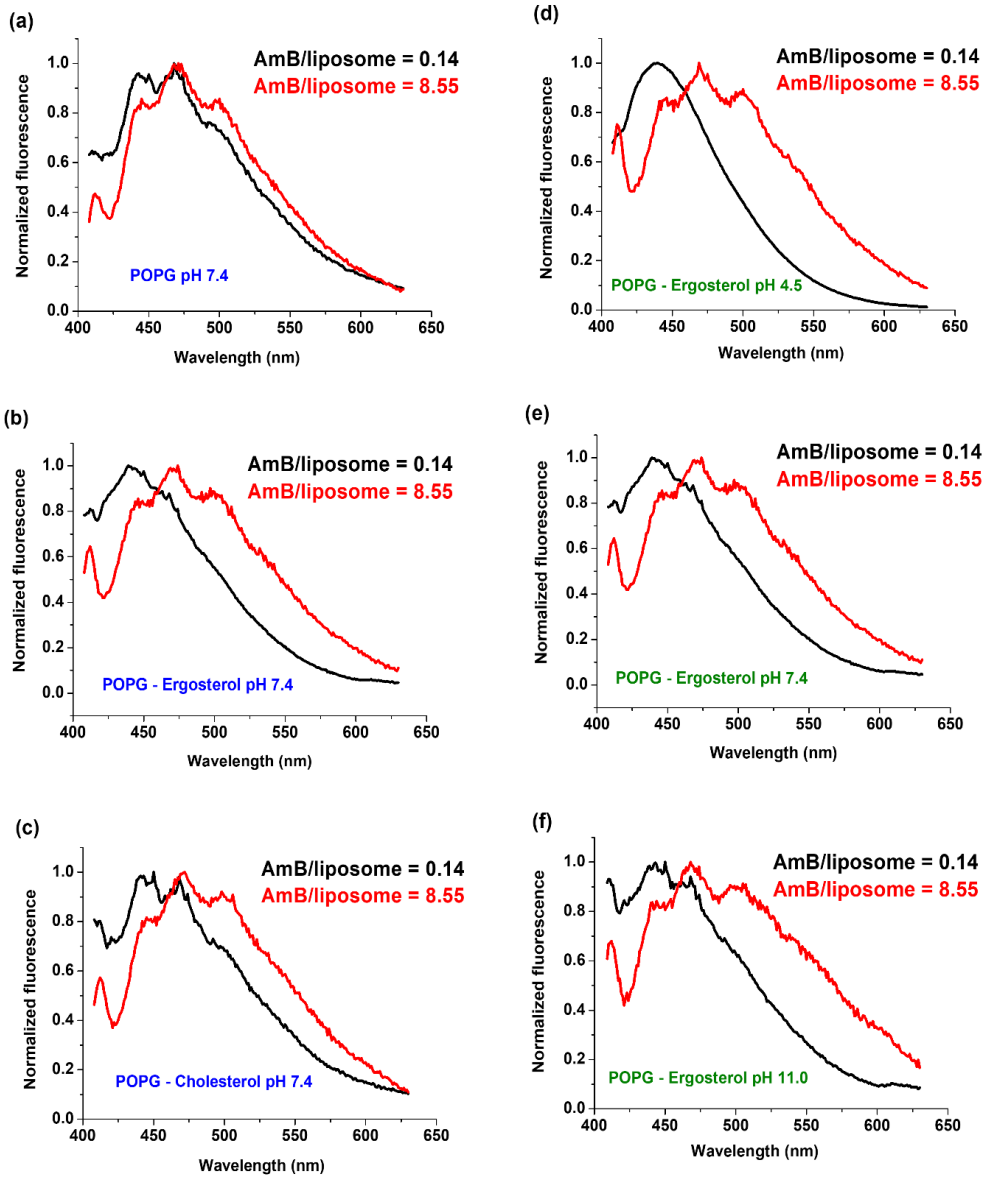

Figure 4.7: Left panel: The peak normalized fluorescence spectra of AmB (2 μM) in the three different liposomes (Only POPG (a), POPG-Ergo (b), POPG-Chol (c)) with minimum and maximum A/L ratio. Right panel: The peak normalized fluorescence spectra of AmB (2 μM) in POPG-Ergo liposomes at different pH (4.5 (d), 7.4 (e), 11.0 (f)).

Figure 4.8 consists of two set of experiments. *Set I* describes the fluorescence lifetime of AmB at minimum and maximum A/L values for each liposomes system (POPG, POPG-Ergo, and POPG-Chol liposomes in pH 7.4). *Set II* describes the fluorescence lifetime of AmB in POPG-Ergo liposomes for three different pH (pH 4.5, 7.4, and 11) at minimum and maximum A/L values. It is clearly observed that the fluorescence decay of AmB in POPG-Ergo liposomes is distinctly slower as compared to POPG and POPG-Chol liposomes when the A/L ratio is small (0.14). All the three decays look similar when the A/L ratio is higher (8.55) (Figure 4.8, b). POPG-Ergo liposomes are prepared in three different pH. The fluorescence decay of AmB is observed to be slowest at pH 4.5 and fastest at pH 11 for low A/L ration. Increase in the A/L ratio increases the rate of decay and does not change this trend (Figure 4.8, c & d).

Finally, Figure 4.9 consists two set of experiments. *Set I* (a, b) describes the changes in the integrated fluorescence intensity of AmB with increasing in A/L values for each liposomes system (POPG, POPG-Ergo, and POPG-Chol liposomes in pH 7.4). *Set II* (c, d) describes the changes in average fluorescence lifetime of AmB in presence of POPG-Ergo liposomes with increasing in A/L values for three different pH (pH 4.5, 7.4, and 11). It is clearly observed that the integrated fluorescence intensity of AmB in all liposomes systems initially decreases and is followed by saturation with increasing A/L values (Figure 4.9, a & b). The average fluorescence lifetime values and the integrated fluorescence intensity of AmB in all liposomes systems follow similar trend at higher A/L value for both cases (Figure 4.9, c & d). From Figure 4.9 (c), the average fluorescence lifetime of AmB with increasing A/L values is distinctly slower in POPG-Ergo liposomes as compared to POPG or POPG-Chol liposomes at pH 7.4. From Figure 4.9 (d), the average fluorescence lifetime of AmB in POPG-Ergo liposomes with increasing A/L

values is distinctly slower as pH is lowered from 11 to 4.5. The results of the absorption and fluorescence spectra of AmB in POPG-Ergo liposomes at three different pH show that the interaction between AmB and Ergo is stronger at pH 4.5 &7.4 than pH 11. The average fluorescence lifetime values of AmB for the three different POPG liposomes at pH 7.4 and POPG-Ergo liposomes at three different pH have been summarized in Table 4.2.

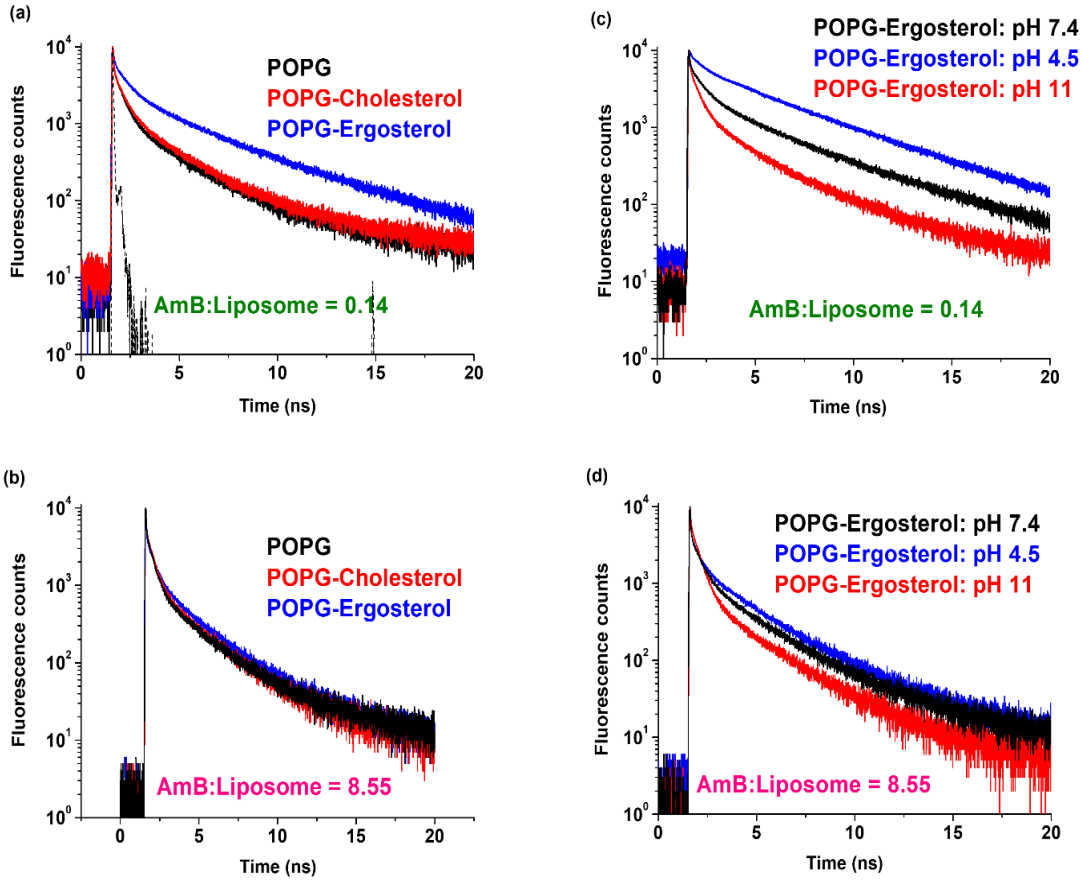

Figure 4.8: Left panel (a, b): Fluorescence decay curves of AmB (2 μM) in the presence of three different POPG liposomes with minimum and maximum A/L values. Right panel (c, d): Fluorescence decay curves of AmB (2 μM) in the presence of POPG-Ergo liposomes at three different pH with minimum and maximum A/L values. The instrument response function is also shown (dotted line) in the top graph of left panel.

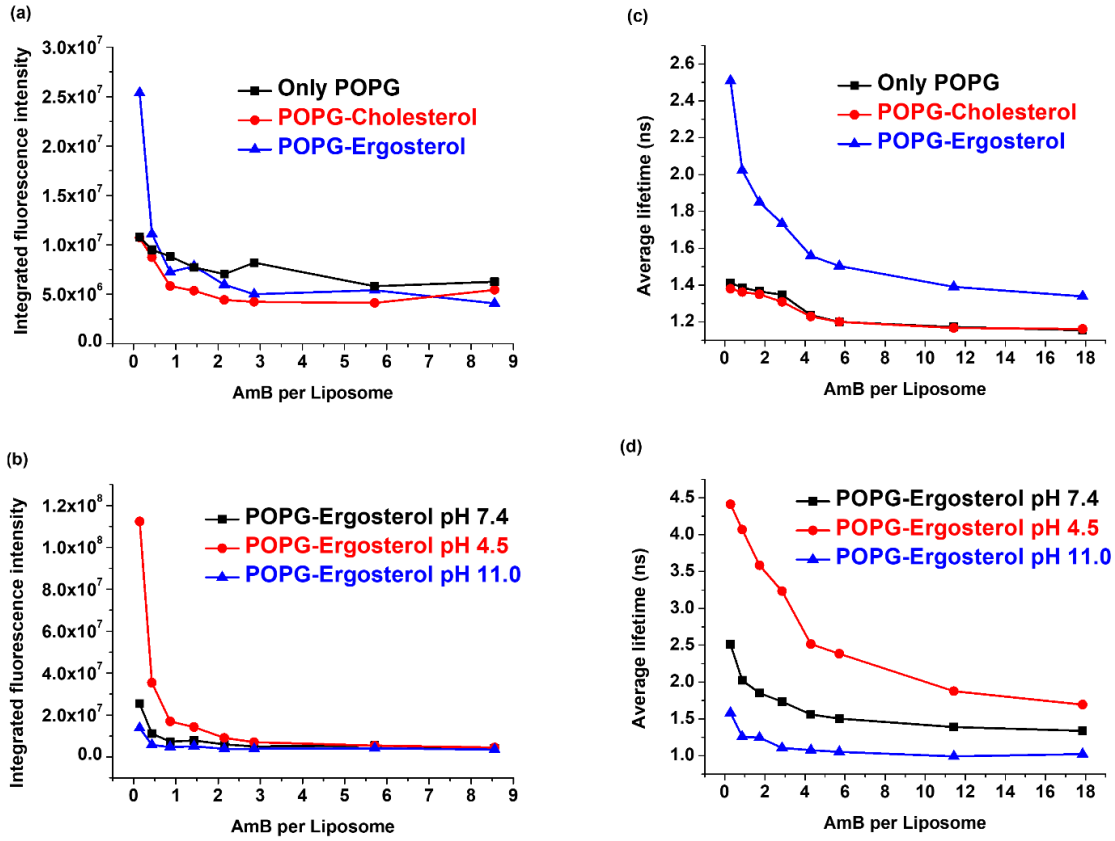

Figure 4.9: Left panel (a, b): Variation in the integrated fluorescence intensity of AmB (2 μM) in the presence of three different POPG liposomes and with POPG-Ergo liposomes at three different pH with increasing A/L values. Right panel (c, d): Variation in the average fluorescence lifetime of AmB (2 μM) in the presence of three different POPG liposomes and with POPG-Ergo liposomes at three different pH with increasing A/L values.

Table 4.1: Summarizes the average transport time constants (τ_{av}, in seconds) of LDS^+ with variation in A/L ratio for all POPG liposomes systems at different pH.

A/L ratio	Only POPG: pH 7.4	POPG-Chol: pH 7.4	POPG-Ergo: pH 7.4	POPG-Ergo: pH 4.5	POPG-Ergo: pH 11.0
0.00	830	810	1388	865	3183
0.01	--	--	--	--	1808
0.02	--	--	--	--	965
0.03	--	--	--	--	750
0.06	--	--	--	--	250
0.07	--	586	--	--	--
0.09	--	--	--	--	113
0.1	--	550	--	--	--
0.11	--	--	--	--	90
0.14	730	420	1400	800	75
0.21	720	353	1200	621	40
0.29	690	270	1050	508	35
0.36	650	233	800	360	27
0.43	635	203	692	320	23
0.5	640	153	600	250	20
0.57	630	130	400	192	18
0.64	600	81	302	150	17
0.71	610	80	194	115	25
0.79	590	78	206	79	20
0.86	--	95	170	97	--
1.0	--	97	--	68	--
1.14	--	84	121	64	--
1.29	--	65	--	49	--
1.43	570	68	79	31	--
1.71	--	51	37	--	--
2.14	551	35	--	18	--
2.29	--	23	26	--	--
2.86	479	20	23	16	--
3.57	420	20	--	--	--
4.29	325	18	15	--	--
5.0	310	23	--	--	--
5.71	244	16	16	15	--
6.43	205	20	--	--	--
7.14	173	14	10	--	--
7.71	145	17	--	--	--
8.57	84	14			

Table 4.2: Summarizes the average fluorescence lifetimes (in nanoseconds) of AmB with variation in A/L ratio for all POPG liposomes systems used in this study at different pH. The lifetime values have an error of 10%.

A/L ratio	Only POPG: pH 7.4	POPG-Chol: pH 7.4	POPG-Ergo: pH 7.4	POPG-Ergo: pH 4.5	POPG-Ergo: pH 11.0
0.29	1.44	1.38	1.41	1.49	1.51
0.87	1.40	1.38	1.39	1.36	1.36
1.73	1.56	1.37	1.37	1.13	1.33
2.86	1.41	1.28	1.34	1.31	1.31
4.29	1.19	1.28	1.24	1.14	1.32
5.71	1.27	1.3	1.2	1.09	1.24
11.43	1.13	1.21	1.17	1.08	1.26
17.86	1.09	1.22	1.15	1.08	1.24

Three individual life time measurements were performed for each system to test the reproducibility. The lifetime values have an error of 10% it means standard deviation of three measurements.

4.3 Discussions

The objectives of these studies are to investigate the effect of an antibiotic, Amphotericin B on the membrane permeability of POPG liposomes as a function of membrane composition (the presence of either ergosterol or cholesterol in the membrane) and the membrane permeability of POPG-Ergo liposomes affects by AmB as a function of pH variation in liposomes system. This work is studied by the SH and spectroscopic techniques. The chemotherapeutic action of AmB is mainly caused by interaction between AmB and sterols which are present in membranes. Several studies reveal that the effect of AmB on the permeability of membranes is more predominant in ergosterol having

membranes compared to cholesterol present in membranes. Therefore, three types of POPG liposomes systems have been selected for investigation of the effect of AmB on the transport of LDS^+ across the bilayer i.e., the membrane permeability. These are POPG (sterol free), POPG-Ergo, and POPG-Chol liposomes systems. From figure 4.2, at A/L values as low as ∽ 0.14, i.e., 0.14 molecules of AmB per liposome, the transport of LDS^+ in the POPG-Ergo liposome is observed to be faster. Thus, the effect of less number of AmB molecules on the membrane permeability of ergosterol incorporated POPG liposomes is more predominant. This indicates that interaction between AmB and Ergo in POPG liposomes disturbes membrane permeability. i.e., the POPG-Ergo liposome is more permeable for LDS^+ ions. In addition to this, the results of absorption, fluorescence spectra and life time studies of AmB in POPG-Ergo liposomes have been supported for interaction of AmB with Ergo in POPG liposomes. The absorption spectra of AmB in POPG liposomes at pH 7.4 shows three major peaks. These appear at ~366, ~387 and ~409 nm (Figure 4.6). These bands are vibronic bands. The absorption band represents the strongly allowed electronic transition from the ground energy state to the excited states with very distinct vibrational substructure (the 0-0 transition at 409 nm). The main absorption band, with the 0–0 vibrational maximum at 409 nm. The short wavelength spectral components represent the high energy excitonic states characteristic of the dimeric and also more complex organization forms of AmB. The peak at 409 nm corresponds to the lowest energy $S_0 \rightarrow S_2$ transition of AmB [209–211]. The absorption spectrum of AmB in POPG-Ergo liposomes is slightly different in the region of 409-416 nm (Figure 4.6). No differeces are observed in the other two liposomes systems. The main cause of these changes in the spectrum is due to the interaction of AmB with Ergo in POPG liposomes. This is further supported from observed life time values of AmB in POPG-Ergo liposomes at an A/L ratio of 0.14. Figure 4.3 reveals that the observed

changes in the transport time constants (τ_{av}) values of LDS^+ with increasing A/L ratio distinctly falls into two kinetic regimes for POPG, POPG-Ergo, and POPG-Chol liposomes. In the first regime, the τ_{av}values of LDS^+ decrease linearly with increasing A/L ratio. They are followed by different slopes and converge at an A/L value of ~1.0. Spectral changes in the absorption and fluorescence studies of AmB in presence of POPG-Chol liposomes and POPG liposomes are not observed. This suggests that there is no interaction between AmB and Chol. It is poignant to mention that the binding constant of AmB with ergostrol is ten times higher than cholesterol as discussed in the introduction section. Therefore, the rate of change in the τ_{av}values of LDS^+ with increasing A/L value is observed to be higher with increase in concentration of AmB in POPG-Chol liposomes. This indicates that the interaction of AmB with Chol in POPG liposomes is dependent on the concentration of AmB. It is interesting to note that the permeability of the POPG bilayer is increased by AmB with increased concentration of AmB. In the second regime (A/L >1), the τ_{av} values of LDS^+ for POPG, POPG-Ergo, and POPG-Chol liposomes remain almost constant at higher A/L value (the highest A/L value is 8.5). Additionally, the fluorescence spectroscopic signatures of AmB (Figures 4.8 & 4.9) show quenching of its fluorescence for all the three liposomes at pH 7.4. The results of SH and spectroscopic studies have shown that for A/L concentrations greater than unity, the membrane permeability is independent of sterols present in the liposomes. This indicates that the aggregated states of the AmB molecules in the lipid bilayer enhance the transport of the LDS^+ ions across liposomes. i.e., the permeability of POPG liposomes is increases.

The interaction of AmB with Ergo is predicted to be two types:

i) π–π electronic interactions between the two double bonds present in one of the cyclohexane rings in Ergo and the heptene moiety of AmB [212].

ii) Interaction between the positively charged amino group (present in the mycosamine part of AmB) and the hydroxyl group of Ergo [51,52].

Our second objective of the study is to investigate the effect of the functional groups charge of AmB on the transport rates of LDS^+ in POPG-Ergo liposomes. Figure 4.4 clearly shows that the effect of charge neutralization of either amino or carboxyl groups of AmB on the transport of LDS^+ is in an opposite way. Figure 4.5 provides a detailed picture on the effects of neutralization of charged functional groups of AmB. At pH 4.5, charge on the carboxylic group of AmB is neutralized. The membrane permeability of POPG-Ergo liposomes is affected drastically by unionized state (neutral form) of carboxyl group of AmB at 0.14 molecules of AmB present per liposome. At pH 11, the charge on the amino group of AmB is neutralized. The effect of unionized state (neutral form) of amino group of AmB on the membrane permeability of POPG-Ergo liposomes remains more or less similar up to a unity A/L value. For A/L values greater than unity, the membrane permeability starts to decrease rapidly due to increase in the concentration of AmB. At pH 7.4, the AmB molecule has zwitterionic characteristics. The effect of zwitterionic state of AmB on the membrane permeability is modest. Figure 4.6 demonstrates the absorption spectra of AmB in presence of POPG-Ergo liposomes in the region of 409-416 nm at pH 4.5 and 7.4. All spectrum appears similar. When pH is lowered from 11 to 4.5, the interactions between AmB and Ergo are increased. This suggests that the interactions between AmB and Ergo are pH dependent. From Figure 4.8, it is clearly observed that the pH dependent interaction of AmB with Ergo in POPG-Ergo liposomes is observed to be higher at pH 4.5 for an A/L value of 0.14. At

the maximum A/L ratio, the life time values of AmB are almost similar for all the three pH. The lifetime values of AmB in POPG-Ergo liposomes are significantly higher at the minimum A/L ratio. The observed trends in the integrated fluorescence intensity and average fluorescence lifetime of AmB in POPG-Ergo liposomes at three different pH (Figure 4.9) are similar to that of those observed in the three different POPG liposomes at pH 7.4 indicating aggregation of AmB molecules within the POPG bilayer. There is also a possibility that, as pH is lowered, the charge on AmB becomes positive. Therefore, possibility of electrostatic interaction with negatively charged POPG lipids cannot be ruled out. In this case, it is expected that the size and zeta potential of the liposomes will be affected. No changes are observed in these two parameters at the highest concentration of AmB used (275 nM for SH experiments where lipid concentration is 50 μM, 2 μM for absorption and fluorescence measurements where lipid concentration is 33.4 μM). This indicates that the possibilty of any interactions cannot be detected by our experimental setup. Therefore, based on our experimental evidence, we speculate that interaction between the positively charged amino group of AmB and the hydroxyl group of Ergo increases with lowering of pH. On the charge neutralization of the carboxyl group of AmB the interactions increase further.

4.4 Summary and conclusions

Here, the Amphotericin B induced membrane permeability of POPG liposomes as a function of membrane composition (the presence of either ergosterol or cholesterol in the membrane) is investigated using SH technique. The effect of AmB on the membrane permeability of POPG-Ergo liposomes as a function of pH variation in liposome system by the SH technique, absorption and fluorescence spectroscopy is also studied. The results of SH and spectroscopy studies of AmB suggested that the interaction between

AmB and Ergo is the main cause for the enhanced permeability of POPG-Ergo liposomes at low values of A/L. It has also been observed that the spectroscopic properties of AmB in the presence of POPG-Ergo liposomes are distinctly different from the other two liposomes indicating specific binding between AmB and Ergo. In addition to this, the effect of neutralizing two charged functional groups of AmB (amino and carboxyl) on the POPG membrane permeability using POPG-Ergo liposomes have also been investigated. It is observed that the interaction of AmB with Ergo primarily depends upon the charged amino group present in the mycosamine moiety of the antibiotic. The spectral (absorption and fluorescence) changes of AmB also supports this argument. In order to understand the alteration in the membrane permeability of AmB-Ergo system, a cartoon diagram of the AmB-Ergo sytem inside a bilayer is illustrated in Figure 4.10. As the length of the AmB-Ergo system is much lesser than the thickness of the POPG bilayer, the lipid molecules near the AmB-Ergo system adjust their positions making the bilayer thin in this region. In literature, the length of sterol-Amphotericin B complex is smaller than the bilayer thickness (~5 nm) [51, 52]. Thus, it is proposed that this is the cause for enhanced membrane permeability.

In addition to this, the results indicate that the membrane permeability of POPG liposomes and POPG-Chol liposomes in presence of AmB are also increased. But the increase is to a lesser extent at low A/L values. The cause of increased permeability of these two systems requires further investigations. Interestingly, at higher A/L value (> 1), the membrane permeability becomes similar for all the three systems. It is thus concluded that the membrane permeability of all three systems are independent of the nature of sterol present in liposomes. The spectroscopic properties of AmB at higher A/L values (>1) suggest that the aggregated states of AmB in the bilayer enhances the bilayer permeability irrespective of the bilayer composition and the pH of the liposomes

system. It is pertinent to know that the binding geometry of AmB with these liposomes needs to be investigated for a better understanding of AmB induced membrane permeability.

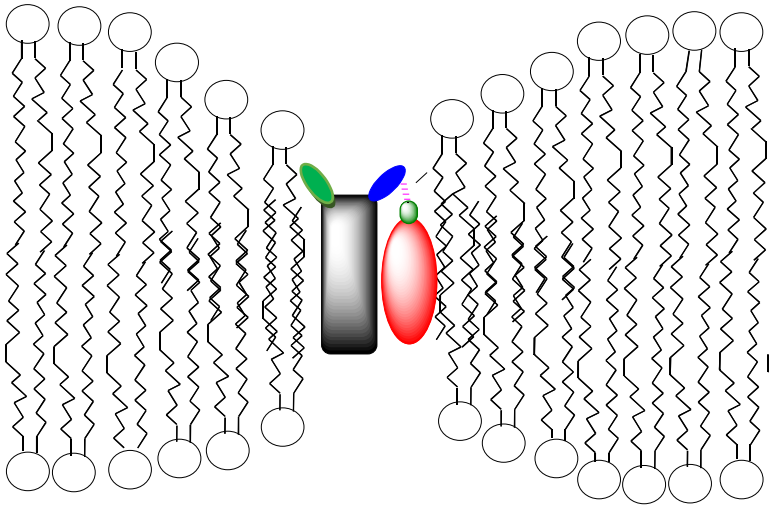

Figure 4.10*: *A schematic illustration of the AmB-Ergo molecular system in side the lipid bilayer which disturbed the ordered arrangement of lipids near to vicinity of AmB-Ergo molecular system in the POPG bilayer, hence increase the membrane permeability.

Chapter 5

pH-Dependent Interaction of Four Different Bile Salts with POPG Liposomes Studied by Dynamic Light Scattering and Second Harmonic Spectroscopy

5.1 Introduction

Bile salts are derived from cholesterol metabolism. The major structural constitutents of bile salts are two or three hydroxyl functional groups in one side and a rigid, large, hydrophobic moiety on another side (Figure 1.3). Unlike conventional surfactants, these molecules (bile salts) are facial amphiphiles as hydrophilic and hydrophobic parts are located on opposite faces [213]. Bile salts consist of convex side of a hydrophobic steroidal backbone and a hydrophilic side having hydroxyl groups on the concave side, making these molecules as facial amphiphiles. The facial representations of NaC, NaDC, UDCA, and UDCA bile salts are shown in Figure 5.1. The physiological activities of bile salts and their derivatives have been extensively studied [214] due to the fact that bile salts and their derivatives play a significant role in many physiological functions such as, digestion, adsorption of fats, solubilisation of lipids in the gut, and the excretion of cholesterol into the intestinal tract. Bile salts themselves do not initiate colonic tumors, but they enhance the induction of tumors by carcinogens [215]. Recent studies reveal that bile salts promote colorectal carcinoma by stimulation of bile acid discharge due to diets having a high content of saturated fats [216,217]. This indicates that bile acids are promoters of colorectal carcinoma, not carcinogens. Several studies suggest that the physiological function of the gastrointestinal mucosa is influenced by the

presence of several physiological molecules [218] such as bile acids. Nugent et. al. suggest that the pH of gall bladder and colon may be acidic during diseased conditions [219]. It has been observed that pH might play an important role in diseases associated with gastrointestinal tract: Measurement of pH in patients with ulcerative colitis shows that in left and right colon the pH values are acidic [219,220]. Additionally, the membrane permeability is altered by bile salts in presence of ionic species. Therefore, it would be interesting to investigate the pH dependent interaction of bile salts with lipid membranes. It gives us an idea on the role of pH in the cytotoxic effects of bile salts in colon.

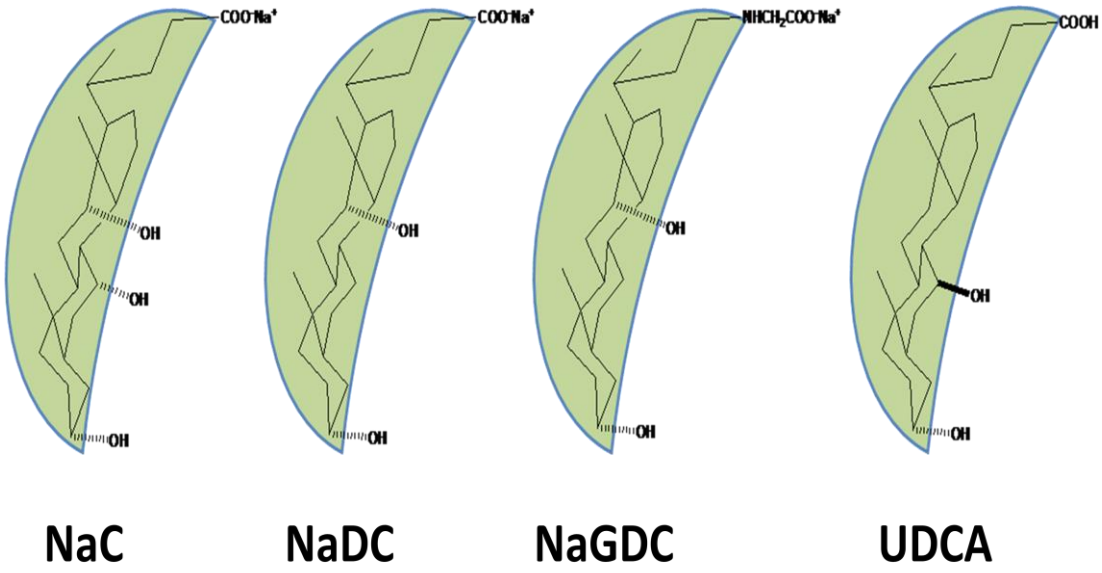

Figure 5.1: Schematic diagram of the facial structures of different bile salts (NaC, NaDC, UDCA, and UDCA). Bile salts consist of convex side of a hydrophobic steroidal backbone and a hydrophilic side having hydroxyl groups on the concave side.

In this work, the pH dependent interaction of four bile salts (sodium cholate (NaC), sodium deoxycholate (NaDC), sodium glycodeoxycholate (NaGDC), and ursodeoxycholic

acid (UDCA)) with POPG liposomes are investigated by dynamic light scattering (DLS) and interfacial second harmonic (SH) spectroscopic techniques. These four bile salt hydrophobicity indices, pK_a values and chemical properties are listed in Table 5.1. The SH and DLS studies are conducted with variation in pH of bile salt- POPG liposome-LDS^+ system from pK_a +1 to pK_a -1, where pK_a corresponds to the pK_a value of the individual bile salt. The integrity of POPG liposomes are studied using the DLS technique by monitoring the size and zeta potential of liposome in presence of bile salts. The permeability of POPG liposomes in presence of bile salts are studied using the SH technique.

Table 5.1: The different chemical properties of the four bile salts. (CMC = Critical micelle concentration).

Bile salts	Hydrophobicity indices	pK_a	CMC (mM)
NaC	0.13	5.2	9-15
NaDC	0.72	6.2	3-10
NaGDC	0.65	4.8	2.1
UDCA	-0.35	5.1	7-19

5.2 Results and Discussions

Four bile salts NaC, NaDC, NaGDC and UDCA are used for the SH studies. The hydrophobicity indices of these bile salts vary widely. The pK_a values of these salts range from 4.8 to 6.2. Thus, selecting different bile salts having wide range of pK_a values can give a comprehensive idea about the effect of pH on liposomal membrane permeability by changing the pH of bile salt- POPG liposomes system. The stock solutions of NaC, NaDC and NaGDC are prepared in milli-Q water (resistivity of 18.2 MΩ.cm at 25°C and a TOC value below 5 ppb). Since, UDCA is sparingly soluble in water, its stock so-

lution is prepared using ethanol as a solvent. Individual bile salt incubated with POPG liposomes at desired pH. Details of preparation of bile salt incubated POPG liposomes are described in Chapter 2. Briefly, an aliquot of bile salt solution is added to preformed POPG liposomes to get the required concentration of bile salt followed by incubation at room temperature for 1 hr. One hour incubation time is allowed to ensure sufficient interaction bile salts and liposomes. The SH studies have been carried out with the organic cations, MG^+ and LDS-698 (LDS^+) as a SH probe [127,140,141]. The LDS^+ ion a positively charged ion which is adsorbed on a negatively charged POPG lipid bilayer of liposome in the SH experiments. At physiological pH, sub milli-molar concentration of bile salt does not appreciably change the bilayer characteristics of liposomes [70,221]. Thus, DLS experiments are performed at different concentrations of individual bile salts present in the POPG liposomes. The effects of different concentrations of individual bile salt on the integrity of liposome can be ascertained. In order to understand the membrane permeability of liposome, the effect of pH on bile salt incubated liposomes is investigated by monitoring the transport of LDS^+ across POPG liposomes containing bile salts.

Details of the SH and hyper-Rayleigh scattering (HRS) measurements are carried out as described in Chapter 2. The effective diameter (the average size of liposome), zeta potential and polydispersity of respective bile salt incubated liposomes are measured at two different pH values: $pK_a + 1$ and $pK_a - 1$ using a Brookhaven 90 Plus size and zeta potential analyzer (Brookhaven Instrument Corp, USA). Here, the pK_a corresponds to the respective bile salt. The average size, polydispersity, and zeta potential of POPG liposomes incubated with different bile salts at two different pH are listed in Table 2.3 (Chapter 2). The studies (The SH experiments, size and zeta potential) are carried out at

pK_a+1 ensure that 90% of the molecules are present in their ionized state, i.e. in their salt form. Similarly, at pK_a-1 ensure that 90% of the molecules are present in their un-ionized state, i.e. in the acid form.

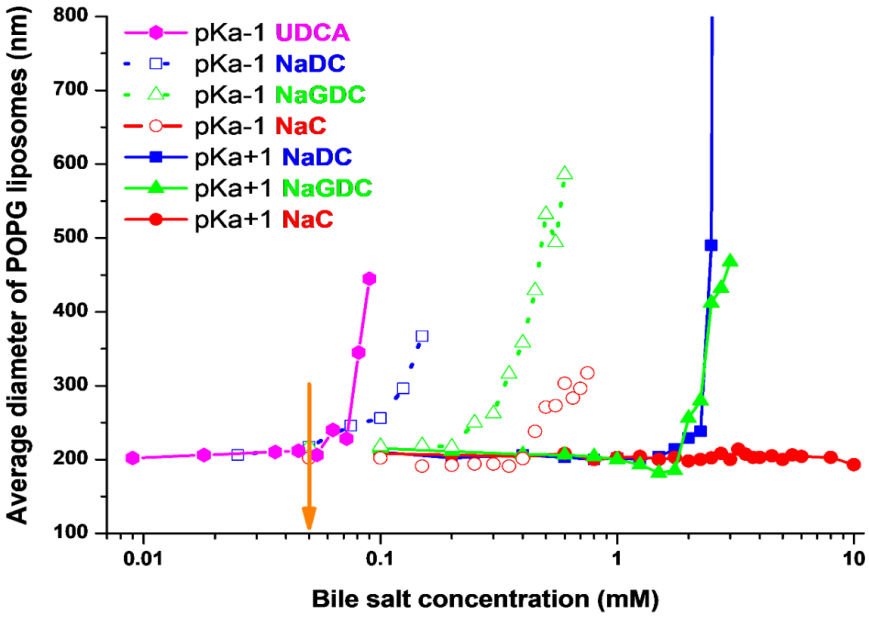

Figure 5.2: Variation in the average diameter of different POPG liposomes with bile salt concentration for four bile salts at two pH conditions. The pH of bile salt- POPG liposomes systems is selected as pK_a-1 and pK_a+1. Here, the pK_a corresponds to respective bile salt.

The Figure 5.2 describes changes in the average diameter of bile salt incubated POPG liposomes with variation in bile salt concentration for two cases: pK_a-1 and pK_a+1. The pK_a corresponds to respective bile salt. In the Figure 5.2, the X-axis is kept deliberately in logarithmic scale in order to accommodate entire range of concentrations of bile salts used. The size measurements of liposomes are carried out at pK_a +1 and pK_a -1 with increasing concentration of individual bile salt up to well below CMC of individual bile salt. It is clearly shown that the integrity of POPG liposomes is observed to be intact at

bile salt concentrations laying well below few mM (less than their critical micelle concentration, Table 5.1). It is pertinent to note that at pH (pH = pK_a+1 for UDCA bile salt), interaction of UDCA with POPG liposome cannot be studied above UDCA concentration of 100 μM. Increasing concentration of UDCA beyond this also increases the concentration of ethanol that disrupts integrity of liposome. This constraints studies at higher concentrations (> 100 μM) of UDCA in POPG liposomes. From Fig. 5.2, at pH= pKa-1, the bile salts are in their unionized (~90%) state (acidic form). The unionized state of bile salts are able to disrupt the POPG liposomes at much lower concentrations of bile salts. These values are 70 μM for UDCA and 100-400 mM for NaGDC, NaC, and NaDC. It is clearly observed that bile salt concentration has significant effect on the integrity of POPG liposomes. Thus, the integrity of liposome may be compromised at higher concentration of bile salts. Therefore, each bile salt concentration of 50 μM is selected for all SH studies. Thus, it is ensured that structural integrity of POPG liposome remains undisturbed at any of the concentrations of bile salt used in this study. In order to get an idea how this bile salt-bile acid transformation affects the permeability of the POPG liposomes in presence of bile salts.

The SH experimental procedure is briefly explained here. The SH studies are carried out at a fixed temperature by a Neslab (JULABO Labortechnik GmbH, Germany) circulating water chiller having a temperature accuracy of ± 1 ^{0}C. The SH experiments are performed as per the given procedure. A concentration of 50 μM of the respective bile salt incubated in POPG liposomes suspension is added into the solution having 5 μM LDS^+ ions in the cuvette. There is an instantaneous increase (< 1 second) in SH intensity due to the electrostatic adsorption of positively charged LDS^+ ions onto a negatively charged outer surface of POPG liposomes as demonstrated earlier [141]. After the addition of

POPG liposomes to the solution containing LDS^+, the SH electric field of ($E_{2\omega}$) of LDS^+ gradually decreases with time. This indicates the transport of LDS^+ ions from the outer lipid bilayer to the inner lipid bilayer of POPG liposomes. The measured experimental data can be converted to the SH electric field then it is fitted to exponential decay functions per following equation 1.12. The transport time constant (τ values) are extracted by exponential fitting of the decay curves of the SH electric field of LDS^+ ion and calculated τ_{av} values. The SH decay curve is fitted from their maximum value of the SH electric filed ($E_{2\omega}$) i.e. just after addition of the liposomes to the buffer solution containing LDS^+ ions.

Figure 5.2 describes time dependent changes in the SH electric field of LDS^+ ($E_{2\omega}$) under different POPG liposomes at two different pH: pH: 7.4 (top) and 5.0 (bottom). The bile salt-liposomes suspension is added to buffer solution containing the LDS^+ ions (5 µM) at 50 seconds.

These different liposomes systems are: The black curve represents the SH electric field of LDS^+ ions across the POPG liposomes (control, i.e., without bile salt). Similarly,

The red curve represents the SH electric field of LDS^+ ions across the 50 µM of NaC bile salt incubated in POPG liposomes.

The blue curve represents the SH electric field of LDS^+ ions across the 50 µM of NaDC bile salt incubated in POPG liposomes.

The green curve represents the SH electric field of LDS^+ ions across the 50 µM of NaGDC bile salt incubated in POPG liposomes.

The pink curve represents the SH electric field of LDS^+ ions across the 50 µM of UDCA bile salt incubated in POPG liposomes

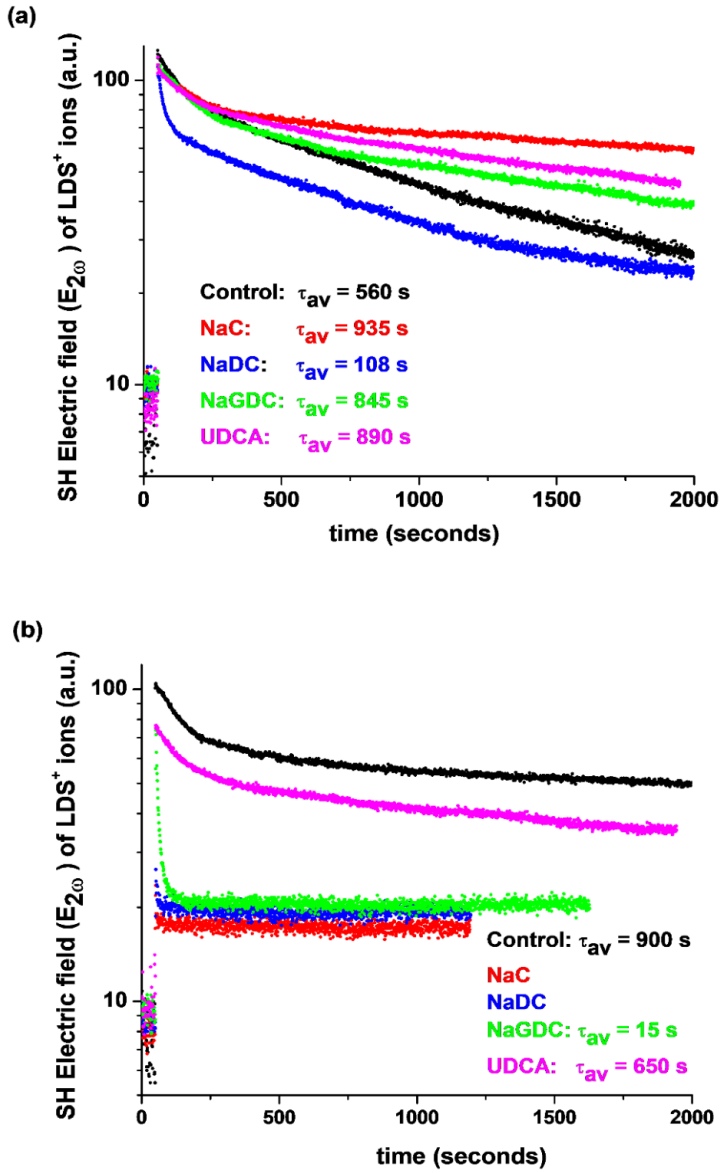

Figure 5.3: Time dependent changes in the SH electric field of LDS^+ ($E_{2\omega}$) under different liposomes systems at two different pH: pH: 7.4 (top) and 5.0 (bottom). The liposome systems are POPG liposomes and respective bile salt (NaC, NaDC, NaGDC, and UDCA) incubated POPG liposomes. The liposomes suspension is added to buffer solution containing the LDS^+ ions (5 µM) at 50 seconds.

From Figure 5.3, it is clearly shown that pH has a significant effect on the transport of LDS^+ ions across POPG liposomes containing bile salts. The fitted parameters are

obtained from decay of SH electric field of LDS^+ after addition of individual bile salt incubated POPG liposomes to the buffer solution containing LDS^+ ions. The τ_{av} values of LDS^+ in all the POPG liposomes systems have been summarized in the Table 5.2.

Table 5.2: Summarizes the average transport time constants (τ_{av}, in seconds) of LDS^+ across the different POPG liposomes at two different pH.

Liposome + Bile salts	pH 7.4 (τ_{av}, sec.)	pH 5 (τ_{av}, sec.)
POPG only	560	900
POPG + NaC	963	-
POPG + NaDC	108	-
POPG + NaGDC	845	15
POPG + UDCA	890	650

At physiological pH -7.4, the results are demonstrated that the τ_{av} values of LDS^+ in POPG liposomes with bile salt are more predominant as compared to POPG liposomes without bile salts (bile salt free POPG liposomes). The τ_{av} values of LDS^+ increase ~1.6 times in the POPG liposomes with NaGDC bile salt as comapared to POPG liposomes. The similar change is observed in NaC bile salt present in POPG liposomes and UDCA bile salt in POPG liposomes. But, In case of NaDC τ_{av} of LDS^+ decreases by 5 fold (from Figure 5.2). When pH of the system is reduced to pH 5.0, τ_{av} values of LDS^+ transport across POPG liposomes in presence of bile salts are significantly affected for NaC, NaDC, and NaGDC bile salts. The τ_{av} values of LDS^+ reduces by a factor of ~60 in each of NaGDC bile salt. The relative decrease of τ_{av} caused by NaC and NaDC in liposomes is very fast and difficult to detect (time resolution of the setup is one second). Interestingly, for UDCA, the changes in the τ_{av} values at pH 5.0 are modest. The results

presented in Figure 5.3 suggest that the pH of bile salt-liposome-LDS^+ system has profound effect on the membrane permeability of POPG liposomes against LDS^+ ions. The permeability of LDS^+ ions variation with pH depends on the bile salt-bile acid transformation. We perform SH studies of bile salt- POPG liposome-LDS^+ system for a range of pH values from $pK_a + 1$ to $pK_a - 1$ with increment of 0.2 pH units.

Figure 5.4 & 5.5 describe time dependent changes in the SH electric field of LDS^+ ($E_{2\omega}$) before and after addition of POPG liposomes with individual bile salt (50 μM) to the buffer solution containing LDS^+ (5 μM) for four different bile salts. (a) NaDC, (b) NaC, (c) NaGDC and (d) UDCA. The transport time constants (τ_{av}) are extracted by exponential fitting of the decay curves of the SH electric field of LDS^+ in POPG liposomes with bile salts. The lifetime values have an error of 10%. The τ_{av} values of LDS^+ in all the POPG liposomes systems are summarized in the Table 5.3. The τ_{av} of the LDS^+ ions are used for plotting the variations in pH of bile salt-POPG liposomes system as shown in Figure 5.6. In Figure 5.4 & 5.5, it is clearly observed that the pH dependent changes in the transport of LDS^+ are similar for three liposome-bile salt system (NaC, NaDC and NaGDC) and it is different for UDCA bile salt.

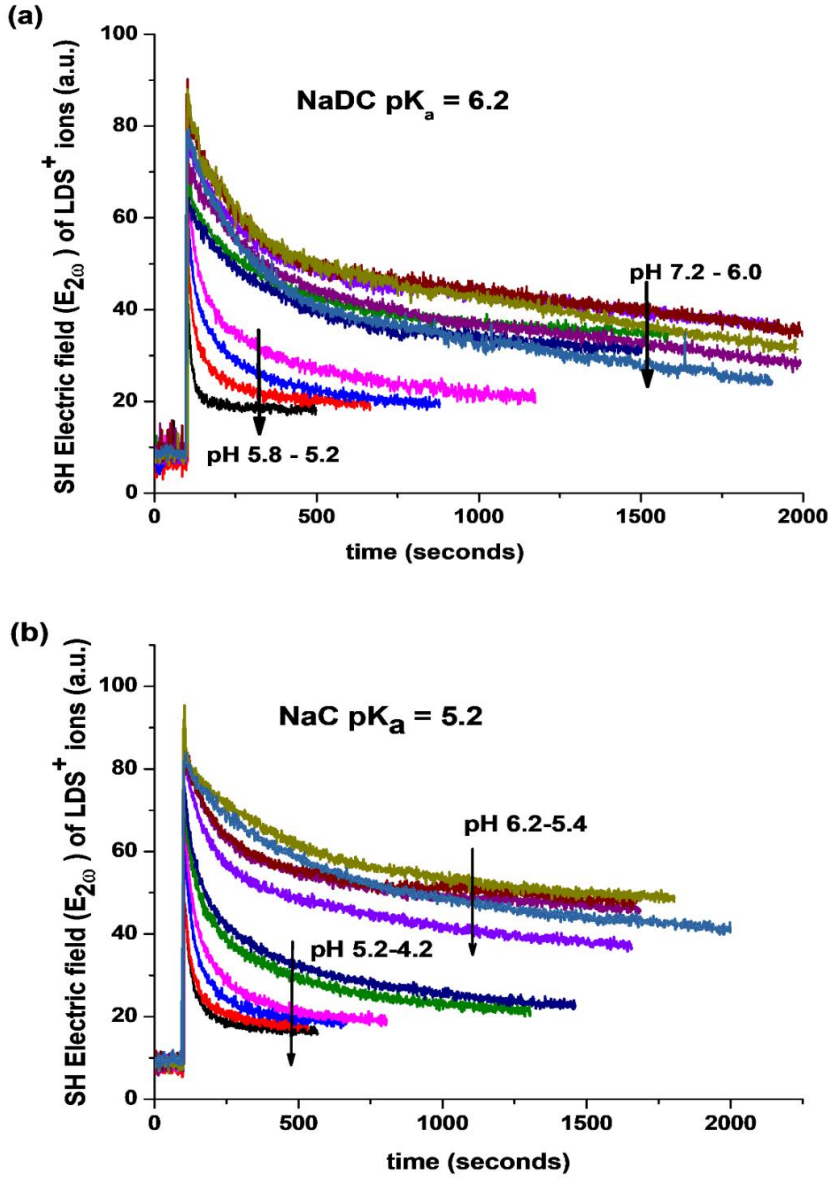

Figure 5.2: Time dependent changes in the SH electric field of LDS^+ ($E_{2\omega}$) are observed in POPG liposomes incubated with respective bile salt. (a) 50 µM of NaDC, (b) 50 µM of NaC. The pH of bile salt-liposomes system is varied in the range of pH values from pK_a + 1 to pK_a -1 with increment of 0.2 pH units. The liposomes suspension is added to buffer solution containing the LDS^+ ions (5 µM) at 50 seconds. The legends are colour matched with the data for clarity.

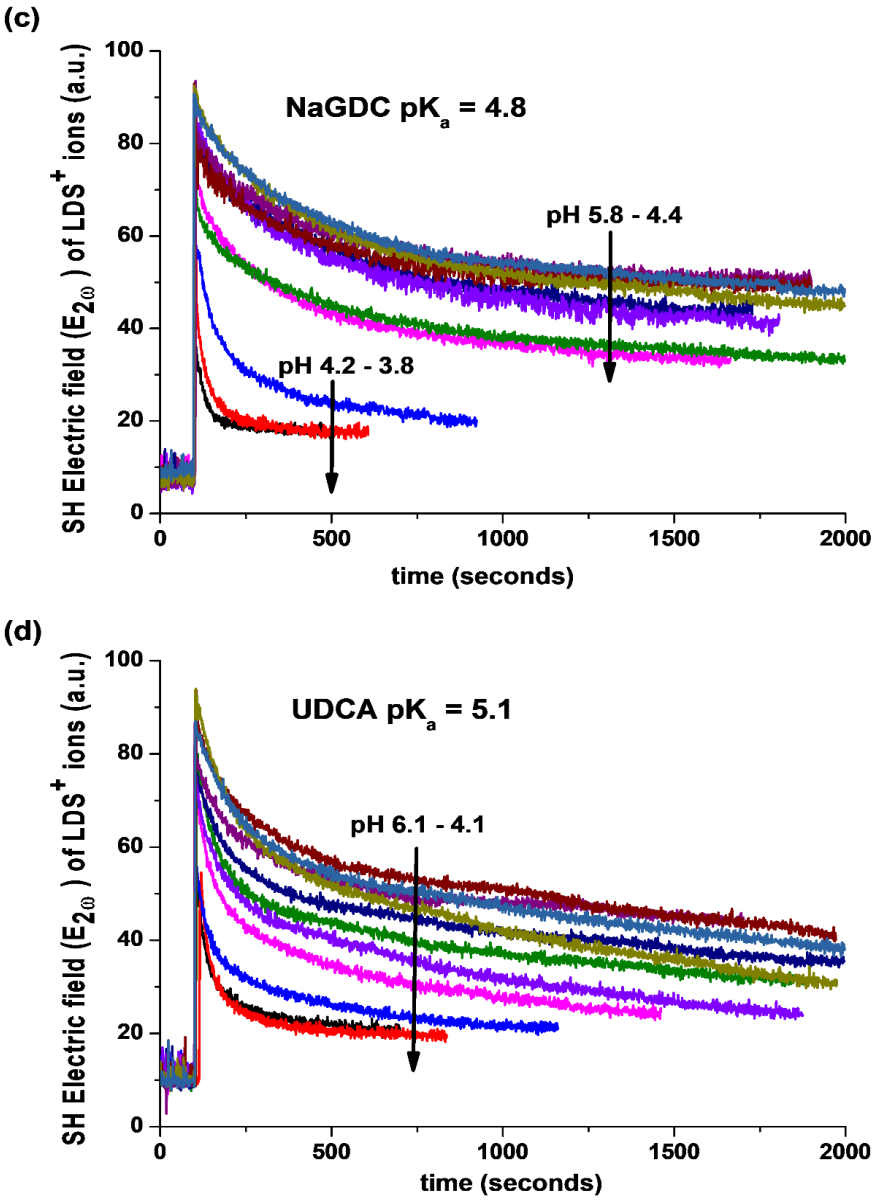

Figure 5.3 : Time dependent changes in the SH electric field of LDS^+ ($E_{2\omega}$) are observed in POPG liposomes incubated with respective bile salt. (c) 50 µM of NaGDC, (d) 50 µM of UDCA. The pH of bile salt-liposomes system is varied in the range of pH values from pK_a + 1 to pK_a -1 with increment of 0.2 pH units. The liposomes suspension is added to buffer solution containing the LDS^+ ions (5 µM) at 50 seconds. The legends are colour matched with the data for clarity.

The observed change in the decay curves of the SH electric field of LDS^+ ($E_{2\omega}$) with variation in pH of bile salt-liposome-LDS^+ system indicate of two distinct regimes for NaC, NaDC, and NaGDC bile salts. These two regimes are followed by below pK_a and above pK_a value of bile salt. A sudden change occurs around pK_a value of the individual bile salt is also seen in Fig. 5.4 & 5.5. Where as, in case of UDCA bile salt, there is a gradual decrease in the decay of the $E_{2\omega}$ with decrease in pH. Since UDCA bile salt is the most hydrophobic of the four bile salts studied. The higher hydrophobicity [219] of UDCA might account for the observed $E_{2\omega}$ trends in Figure 5.5 (d).

Table 5.3: Summarizes the average transport time constants ($\tau_{av,}$ in seconds) of LDS^+ across the different bile salt-POPG liposomes. The pH of bile salt-liposomes system is varied in the range of pH values from pK_a + 1 to pK_a -1 with increment of 0.2 pH units.

NaC		NaDC		NaGDC		UDCA	
pH	τ_{avg} (sec.)	pH	τ_{avg} (sec.)	pH	τ_{avg} (sec.)	pH	τ_{avg} (sec.)
6.2	673.5	7.2	669.78	5.8	548.75	6.1	578.31
6	543.81	7.0	721.72	5.6	616.55	5.9	530.76
5.8	366.59	6.8	560.58	5.4	235.63	5.7	526.86
5.6	398.17	6.6	778.42	5.2	350.77	5.5	359.87
5.4	517.53	6.4	556.06	5	615.37	5.3	240.02
5.2	94.74	6.2	506.75	4.8	583.07	5.1	271.32
5	70.63	6.0	132.63	4.6	286.2	4.9	159.18
4.8	25.38	5.8	55.23	4.4	225.67	4.7	89.91
4.6	24.67	5.6	26.18	4.2	62.47	4.5	46.08
4.4	27.60	5.4	19.57	4	24.99	4.3	23.30
4.2	23.67	5.2	11.00	3.8	22.67	4.1	22.98

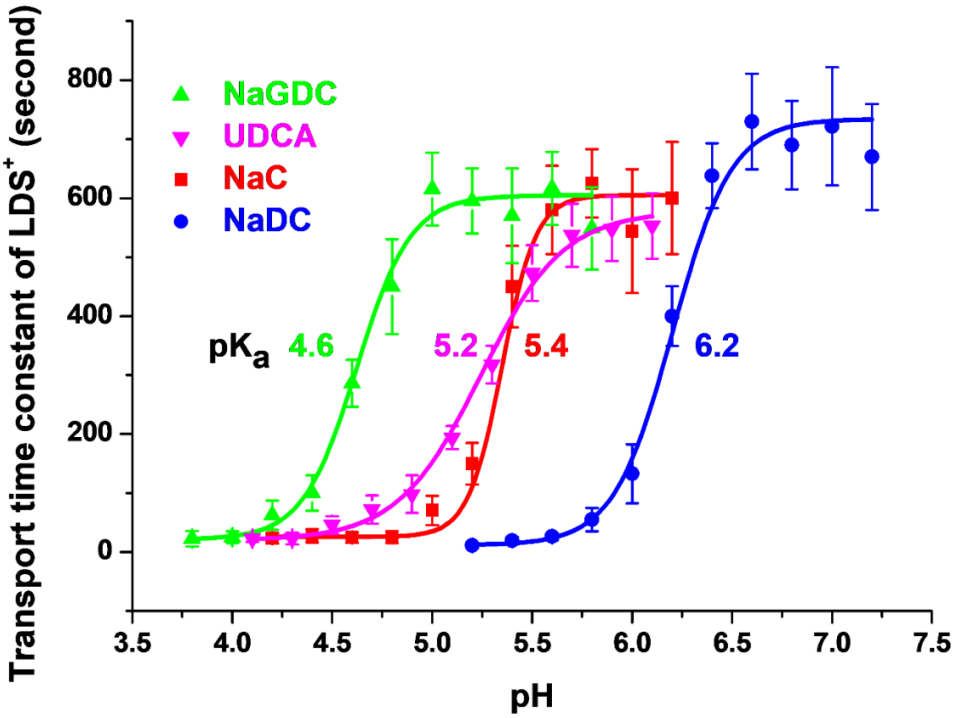

Figure 5.4: Changes in the average transport time constants (τ_{av}) of LDS^+ ions with variation in the pH of bile salt-POPG liposomes system. The pH of bile salt-liposomes system is varied in the range of pH values from pK_a + 1 to pK_a -1 with increment of 0.2 pH units. Where, the pK_a corresponds to respective bile salt. The data points are fitted with a sigmoidal function. The inflexion points are mentioned in the graph for each bile salts and they match closely with their respective pK_a.

Finally, figure 5.6 describes the τ_{av}values of the LDS^+ ions across POPG liposomes in the presence of bile salts with variation in pH. The trends in the τ_{av} values with decreasing pH is clearly demonstrate in the "S" shape curve for all four bile salts. The τ_{av} values of the LDS^+ data set is fitted with a sigmoidal function for each bile salt. The point of inflection is obtained from fitting parameters. The point of inflection matches closely with the pK_a of corresponding bile salt. A sharp transition decay is observed for three bile salts NaC, NaDC, and NaGDC bile salts whereas, it is gradual for UDCA bile salt. From figure 5.6, it is observed that as pH varies from pK_a+1 to pK_a-1for each bile

salt, the τ_{av} values of LDS^+ decrease. The bile salts in their neutral form are more conducive in enhancing the permeability of the POPG membrane as compared to the bile salts in ionic form. There is increased interest in the investigation of the cytotoxic effect of bile salts in colon epithelial cells. The main targets of bile acids within the gastrointestinal tract are epithelial cells [222] and these cells are known to be transformed to cancerous. High content of saturated fats in diet produces elevated levels of bile acids in the colonic lumen. As bile acid concentration in the colonic lumen increases, there may be an increase in cytotoxic effects of bile acids [223]. In addition to this, the epidemiologic studies reveal that for an increase in high serum or fecal bile acid concentrations, there is an increased risk of colorectal cancer [224]. Therefore, at lower concentration level, the physiological activity of bile acids are cytoprotective (physiological detergents and regulators of cell fate and signal). However, at higher concentration level, these are cytotoxic. The bile acids are considered as tumor-promoting agents in colorectal cancer development [225].

The concentrations of bile acids in the final tract of the colon is low under physiological conditions. The concentration of bile salts is higher in the gallbladder (~300 mM) and the small intestine (~10 mM). Under pathological circumstances or fat-rich diet, there might be concentrations of bile salts as high as 1 mM in cecum or in fecal. Under these conditions, the concentration of NaDC can reach values around 700–800 μM [226]. Based on our results it can be safely speculated that high concentration of NaDC plays a crucial role in membrane damage (changing the membrane permeability). We know that the role of pH in the colon is of vital importance. Since the colonic pH remains slightly acidic (~ 6.0), it is perhaps worthwhile to speculate that in this condition NaDC have more cytotoxic effects and are followed by NaC. The other two NaGDC and UDCA bile

salts do not affect the membrane integrity. Our results thus point out one aspect of bile salt induced cytotoxicity is by damaging the membrane integrity.

5.3 Summary and conclusions

In this chapter, the effect of bile acid – bile salt transformation on the permeability and integrity of POPG liposomes have been investigated by DLS and SH spectroscopy. Our results suggest that the bile salts in their neutral form are much superior for alteration of the POPG membrane properties as compared to their in ionic form. As pH of the colon is slightly acidic, the bile salts are considered to be responsible for colorectal cancer. Our results indicate that out of the four bile salts, NaDC and NaC bile salts affect the colon by altering the membrane properties causing cellular damage.

Chapter 6

Summary and future prospective

In this thesis, the interactions of amphiphilic molecules with a membrane lipid bilayer have been investigated. To monitor the adsorption and transport of an organic cation (LDS^+) across the lipid bilayer in real time we have used the interfacial specific second harmonic (SH) spectroscopic technique. Amphiphilic molecules like pluronic polymers, the antibiotic Amphotericin B, and bile salts have been used in thesis. The LDS^+ ion has been employed as an optical SH probe in the SH studies due to a strong second-order non linearity at the wavelength (800 nm) of a Ti-sapphire laser generating femtosecond pulses (pulse width ~150 fs). The SH spectroscopic studies have been performed using the quasi-CW output of the Ti-sapphire by tuning the laser wavelength to 800 nm and detecting the SH intensity at 400 nm.

Pluronic polymers (F-127, F-68 and L-61) induced membrane permeability of the POPG liposomes have been investigated. In this study, the effect of the variation in the length of either hydrophilic (poly-ethylene oxide, PEO) or hydrophobic (poly-propylene oxide, PPO) units in the polymer by the membrane transport of LDS^+ ion was studied. The individual PPO and PEO units of the polymer were observed to play a key role in deciding the membrane permeability. The transportof LDS^+ ions across the POPG lipid bilayer was observed to depend critically on the length of the hydrophobic (PO) segment present in the polymer. This has been attributed to the significant alteration in the bilayer packing near the vicinity of the adsorbed polymer. The change was more pronounced for the polymer unit with longer hydrophobic (PO) segment. In addition, the role of polymer structure and temperature on the insertion and location of the hydrophobic part

(PPO) of the polymer inside the membrane were also investigated by monitoring the transport of the LDS^+. The most hydrophobic of the series, was observed to insert itself spontaneously into the bilayer. The results obtained in this study are expected to provide further insight into the nature of pluronic polymer induced membrane permeability.

In this study, the membrane permeability induced by the polyene antibiotic Amphotericin B (AmB) in the negatively charged POPG liposome bilayer containing either ergosterol (Ergo) or cholesterol (Chol) by monitoring the bilayer transport of the LDS^+ has been investigated. The transportof LDS^+ ions across the lipid bilayer with and without sterol was observed to depend on Amphotericin B/Liposome (A/L) ratio. The transport of LDS^+ ions across the POPG lipid bilayer with and without sterol falls into two kinetic regimes. In the first regime, at low A/L value, the transport of LDS^+ ions across with and without sterol incorporated POPG lipid bilayer decreases linearly with different slopes. The membrane permeability of ergosterol incorporated POPG liposomes was higher compared to cholesterol incorporated POPG liposomes and only POPG liposomes. The interaction between AmB and Ergo was found to be responsible for the enhanced bilayer permeability. In the second regime, at higher the A/L value, the bilayer permeability becomes independent of the nature of sterol. The results suggest that with increasing A/L value, the aggregated states of AmB in the bilayer which enhances the bilayer permeability irrespective of the bilayer composition. The spectral (absorption and fluorescence) changes of AmB in liposomes also support this argument. It was observed that interaction of AmB with Ergo is primarily dependent upon the charged amino group present in the mycosamine moiety of the antibiotic. We believe that these results will help further understand the action of the antibiotic present in a bilayer.

We have also studied the pH dependent interactions of four bile salts with the negatively charged POPG liposomes. The results indicate that in their neutral form (i.e bile acids), these are able to alter the POPG membrane properties significantly more compared to their ionic (i.e. bile salts) form. Therefore, one of the pathways of bile salt induced cytotoxicity in the gastrointestinal tract, may occur due to the potential membrane damaging action of these bile salts at acidic pH.

Thus in the present thesis three important aspects related to the liposomes composition such as copolymer composition, sterol incorporate liposomes, and pH on the transport of probe molecules have been investigated mainly by SH spectroscopy and also supported by other spectroscopic tools. The results presented in the thesis find utility in understanding the transport of many important biomolecules across the cell membranes.

Future directions:

These results show the potential of SH spectroscopy as an important tool to understand, the nature of the interactions and the manner in which amphiphilic molecules are able to alter the membrane permeability of the POPG liposome bilayer. In order to get a more comprehensive picture, the interaction of amphiphilic molecules with the lipid head group needs to be investigated in more detail. For example, it is important to know the binding geometry of AmB with these liposomes. Such studies provide insights about the molecular mechanism behind how these molecules are able to induce membrane permeability.

References

1. Lodish, H.; Berk, A.; Zipurshy, S. L; Kaiser, C. A.; Krieger, M.; Bretscher, A. *Molecular Cell Biology*; W H Freeman, **2000**.
2. Gennis, R. B. *Biomembranes-Molecular Structure and Function*; Springer- Verlag, New York, **1989**.
3. Winkle, L. J. V.; Bussolati, O.; Gazzola, G.; McGiven, j.; Mackenzie, B.; Saier, M. H.; Taylor, P. M.; Rennie, M. J.; Low, S. Y. *Biomembrane Transport*, Vol 1.; Academic Press Inc., **1999**.
4. Chapman. D. *Liposomal Technol.* **1983**, *1*, 1–18.
5. Bangham, A. D.; Hill, M. W. . M. N. G. A. *Methods in Membrane Biology*; Springer USA, **1974**.
6. Seydel, J. K.; Wiese, M. *Drug-Membrane Interactions*; Weinheim, Wiley-VCH Verlag GmbH, **2002**.
7. Przestalski, S.; Sarapuk, J.; Kleszczyńska, H.; Gabrielska, J.; Hładyszowski, J.; Trela, Z.; Kuczera, J. *Acta Biochim. Pol.* **2000**, *47* (3), 627–638.
8. Lyubartsev, A. P.; Rabinovich, A. L. *Soft Matter* **2011**, *7* (1), 25–39.
9. Loura, L. M. S.; Ramalho, J. P. P. *Molecules* **2011**, *16* (7), 5437–5452.
10. Gumbart, J. C.; Roux, B.; Chipot, C. *J. Chem. Theory Comput.* **2013**, *9* (1), 794–802.
11. Marie, E.; Sagan, S.; Cribier, S.; Tribet, C. *J. Membr. Biol.* **2014**, *247* (9–10), 861–881.
12. Pan, A. C.; Xu, H.; Palpant, T.; Shaw, D. E. *J. Chem. Theory Comput.* **2017**, *13* (7), 3372–3377.
13. Peetla, C.; Stine, A.; Labhasetwar, V. *Mol. Pharm.* **2009**, *6* (5), 1264–1276.
14. Sun, Y.; Lee, C. C.; Hung, W. C.; Chen, F. Y.; Lee, M. T.; Huang, H. W. *Biophys. J.* **2008**, *95* (5), 2318–2324.
15. Nussio, M. R.; Sykes, M. J.; Miners, J. O.; Shapter, J. G. *Langmuir* **2009**, *25* (2), 1086–1090.
16. Nerdal, W.; Gundersen, S. A.; Thorsen, V.; Høiland, H.; Holmsen, H. *Biochim. Biophys.*

Acta - Biomembr. **2000**, *1464* (1), 165–175.

17. Paloncýová, M.; Devane, R.; Murch, B.; Berka, K.; Otyepka, M. *J. Phys. Chem. B* **2014**, *118* (4), 1030–1039.
18. Nussio, M. R.; Sykes, M. J.; Miners, J. O.; Shapter, J. G. *ChemMedChem* **2007**, *2* (3), 366–373.
19. Batrakova, E. V.; Kabanov, A. V. *J. Control. Release* **2008**, *130* (2), 98–106.
20. Kabanov, A. V; Batrakova, E. V; Yu, V. **2002**, *82*, 189–212.
21. Pitto-Barry, A.; Barry, N. P. E. *Polym. Chem.* **2014**, *5* (10), 3291–3297.
22. Kabanov, A. V; Lemieux, P.; Vinogradov, S.; Alakhov, V. *Adv. Drug Deliv. Rev.* **2002**, *54* (2), 223–233.
23. Alexandridis, P.; Lindman, B. *Amphiphilic Block Copolymers-Self-Assembly and Applications*; Elsevier Science B.V., **2000**.
24. Rey-Rico, A.; Cucchiarini, M. *Int. J. Mol. Sci.* **2018**, *19* (3), 777–790.
25. Huin, C.; Gall, T. Le.: Barteau, B.; Pitard, B.; Montier, T.; Lehn, P.; Cheradame, H.; Guégan, P. *J. Gene Med.* **2011**, *13*, 538–548.
26. Yang, Z.; Sahay, G.; Sriadibhatla, S; Kabanov, A. V. *Bioconjug Chem.* **2008**, *19* (10), 1987–1994.
27. Binder, W. H.; Barragan, V.; Menger, F. M. *Angew. Chemie - Int. Ed.* **2003**, *42* (47), 5802–5827.
28. Schulz, M.; Olubummo, A.; Binder, W. H. *Soft Matter* **2012**, *8* (18), 4849–4864.
29. Yaroslavov, A. A.; Melik-Nubarov, N. S.; Menger, F. M. *Acc. Chem. Res.* **2006**, *39* (10), 702–710.
30. Melik-Nubarov, N. S.; Pomaz, O. O.; Dorodnych; Badun, G. A.; Ksenofontov, A. L.; Schemchukova, O. B.; Arzhakov, S. A. *FEBS Lett.* **1999**, *446* (1), 194–198.
31. Wu, G.; Khant, H. A.; Chiu, W.; Ka Yee C. Lee. *Soft Matter* **2009**, *5* (7), 1496–1503.
32. Wu, G.; Lee, K. Y. C. *J. Phys. Chem. B* **2009**, *113* (47), 15522–15531.
33. Hezaveh, S.; Samanta, S.; De Nicola, A.; Milano, G.; Roccatano, D. *J. Phys. Chem. B*

2012, *116* (49), 14333–14345.

34. Rabbel, H.; Werner, M.; Sommer, J. U. *Macromolecules* **2015**, *48* (13), 4724–4732.
35. Ileri Ercan, N.; Stroeve, P.; Tringe, J. W.; Faller, R. *Langmuir* **2016**, *32* (39), 10026–10033.
36. Kayser, A. L. . A. F. K. . O. *Appl Microbiol Biotechnol* **2005**, *68*, 151–162.
37. Nicolaou, K. C.; Daines, R. A.; Uenishi, J.; Li, W. S.; Papahatjis, D. P.; Chakraborty, T. K. *J. Am. Chem. Soc* **1988**, *110*, 4672–4685.
38. Ghannoum, M. A.; B.Rice, L. *Clin. Microbiol. Rev.* **1999**, *12* (4), 501–517.
39. Brajtburg, J.; Powderly, W. G.; Kobayashi, G. S.; Medoff', G. *Antimicrob. Agents Chemotherpy* **1990**, *34* (2), 183–188.
40. Gallis, H. A.; Drew, R. H.; Pickard, W. W. *Rev. Infect. Dis.* **1990**, *12* (2), 308–329.
41. Odds, F. C.; Brown, A. J. P.; Gow, N. A. R. *Trends Microbiol.* **2003**, *11* (6), 272–279.
42. De Kruijff, B.; Demel, R. A. *Biochim. Biophys. Acta* **1974**, *339*, 57–70.
43. Neumann, A.; Baginski, M.; Czub, J. *J. Am. Chem. Soc.* **2010**, *132* (51), 18266–18272.
44. Baginski, M.; Resat, H.; McCammon, J. A. *Mol. Pharmacol.* **1997**, *52* (4), 560–570.
45. Hsuchen, C. C.; Feingold, D. S. *Antimicrob. Agents Chemother.* **1973**, *4* (3), 309–315.
46. Gary-Bobo, C. M. *Bohemia* **1989**, *71*, 37–47.
47. Teerlink, T.; de Kruijff, B.; Demel, R. A. *Biochim. Biophys. Acta - Biomembr.* **1980**, *599* (2), 484–492.
48. Foglia, F.; Fragneto, G.; Clifton, L. A.; Lawrence, M. J.; Barlow, D. J. *Langmuir* **2014**, *30* (30), 9147–9156.
49. Nakagawa, Y.; Umegawa, Y.; Takano, T.; Tsuchikawa, H.; Matsumori, N.; Murata, M. *Biochemistry* **2014**, *53* (19), 3088–3094.
50. Bolard, J. *Biochim. Biophys. Acta* **1986**, *864* (3), 257–304.
51. Palacios, D. S.; Dailey, I.; Siebert, D. M.; Wilcock, B. C.; Burke, M. D. *Proc. Natl. Acad. Sci.* **2011**, *108* (17), 6733–6738.
52. Gray, K. C.; Palacios, D. S.; Dailey, I.; Endo, M. M.; Uno, B. E.; Wilcock, B. C.; Burke,

M. D. *Proc. Natl. Acad. Sci.* **2012**, *109* (7), 2234–2239.

53. Umegawa, Y.; Tahara, K.; Matsumori, N.; Nakagawa, Y.; Murata, M.; Tsuchikawa, H.; Oishi, T. *Biochemistry* **2012**, *51* (1), 83–89.
54. Hamilton-Miller, J. M. T. *Bacteriol. Rev.* **1973**, *37* (2), 166–196.
55. Vlahcevic, Z. R.; Pandak, W. M.; Stravitz, R. T. *Gastroenterol. Clin. North Am.* **1999**, *28* (1), 1–25.
56. Martin, G, P.; El-Hariri, L. M.; Marriott, C. *J. Pharm. Pharmacol.* **1992**, *44*, 646–650.
57. Garidel, P.; Hildebrand, A.; Knauf, K.; Blume, A. *Molecules* **2007**, *12*, 2292–2326.
58. Kazuo Chijiiwa; Minako Nagai. *Biochim. Biophys. Acta* **1989**, *1001* (2), 111–114.
59. Chijiiwa, K.; Nagai, M. *Arch. Biochem. Biophys.* **1989**, *270* (2), 472–477.
60. Vlahcevic, Z. R.; Gurley, E. C.; Heuman, D. M.; Hylemon, P. B. *J Lipid Res* **1990**, *31* (6), 1063–1071.
61. Schubert, R.; Jaroni, H.; Schoelmerich, J.; Schmidt, K. H. *Digestion* **1983**, *28*, 181–190.
62. Schubert, R.; Schmidt, K. heinz. *Biochemistry* **1988**, *27* (24), 8787–8794.
63. Acta, A. K. B. B.; Schubert, R.; Beyer, K.; Wolburg, H.; Schmidt, K. *Biochemistry* **1986**, *25*, 5263–5269.
64. Sreekanth, V.; Bajaj, A. *J. Phys. Chem. B* **2013**, *117* (40), 12135–12144.
65. Thakur, R.; Das, A.; Adhikari, C.; Chakraborty, A. *Phys. Chem. Chem. Phys.* **2014**, *16* (29), 15681–15691.
66. Esteves, M.; Ferreira, M. J.; Kozica, A.; Fernandes, A. C.; Gonçalves Da Silva, A.; Saramago, B. *Langmuir* **2015**, *31* (32), 8901–8910.
67. Mahajan, S.; Mahajan, R. K. *J. Colloid Interface Sci.* **2012**, *387* (1), 194–204.
68. Sen, S.; Paul, B. K.; Guchhait, N. *J. Colloid Interface Sci.* **2017**, *505*, 266–277.
69. Yadav, T.; Tikariha, D.; Sinha, S.; Ghosh, K. K. *J. Mol. Liq.* **2017**, *233*, 23–28.
70. Mohapatra, M.; Mishra, A. K. *J. Phys. Chem. B* **2010**, *114* (46), 14934–14940.
71. Aamson, A. W. *Physical Chemistry of Surfaces*, 4th ed.; Wiley: New York, **1982**.
72. Bloembergen, N. *Nonlinear Optics*; Wiley: New York, **1965**.

73. Dick, B.; Gierulski, A.; Marowsky, G.; Reider, G. A. *Appl. Phys. B Photophysics Laser Chem.* **1985**, *38* (2), 107–116.

74. Dick, B. *Chem. Phys.* **1985**, *96* (2), 199–215.

75. Williams, D. J. E. In *ACS Symposium Series 233; American Chemical Society*; Washington, DC, **1985**.

76. Felderhof, B. U.; Marowsky, G. *Appl. Phys. B Photophysics Laser Chem.* **1987**, *44* (1), 11–17.

77. Mizrahi, V.; Sipe, J. E. *J. Opt. Soc. Am. B* **1988**, *5* (3), 660–667.

78. Richmond, G. L.; Robinson, J. M.; Shannon, V. L. *Prog. Surf. Sci.* **1988**, *28* (1), 1–70.

79. Shen, Y. R. *Annu. Rev. Phys. Chem.* **1989**, *40* (1), 327–350.

80. Marlow, F.; Werner, L.; Hill, W. *Surf. Sci.* **1991**, *249* (1–3), 365–372.

81. Eisenthal, K. *Annu. Rev. Phys. Chem.* **1992**, *43* (1), 627–661.

82. Corn, R. M.; Higgins, D. A. *Chem. Rev.* **1994**, *94* (2), 107–125.

83. Bain, C. D. *J. Chem. Soc. Faraday Trans.* **1995**, *91* (9), 1281–1296.

84. Luca, A. A. T.; Hebert, P.; Brevet, P. F.; Girault, H. H. *J. Chem. Soc. Faraday Trans.* **1995**, *91* (12), 1763–1768.

85. Eisenthal, K. B. *Chem. Rev.* **1996**, *96* (4), 1343–1360.

86. Eisenthal, K. B. *Chem. Rev.* **2006**, *106* (4), 1462–1477.

87. Bredenbeck, J.; Ghosh, A.; Nienhuys, H. K.; Bonn, M. *Acc. Chem. Res.* **2009**, *42* (9), 1332–1342.

88. Johnson, C. M.; Baldelli, S. *Chem. Rev.* **2014**, *114* (17), 8416–8446.

89. Roy, S.; Covert, P. A.; Fitzgerald, W. R.; Hore, D. K. *Chem. Rev.* **2014**, *114* (17), 8388–8415.

90. Yan, E. C. Y.; Fu, L.; Wang, Z.; Liu, W. *Chem. Rev.* **2014**, *114* (17), 8471–8498.

91. Nihonyanagi, S.; Yamaguchi, S.; Tahara, T. *Chem. Rev.* **2017**, *117* (16), 10665–10693.

92. Franken, P. A.; Hill, A. E.; Peters, C. W.; Weinreich, G. *Phys. Rev. Lett.* **1961**, *7* (4), 118–119.

93. Terhune, R. W.; Maker, P. D.; Savage, C. M. *Phys. Rev. Lett.* **1962**, *8* (10), 404–406.

94. Boyd, R. . *Nonlinear Optics*; Academic Press,New York, **1992**.

95. Shen, Y. R.; Martini, F. de. in: V. M. A. and D. L. M. (Eds. . In *Introduction to surface and superlattice excitations*; North-Holland, **1982**; p 629.

96. Heinz, T. F. University of California,Berkeley, **1982**.

97. Sipe, J. E.; Stegman, G. I. in: V. M. A. *Surface Polaritons*; Mills, D. L., Ed.; North-Holland, **1982**.

98. Fukui, M.; Stegman, G. I. *Electromagnetic Surface Modes*; Boardman, A. D., Ed.; John Wiley & Sons, **1982**.

99. Clays, K.; Persoons, A. *Phys. Rev. Lett.* **1991**, *66*, 2980–2983.

100. Terhune, R. W.; Maker, P. D.; Savage, C. M. *Phys. Rev. Lett.* **1965**, *14*, 681–684.

101. Shen, Y. . *The Principles of Nonlinear Optics*; Wiley, New York, **1984**.

102. Ponath, H, E.; Stegeman, G, I. *Nonlinear Surface Electromagnetic Phenomena*; Elsevier Science Publishers,North Holland, **1991**.

103. Wang, H.; Yan, E. C. Y.; Borguet, E.; Eisenthal, K. B. *Chem. Phys. Lett.* **1996**, *259* (1–2), 15–20.

104. Wan, C.; Johnson, C. K. *J. Phys. Chem.* **1994**, *98* (8), 1999–2001.

105. V, O. A. P. V. E. *Phys. Rev. B* **1995**, *51* (24), 17591–17599.

106. Gorter, E.Grendel, F. *J. Exp. Med.* **1925**, *41* (4), 439–443.

107. Bangham, A. D.; Horne, R. W. *J. Mol. Biol.* **1964**, *8* (5), 660–668.

108. Szoka, Francis Papahadjopoulos, D. *Ann Rev. Biophys Bioeng* **1980**, *9*, 467–508.

109. Cafiso, D. *Methods Enzym.* **1989**, *172*, 331–345.

110. Cafiso, D. S.; Hubbell, W. L. *Biophys. J.* **1983**, *44* (1), 49–57.

111. Buster, D. C.; Hinton, J. F.; Millett, F. S.; Shungu, D. C. *Biophys. J.* **1988**, *53* (2), 145–152.

112. Xiang, T. X.; Anderson, B. D. *Biophys. J.* **1997**, *72* (1), 223–237.

113. Cruciani, O.; Mannina, L.; Sobolev, A. P.; Cametti, C.; Segre, A. *Molecules* **2006**, *11*

(5), 334–344.

114. Mel'nikov, S. M.; Seijen Ten Hoorn, J. W. M.; Eijkelenboom, A. P. A. M. *Chem. Phys. Lipids* **2004**, *127* (2), 121–141.

115. Vermathen, M.; Vermathen, P.; Simonis, U.; Bigler, P. *Langmuir* **2008**, *24* (21), 12521–12533.

116. Vermathen, M.; Marzorati, M.; Vermathen, P.; Bigler, P. *Langmuir* **2010**, *26* (13), 11085–11094.

117. Kaiser, S.; Hoffmann, H. *J. Colloid Interface Sci.* **1996**, *184* (1), 1–10.

118. Voelker, D.; Smejtek, P. *Biophys. J.* **1996**, *70* (2 I), 818–830.

119. Terce, F.; Tocanne, J. F.; Laneelle, G. *Eur. J. Biochem.* **1982**, *125* (1), 203–207.

120. Aubard, J.; Lejoyeux, P.; Schwaller, M. A.; Dodin, G. *J. Phys. Chem.* **1990**, *94* (4), 1706–1711.

121. Casals, C.; Miguel, E.; Perez-Gil, J. *Biochem. J.* **1993**, *296* (3), 585–593.

122. Kuzelová, K.; Brault, D. *Biochemistry* **1994**, *33* (32), 9447–9459.

123. Kuzelova, K.; Brault, D. *Biochemistry* **1995**, *34* (35), 11245–11255.

124. Maman, N.; Dhami, S.; Phillips, D.; Brault, D. *Biochim. Biophys. Acta* **1999**, *1420* (1), 168–178.

125. Bonneau, S.; Maman, N.; Brault, D. *Biochim. Biophys. Acta - Biomembr.* **2004**, *1661* (1), 87–96.

126. Nathalie Maman, D. B. *Biochim. Biophys. Acta* **1998**, *1414*, 31–42.

127. Srivastava, A.; Eisenthal, K. B. *Chem. Phys. Lett.* **1998**, *292* (3), 345–351.

128. Yan, E. C. Y.; Eisenthal, K. B. *Biophys. J.* **2000**, *79* (2), 898–903.

129. Yan Liu, Elsa C. Y. Yan, Xiaolin Zhao, and K. B. E. *Langmuir* **2001**, *17* (3), 2063–2066.

130. Liu, Y.; Yan, E. C. Y.; Eisenthal, K. B. *Biophys. J.* **2001**, *80* (2), 1004–1012.

131. Shang, X.; Liu, Y.; Yan, E.; Eisenthal, K. B. *J. Phys. Chem. B* **2001**, *105* (51), 12816–12822.

132. Liu, J.; Subir, M.; Nguyen, K.; Eisenthal, K. B. *J. Phys. Chem. B* **2008**, *112* (48), 15263–15266.

133. Liu, J.; Shang, X.; Pompano, R.; Eisenthal, K. B. *Faraday Discuss.* **2005**, *129*, 291–299.

134. Zeng, J.; Eckenrode, H. M.; Dounce, S. M.; Dai, H. L. *Biophys. J.* **2013**, *104* (1), 139–145.

135. Zeng, J.; Eckenrode, H. M.; Dai, H. L.; Wilhelm, M. J. *Colloids Surfaces B Biointerfaces* **2015**, *127*, 122–129.

136. Wilhelm, M. J.; Sheffield, J. B.; Gonella, G.; Wu, Y.; Spahr, C.; Zeng, J.; Xu, B.; Dai, H. L. *Chem. Phys. Lett.* **2014**, *605–606*, 158–163.

137. Wilhelm, M. J.; Sheffield, J. B.; Sharifian Gh., M.; Wu, Y.; Spahr, C.; Gonella, G.; Xu, B.; Dai, H. L. *ACS Chem. Biol.* **2015**, *10* (7), 1711–1717.

138. Wilhelm, M. J.; Sharifian Gh., M.; Dai, H. L. *Biochemistry* **2015**, *54* (29), 4427–4430.

139. Sharifian Gh, M.; Wilhelm, M. J.; Dai, H. L. *J. Phys. Chem. Lett.* **2016**, *7* (17), 3406–3411.

140. Saini, R. K.; Dube, A.; Gupta, P. K.; Das, K. *J. Phys. Chem. B* **2012**, *116* (14), 4199–4205.

141. Varshney, G. K.; Saini, R. K.; Gupta, P. K.; Das, K. *Langmuir* **2013**, *29* (9), 2912–2918.

142. Varshney, G. K.; Kintali, S. R.; Gupta, P. K.; Das, K. *Langmuir* **2016**, *32* (40), 10415–10421.

143. Varshney, G. K.; Kintali, S. R.; Das, K. *Langmuir* **2017**, *33* (33), 8302–8310.

144. LaVan, D. A.; McGuire, T.; Langer, R. *Nat. Biotechnol.* **2003**, *21* (10), 1184–1191.

145. Allen, T. M.; Hansen, C.; Martin, F.; Redemann, C.; Yau-Young, A. *BBA - Biomembr.* **1991**, *1066* (1), 29–36.

146. Torchilin, V. P. *Nat. Rev. Drug Discov.* **2005**, *4* (2), 145–160.

147. Tardi, P. G.; Boman, N. L.; Cullis, P. R. *J. Drug Target.* **1996**, *4* (3), 129–140.

148. Singh, A. K.; Kilpatrick, P. K.; Carbonell, R. G. *Biotechnol. Prog.* **1996**, *12* (2), 272–280.

149. Charrier, A.; Thibaudau, F. *Biophys. J.* **2005**, *89* (2), 1094–1101.

150. Liang, X.; Mao, G.; Ng, K. Y. S. *J. Colloid Interface Sci.* **2005**, *285* (1), 360–372.

151. Kostarelos, K.; Tadros, T. F.; Luckham, P. F. *Langmuir* **1999**, *15* (2), 369–376.

152. Kostarelos, K.; Luckham, P. F.; Tadros, T. F. *J. Colloid Interface Sci.* **1997**, *191* (2), 341–348.

153. Haskell, R. J. *J. Pharm. Sci.* **1998**, *87* (2), 125–129.

154. Hunter, D. J. *Zeta Potential in Colloids Science: Principles and Applications*; Academic Press Inc. (London) Ltd., **1988**.

155. Shaw, D. J. *Introduction to Colloidal and Surface Chemistry*; Butterworth Heinemann,UK, **1992**.

156. Rohatgi-Mukherjee, K. K. *Fundamentals of Photochemistry*; Wiley Eastern Ltd: India, **1986**.

157. R. Lakowicz, J. *Principles of Fluorescence Spectroscopy*, 3rd ed.; Springer New York, **2006**.

158. Birks, J. B. *Photo Physics of Aromatic Molecules*; Wiley-Interscience: New York, **1970**.

159. Gilbert, A; Baggott, J.; Wagner, P. J. *Essential of Molecular Photochemistry*; Blackwell Science Inc.: Cambridge, USA, **1991**.

160. Sauer, M.; Hofkens, J.; Enderlein, J. *Handbook of Fluorescence Spectroscopy and Imaging*; WILEY-VCH Verlag GmbH & Co. KGaA, Weinheim, **2011**.

161. Lantz, R. C.; Chen, G. J.; Solyom, A. M.; Jolad, S. D.; Timmermann, B. N. *Phytomedicine* **2005**, *12*, 445–452.

162. Shi, M.; Cai, Q.; Yao, L.; Mao, Y.; Ming, Y.; Ouyang, G. *Cell Biol. Int.* **2006**, *30* (3), 221–226.

163. Surh, Y. J. *Food Chem. Toxicol.* **2002**, *40* (8), 1091–1097.

164. O'Connor, D. V.; Phillips, D. *Time-Correlated Single-Photon Counting*; Academic Press: London, **1984**.

165. Duan, X. M.; Konami, H.; Okada, S.; Oikawa, H.; Matsuda, H.; Nakanishi, H. *J. Phys.*

Chem. **1996**, *100* (45), 17780–17785.

166. Ashwell, G. J.; Jackson, P. D.; Crossland, W. A. *Nature* **1994**, *368*, 438–440.

167. Kim, O. K.; Choi, L. S.; Zhang, H. Y.; He, X. H.; Shih, Y. H. *J. Am. Chem. Soc.* **1996**, *118* (48), 12220–12221.

168. Xu, J.; Lu, X.; Zhou, G.; Zhang, Z. *Thin Solid Films* **1998**, *312* (1–2), 295–299.

169. Varshney, G. K. Homi Bhabha National Institute, India, **2018**.

170. Binder, W. H. *Angew. Chemie - Int. Ed.* **2008**, *47* (17), 3092–3095.

171. Amado, E.; Kressler, J. *Curr. Opin. Colloid Interface Sci.* **2011**, *16* (6), 491–498.

172. Johnsson, M.; Silvander, M.; Karlsson, G.; Edwards, K. *Langmuir* **1999**, *15* (19), 6314–6325.

173. Erukova, V. Y.; Krylova, O. O.; Antonenko, Y. N.; Melik-Nubarov, N. S. *Biochim. Biophys. Acta - Biomembr.* **2000**, *1468* (1–2), 73–86.

174. Johnsson, M.; Bergstrand, N.; Edwards, K.; Stålgren, J. J. R. *Langmuir* **2007**, *17* (13), 3902–3911.

175. Krylova, O. O.; Melik-Nubarov, N. S.; Badun, G. A.; Ksenofontov, A. L.; Menger, F. M.; Yaroslavov, A. A. *Chem. - A Eur. J.* **2003**, *9* (16), 3930–3936.

176. Maskarinec, S. A.; Lee, K. Y. C. *Langmuir* **2003**, *19* (5), 1809–1815.

177. Firestone, M. A.; Wolf, A. C. **2003**, 1539–1549.

178. Krylova, O. O.; Pohl, P. *Biochemistry* **2004**, *43* (12), 3696–3703.

179. Zhirnov, A. E.; Demina, T. V.; Krylova, O. O.; Grozdova, I. D.; Melik-Nubarov, N. S. *Biochim. Biophys. Acta - Biomembr.* **2005**, *1720* (1–2), 73–83.

180. Demina, T.; Grozdova, I.; Krylova, O.; Zhirnov, A.; Istratov, V.; Frey, H.; Kautz, H.; Melik-Nubarov, N. *Biochemistry* **2005**, *44* (10), 4042–4054.

181. Liang, X.; Mao, G.; Ng, K. Y. S. *J. Colloid Interface Sci.* **2005**, *285* (1), 360–372.

182. Chang, L. C.; Lin, C. Y.; Kuo, M. W.; Gau, C. S. *J. Colloid Interface Sci.* **2005**, *285* (2), 640–652.

183. Gau-Racine, J.; Lal, J.; Zeghal, M.; Auvray, L. *J. Phys. Chem. B* **2007**, *111* (33), 9900–

9907.

184. Frey, S. L.; Zhang, D.; Carignano, M. A.; Szleifer, I.; Lee, K. Y. C. *J. Chem. Phys.* **2007**, *127* (11).

185. Frey, S. L.; Lee, K. Y. C. *Langmuir* **2007**, *23* (5), 2631–2637.

186. Wu, G.; Lee, K. Y. C. *Langmuir* **2009**, *25* (4), 2133–2139.

187. Chieng, Y. Y.; Chen, S. B. *J. Phys. Chem. B* **2009**, *113* (45), 14934–14942.

188. Wang, J. Y.; Chin, J.; Marks, J. D.; Lee, K. Y. C. *Langmuir* **2010**, *26* (15), 12953–12961.

189. Cheng, C. Y.; Wang, J. Y.; Kausik, R.; Lee, K. Y. C.; Han, S. *Biomacromolecules* **2012**, *13* (9), 2624–2633.

190. Hezaveh, S.; Samanta, S.; De Nicola, A.; Milano, G.; Roccatano, D. *J. Phys. Chem. B* **2012**, *116* (49), 14333–14345.

191. Nawaz, S.; Redhead, M.; Mantovani, G.; Alexander, C.; Bosquillon, C.; Carbone, P. *Soft Matter* **2012**, *8* (25), 6744–6754.

192. Hädicke, A.; Blume, A. *J. Colloid Interface Sci.* **2013**, *407*, 327–338.

193. Wood, I.; Martini, M. F.; Albano, J. M. R.; Cuestas, M. L.; Mathet, V. L.; Pickholz, M. *J. Mol. Struct.* **2016**, *1109*, 106–113.

194. Goliaei, A.; Lau, E. Y.; Adhikari, U.; Schwegler, E.; Berkowitz, M. L. *J. Phys. Chem. B* **2016**, *120* (33), 8631–8641.

195. Adhikari, U.; Goliaei, A.; Tsereteli, L.; Berkowitz, M. L. *J. Phys. Chem. B* **2016**, *120* (26), 5823–5830.

196. Fusco, S.; Borzacchiello, A.; Netti, P. A. *Journal of Bioactive and Compatible Polymers*. March 2006, pp 149–164.

197. Basáñez, G.; Nieva, J. L.; Rivas, E.; Alonso, A.; Goñi, F. M. *Biophys. J.* **1996**, *70* (5), 2299–2306.

198. Zotchev, S. *Curr. Med. Chem.* **2012**, *10* (3), 211–223.

199. Baginski, M.; Czub, J.; Sternal, K. *Chem. Rec.* **2006**, *6* (6), 320–332.

200. Charbonneau, C.; Fournier, I.; Dufresne, S.; Barwicz, J.; Tancrède, P. *Biophys. Chem.*

2001, *91* (2), 125–133.

201. Vertut-Croquin, A.; Bolard, J.; Chabbert, M.; Gary-Bobo, C. *Biochemistry* **1983**, *22* (12), 2939–2944.
202. Chen, W. C.; Bittman, R. *Biochemistry* **1977**, *16* (19), 4145–4149.
203. Hsuchen, C.-C.; Feingold, D. S. *Selective Membrane Toxicity of the Polyene Antibiotics: Studies on Lecithin Membrane Models (Liposomes) Downloaded From*; **1973**.
204. Baginski, M.; Resat, H.; Borowski, E. *Biochim. Biophys. Acta - Biomembr.* **2002**, *1567* (SUPPL.), 63–78.
205. Neumann, A.; Czub, J.; Baginski, M. *J. Phys. Chem. B* **2009**, *113* (48), 15875–15885.
206. Fujii, G.; Chang, J. E.; Coley, T.; Steere, B. *Biochemistry* **1997**, *36* (16), 4959–4968.
207. Nakagawa, Y.; Umegawa, Y.; Matsushita, N.; Yamamoto, T.; Tsuchikawa, H.; Hanashima, S.; Oishi, T.; Matsumori, N.; Murata, M. *Biochemistry* **2016**, *55* (24), 3392–3402.
208. Baginski, M.; Sternal, K.; Czub, J.; Borowski, E. *Acta Biochim. Pol.* **2005**, *52* (3), 655–658.
209. Gruszecki, W. I.; Gagoś, M.; Hereć, M. *Journal of Photochemistry and Photobiology B: Biology*. January 2003, pp 49–57.
210. Gruszecki, W. I.; Luchowski, R.; Gagoś, M.; Arczewska, M.; Sarkar, P.; Hereć, M.; Myśliwa-Kurdziel, B.; Strzałka, K.; Gryczynski, I.; Gryczynski, Z. *Biophys. Chem.* **2009**, *143* (1–2), 95–101.
211. Wasko, P.; Luchowski, R.; Tutaj, K.; Grudzinski, W.; Adamkiewicz, P.; Gruszecki, W. I. *Mol. Pharm.* **2012**, *9* (5), 1511–1520.
212. Baran, M.; Borowski, E.; Mazerski, J. *Biophys. Chem.* **2009**, *141* (2–3), 162–168.
213. Mukhopadhyay, S.; Maitra, U. *Curr. Sci.* **2004**, *87* (12), 1666–1683.
214. Hofmann, A. F. *Arch Intern Med.* **1999**, *159*, 2647–2658.
215. Wynder, T. N. N. E. M. J. H. W. E. L. *J. Natl. Cancer Inst.* **1974**, *53* (4), 1093–1097.
216. Bernstein, H.; Bernstein, C.; Payne, C. M.; Dvorakova, K.; Garewal, H. *Mutat. Res.* -

Rev. Mutat. Res. **2005**, *589* (1), 47–65.

217. Ou, J.; DeLany, J. P.; Zhang, M.; Sharma, S.; O'Keefe, S. J. D. *Nutr. Cancer* **2012**, *64* (1), 34–40.

218. Ana I. Haza, Björn Glinghammar, Alf Grandien, and J. R. *Nutr. Cancer* **2009**, *36* (1), 79–89.

219. Nugent, S. G.; Kumar, D.; Rampton, D. S.; Evans, D. F. *Gut* **2001**, *48* (4), 571–577.

220. Rubin, D. T.; Bunnag, A. P.; Surma, B. L.; Mikolajczyk, A. *Gastroenterology* **2009**, *136* (5), A-349.

221. Mohapatra, M.; Mishra, A. K. *Langmuir* **2013**, *29*, 14934–14940.

222. Barrasa, J. I.; Olmo, N.; Lizarbe, M. A.; Turnay, J. *Toxicol. Vitr.* **2013**, *27* (2), 964–977.

223. Reddy, B. S. **1979**, 3766–3768.

224. Tong, J. L.; Ran, Z. H.; Shen, J.; Fan, G. Q.; Xiao, S. D. *Yonsei Med. J.* **2008**, *49* (5), 792–803.

225. Bernstein, C.; Holubec, H.; Bhattacharyya, A. K.; Nguyen, H.; Payne, C. M.; Zaitlin, B.; Bernstein, H. *Arch. Toxicol.* **2011**, *85* (8), 863–871.

226. Longpre, J. M.; Loo, G. *Apoptosis* **2008**, *13* (9), 1162–1171.